

AD-A134 343

ANALYTICAL AND EXPERIMENTAL INVESTIGATION OF SOIL
REINFORCING(U) PURDUE UNIV LAFAYETTE IN SCHOOL OF CIVIL
ENGINEERING R D HOLTZ ET AL. OCT 83 AFESC/ESL-TR-82-31

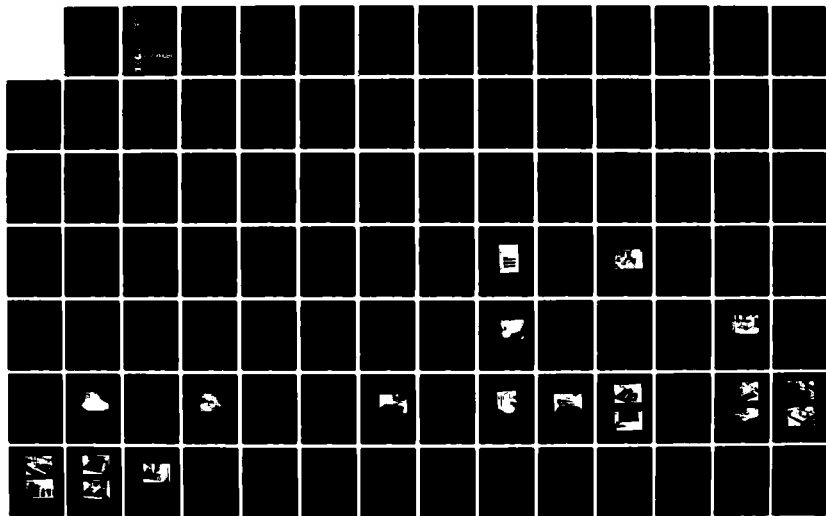
1/2

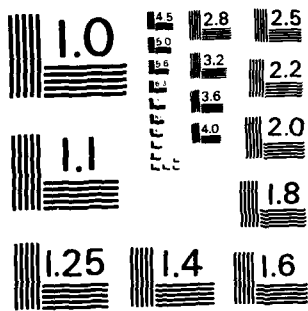
UNCLASSIFIED

F08635-71-K-0036

F/G 13/13

NL





MICROCOPY RESOLUTION TEST CHART
NATIONAL BUREAU OF STANDARDS - 1963 - A



ESL-TR-82-31

ANALYTICAL & EXPERIMENTAL INVESTIGATION OF SOIL REINFORCING

R.D. HOLTZ & M.E. HARR
SCHOOL OF CIVIL ENGINEERING
PURDUE UNIVERSITY
WEST LAFAYETTE, INDIANA 47907

OCTOBER 1983

FINAL REPORT
1 JANUARY 1981 - 30 JUNE 1982

DTIC
SELECTED
NOV 2 1983
S D

APPROVED FOR PUBLIC RELEASE: DISTRIBUTION UNLIMITED

AD-A134343



DTIC FILE COPY



ENGINEERING & SERVICES LABORATORY
AIR FORCE ENGINEERING & SERVICES CENTER
TYNDALL AIR FORCE BASE, FLORIDA 32403

00 11 01 00M

NOTICE

PLEASE DO NOT REQUEST COPIES OF THIS REPORT FROM
HQ AFESC/RD (ENGINEERING AND SERVICES LABORATORY).

ADDITIONAL COPIES MAY BE PURCHASED FROM:

NATIONAL TECHNICAL INFORMATION SERVICE

5285 PORT ROYAL ROAD

SPRINGFIELD, VIRGINIA 22161

FEDERAL GOVERNMENT AGENCIES AND THEIR CONTRACTORS
REGISTERED WITH DEFENSE TECHNICAL INFORMATION CENTER
SHOULD DIRECT REQUESTS FOR COPIES OF THIS REPORT TO:

DEFENSE TECHNICAL INFORMATION CENTER

CAMERON STATION

ALEXANDRIA, VIRGINIA 22314

UNCLASSIFIED

SECURITY CLASSIFICATION OF THIS PAGE (When Data Entered)

| REPORT DOCUMENTATION PAGE | | READ INSTRUCTIONS BEFORE COMPLETING FORM |
|---|------------------------------------|---|
| 1 REPORT NUMBER ESL-TR-82-31 | 2 GOVT ACCESSION NO. AD-A134343 | 3 RECIPIENT'S CATALOG NUMBER |
| 4 TITLE (and Subtitle) ANALYTICAL AND EXPERIMENTAL INVESTIGATION OF SOIL REINFORCING | | 5 TYPE OF REPORT & PERIOD COVERED Final Report, Phase I 1 Jan 1981 to 30 Jun 1982 |
| | | 6 PERFORMING ORG. REPORT NUMBER |
| 7 AUTHOR(s) R. D. Holtz and M. E. Harr | | 8 CONTRACT OR GRANT NUMBER(s) F08635-71-K-0036 |
| 9 PERFORMING ORGANIZATION NAME AND ADDRESS School of Civil Engineering Purdue University West Lafayette, Indiana 47907 | | 10 PROGRAM ELEMENT PROJECT, TASK AREA & WORK UNIT NUMBERS PE 62601F JON 26730002 |
| 11 CONTROLLING OFFICE NAME AND ADDRESS Air Force Engineering and Services Center Engineering and Services Laboratory (RDC) Tyndall Air Force Base, FL 32403 | | 12 REPORT DATE October 1983 |
| | | 13 NUMBER OF PAGES 129 |
| 14 MONITORING AGENCY NAME & ADDRESS (if different from Controlling Office) | | 15 SECURITY CLASS. (of this report) Unclassified |
| | | 15a DECLASSIFICATION DOWNGRADING SCHEDULE |
| 16 DISTRIBUTION STATEMENT (of this Report): Approved for public release, distribution unlimited. | | |
| 17 DISTRIBUTION STATEMENT (of the abstract entered in Block 20, if different from Report) | | |
| 18 SUPPLEMENTARY NOTES Availability of this report is specified on reverse of front cover. | | |
| 19 KEY WORDS (Continue on reverse side if necessary and identify by block number) Soil reinforcing, geotextiles, plate load tests, laboratory tests, analytical models, geogrids, stress and strain diffusion, unpaved runways | | |
| 20 ABSTRACT (Continue on reverse side if necessary and identify by block number): -Significant improvements in the capacity and service life of reinforced earth structures require an improved understanding of the fundamental behavior of these systems. Both experimental and analytical investigations were carried out to develop models for the interaction of geotextile-type reinforcement and granular soils. Reinforcement configurations and systems investigated were thought to be applicable to alternate launch and recovery surfaces (ALRS). Model ALRS systems using geotextiles and geogrids as reinforcement were tested in the laboratory in a variety of configurations. These were loaded to | | |

DD FORM 1473 1 JAN 73 EDITION OF 1 NOV 65 IS OBSOLETE

UNCLASSIFIED

SECURITY CLASSIFICATION OF THIS PAGE (When Data Entered)

20. Abstract (continued)

failure, quasi-statically, by both plane strain and axisymmetric rigid plates. Load-deformation characteristics as well as the shape of the deflected basin are reported.

Significant increases in bearing capacity and modulus of subgrade reaction as a function of depth and number of layers of reinforcement were observed. However, there was a decrease in improvement as the depth to the first layer increased. Edge fixity conditions were found to be relatively unimportant, and the benefit of multiple-reinforcement layers was greater if the depth and spacing were small compared to the diameter of the loaded area. Surprisingly, little difference was observed in the response of the geogrids and geotextiles, probably because sand was used in the experiments. Geometric scaling of bearing capacity, based on the diameters of the loaded areas, was not possible.

Two new analytical models and numerical solutions for fabric-reinforced soil systems were developed. One is based on probabilistic concepts for vertical stress diffusion, and the other considers the diffusion of strain through a particulate medium. Both approaches have considerable potential in foundation engineering as well as in soil-fabric reinforcement systems.

| | |
|--------------------|-------------------------------------|
| Accession For | |
| NTIS GRA&I | <input checked="" type="checkbox"/> |
| DTIC TAB | <input type="checkbox"/> |
| Unannounced | <input type="checkbox"/> |
| Justification | |
| By | |
| Distribution/ | |
| Availability Codes | |
| Dist | Avail and/or Special |
| A/1 | |



SUMMARY

Significant improvements in the capacity and service life of reinforced earth structures require an improved understanding of the fundamental behavior of these systems. Both experimental and analytical investigations were carried out to develop models for the interaction of geotextile-type reinforcement and granular soils. Reinforcement configurations and systems investigated were thought to be applicable to temporary runways, also known as alternate launch and recovery surfaces (ALRS). Model ALRS systems using geotextiles and geogrids as reinforcement were tested in the laboratory in a variety of configurations. These were loaded to failure, quasi-statically, by both plane strain and axisymmetric rigid plates. Load-deformation characteristics, as well as the shape of the deflected basin, are reported.

Two new analytical models for fabric-reinforced soil systems were developed. The first is based on probabilistic concepts for vertical stress diffusion in a particulate medium. Numerical solutions were obtained for some practical subgrade-reinforcing situations. The efficiency of the membrane was found to increase as the underlying subgrade becomes more compressible, as long as the geotextile is sufficiently strong and possesses sufficient frictional resistance. Another model was developed which considers the diffusion of strain through a particulate medium. This model predicts surface deflection profiles as well as strains with depth, and the approach has considerable potential in foundation engineering as well as in soil-fabric reinforcement systems.

Significant increases in bearing capacity and modulus of subgrade reaction as a function of both the location (depth) of the reinforcement and the number of reinforcement layers were observed. However, there was a decrease in improvement as the depth to the first layer increased. The "critical depth," if it exists, is probably about one-third the width (or diameter) of the loaded area. Edge fixity conditions were found to be relatively unimportant, and the benefit of multiple-reinforcement layers was found to be greater if the depth and spacing were small compared to the diameter of the loaded area. Surprisingly, little difference in response between geogrids and geotextiles was observed, probably because the sand used in the experiments did not provide the interlock component apparently necessary for the optimum functioning of the geogrids. Scaling of maximum load, bearing capacity, etc., based on the diameters of the loaded areas was unsuccessful. Surface deflection profiles due to the loaded plate at one-half maximum load could be reasonably predicted from the strain diffusion hypothesis developed earlier.

Implications of the research findings for practical ALRS systems, as well as an outline of plans for Phase II research, are also presented.

PREFACE

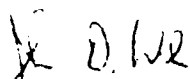
This report was prepared by the School of Civil Engineering, Purdue University, Lafayette, Indiana, 47907, with research directed by Professors R. D. Holtz and M. E. Harr. Work was done under Contract F08635-71-K-0036, for the Air Force Engineering and Services Laboratory, Air Force Engineering and Services Center, Tyndall Air Force Base, Florida.

This report summarizes work done between January 1981 and June 1982. AFESC/RD project officers were Captains R. R. Costigan and J. D. Wilson.

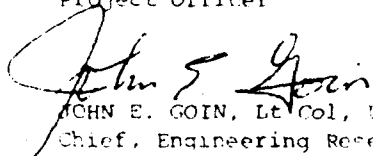
The authors acknowledge the assistance of P. Bourdeau, R. A. McMillion, M. Gunaratne, M. W. Buis, T. A. Haliburton, F. Glossic, and G. P. Harston with various aspects of the research. They also thank Catherine Ralston for preparing the manuscript and N. Sivakugan for making the drawings.

This report has been reviewed by the Public Affairs Office (PA) and is releasable to the National Technical Information Service (NTIS). At NTIS, it will be available to the general public, including foreign nationals.

This technical report has been reviewed and is approved for publication.


JOHN D. WILSON, Capt, USAF
Project Officer


JAMES R. VAN ORMAN
Chief, Rapid Runway Repair Branch


JOHN E. GOIN, Lt Col, USAF
Chief, Engineering Research Division


ROBERT E. BRANDON
Deputy Director
Engineering and Services Laboratory

TABLE OF CONTENTS

| Section | Title | Page |
|---------|--|------|
| I. | INTRODUCTION AND TECHNICAL BACKGROUND | 1 |
| | 1. Earth Reinforcing | 1 |
| | 2. Related Work on Reinforced Roads; MESL | 3 |
| | 3. Haliburton's Work and Critique by van den Berg | 4 |
| | 4. Materials for Reinforcing | 5 |
| | 5. Related Work on RRR and ALRS | 6 |
| | 6. Objectives of the Present Research | 6 |
| | 7. Outline of this Report | 6 |
| II. | ANALYTICAL WORK | 7 |
| | 1. Introduction | 7 |
| | 2. Homogeneous Medium | 7 |
| | a. Plane Strain Case | 7 |
| | b. Three-Dimensional Case | 9 |
| | 3. Multilayer Medium | 9 |
| | 4. Soil-Fabric Medium | 13 |
| | 5. Strain Diffusion | 13 |
| | 6. Examples of Models | 16 |
| | a. Homogeneous Medium - Infinite Strip | 16 |
| | b. Homogeneous Medium - Circular Area | 16 |
| | c. Strain Diffusion | 16 |
| | d. Displacements and Settlements | 27 |
| III. | EXPERIMENTAL WORK | 29 |
| | 1. Introduction | 29 |
| | 2. Description of Experimental Program | 29 |
| | a. Variables | 29 |
| | b. Code | 30 |
| | 3. Description of Apparatus and Equipment | 30 |
| | a. Loading Box and Reaction Frame | 30 |
| | b. MTS "Closed Loop" Hydraulic Loading System | 34 |
| | c. Sand | 34 |
| | d. Reinforcement | 41 |
| | e. Loading Plates | 48 |
| | f. Instrumentation and Data Acquisition System | 48 |

TABLE OF CONTENTS (CONTINUED)

| Section | Title | Page |
|---------|--|------|
| 4. | Fabrication and Construction of Test Specimens | 50 |
| | a. Sand Placement and Density Control | 50 |
| | b. Fabric and Geogrid Placement | 59 |
| | c. Mounting of the Load Plate and Load Cell | 62 |
| | d. Instrumentation | 62 |
| | e. Loading Test | 62 |
| 5. | Experimental Results | 66 |
| | a. Photographs of Tests After Failure | 66 |
| | b. Loading vs. Settlement of Plates | 66 |
| | c. Ultimate Load and Stress | 78 |
| | d. Effect of Reinforcement Depth and Spacing | 81 |
| | e. Effect of Number of Layers of Reinforcement | 83 |
| | f. Function of Type of Material | 85 |
| | g. Effect of Partial and Full-Edge Fixity of the Reinforcement | 85 |
| | h. Scaling Effects | 85 |
| | i. Box Size and Edge Effects | 91 |
| | j. Haliburton's "Optimum Depth" Concept | 91 |
| | k. Deflection Basin Measurements and Rut Development | 91 |
| IV. | IMPLICATIONS FOR ALTERNATE LAUNCH AND RECOVERY SURFACES | 99 |
| V. | OUTLINE OF PLANS FOR PHASE II RESEARCH | 101 |
| | 1. Field Tests | 101 |
| | 2. Additional Laboratory and Analytical Investigations | 101 |
| | 3. Additional Analytical Work | 102 |
| VI. | CONCLUSIONS AND RECOMMENDATIONS | 103 |
| | 1. Conclusions | 103 |
| | 2. Recommendations | 103 |
| | REFERENCES | 105 |

TABLE OF CONTENTS (CONCLUDED)

| Section | Title | Page |
|----------|--|------|
| APPENDIX | | |
| A | Bourdeau, Harr, and Holtz (1982) | 110 |
| B | Listing of Computer Programs | 115 |

LIST OF FIGURES

| Figure | Title | Page |
|--------|--|------|
| 1 | Load Geometry | 8 |
| 2 | Infinite Strip Geometry | 10 |
| 3 | Uniform Load over Circular Area | 10 |
| 4 | Layered Medium (After Reference 42) | 12 |
| 5 | Strain Diffusion Under a Circularly Loaded Rigid Plate | 15 |
| 6 | Strain Diffusion for a Layered Medium | 17 |
| 7 | Expected Vertical Stress at Depth $z = a$ Under a Unit Load Distributed Over (a) an Infinite Strip, and (b) a Circular Area for $\nu = 0.25$ in a Homogeneous Medium | 18 |
| 8 | Relative Surface Deflections Given a Uniform Displacement over a Circular Area of Radius A , $\mu = 3.0$ | 19 |
| 9 | Relative Surface Deflections Given a Uniform Displacement over a Circular Area of Radius A , $\mu = 2.0$ | 20 |
| 10 | Relative Surface Deflections Given a Uniform Displacement over a Circular Area of Radius A , $\mu = 1.0$ | 21 |
| 11 | Relative Surface Deflections Given a Uniform Displacement over a Circular Area of Radius A , $\mu = 0.3$ | 22 |
| 12 | Relative Surface Deflections Given a Uniform Displacement over a Circular Area of Radius A , $\mu = 0.2$ | 23 |
| 13 | Relative Surface Deflections Given a Uniform Deflection over a Circular Area of Radius A , $\mu = 0.1$ | 24 |
| 14 | Relative Surface Deflections Given a Uniform Displacement over a Circular Area of Radius A , $\mu = 0$ | 25 |
| 15 | Illustration of Geometric Test Variables. Note: $D = B$ for PS Tests | 31 |

LIST OF FIGURES (CONTINUED)

| Figure | Title | Page |
|--------|--|------|
| 16 | Test Box | 35 |
| 17 | Loading Frame (Reference 47) | 36 |
| 18 | General View of Test Box, Data Acquisition System and Controls for the MTS Loading System | 37 |
| 19 | Grain Size Distribution of Ottawa Flint Sand | 38 |
| 20 | Results of Direct Shear Tests on Ottawa Flint Sand | 40 |
| 21 | Results of Wide Strip Tensile Tests on Woven Polyester, Warp Direction | 42 |
| 22 | Tensile Stress-Strain Relationship for (a) SR1 and (b) SR2 Geogrids | 46 |
| 23 | Results of Creep Tensile Tests on (a) SR1 and (b) SR2 Geogrids | 46 |
| 24 | Results of Pullout and Shear Box Tests on Various Materials Including Geogrids ("Tensar" [®]) and Geotextiles (after Ref- erences 4 and 48) | 47 |
| 25 | DCDT Support Beam, Load Cell, and 6-inch Diameter Load Plate | 49 |
| 26 | Location of DCDTs for Each Test Configuration (see also Table 4) | 51 |
| 27 | MACSYM 2 Data Acquisition System and Heath Printer | 53 |
| 28 | Schematic Diagram of Test Instrumentation and Data Acquisition System | 54 |
| 29 | Vibrator and Plate | 56 |
| 30 | Vibration Pattern | 57 |
| 31 | Density Can in Corner of Test Box | 58 |
| 32 | Sand Loosely Dumped on Fabric Layer | 61 |
| 33 | Closeup of Load Cell and Load Plate | 63 |

LIST OF FIGURES (CONTINUED)

| Figure | Title | Page |
|--------|--|------|
| 34 | DCDT Support Beam | 64 |
| 35 | View of Geogrid (SR2) Specimen After a Plane Strain Test. Loading Beam, Load Cell, and Top Sand Layer Have All Been Removed | 65 |
| 36 | Side View Showing "Permanent Set" in Geogrid (SR2) After a PS Test | 65 |
| 37 | Test after Failure with Fabric Reinforcement Using a 3-inch Diameter Plate | 67 |
| 38 | Closeup View of Figure 37 | 67 |
| 39 | Test Shown in Figures 37 and 38 After Raising of the Plate | 68 |
| 40 | Plane Strain Test Setup Prior to Loading | 68 |
| 41 | Plane Strain Test After Failure | 69 |
| 42 | View from Above of Plane Strain Test After Failure | 69 |
| 43 | Tests with Fabric Partially Clamped, Prior to Placement of the Final Sand Layer | 70 |
| 44 | After Failure of Test with Partial Fixity | 70 |
| 45 | Same Tests as in Figures 43 and 44, After Top Sand Layer Was Removed. The Black Arrow Drawn on the Fabric Points to a Dashed Line Which Indicates How Much the Fabric Has Moved from its Initial Position (About 1 inch) | 71 |
| 46 | Load-Settlement Response of 3CP and 6CP Tests | 73 |
| 47 | Load-Settlement Response of 3CP and 3CP1W Tests with Reinforcement at Three Depths (Expanded Settlement Scale) | 74 |
| 48 | Load-Settlement Response of 3CP Tests, Grids, vs. Fabric Reinforcement | 75 |
| 49 | Load-Settlement Response of 6CP Tests, One vs. Two Layers of Fabric Reinforcement | 76 |

LIST OF FIGURES (CONCLUDED)

| Figure | Title | Page |
|--------|--|------|
| 50 | Load-Settlement Response of PS Tests with Fabric and Grids | 77 |
| 51 | Load-Settlement Response of Tests with Partial Edge Fixity of the Fabric | 79 |
| 52 | Maximum Load on the Plate vs. the Depth, d , to the First Reinforcement Layer | 82 |
| 53 | Modified Bearing Capacity Ratio (CR) vs. Depth of the First Reinforcement Layer | 84 |
| 54 | Maximum Load on the Plate at Failure vs. the Ratio of the Depth of Burial to the Reinforcement to the Diameter of the Loading Plate, d/D | 86 |
| 55 | Stress at Maximum Load q_{max} vs. the Ratio d/D | 88 |
| 56 | Modified Bearing Capacity Ratio BCR vs. the Ratio d/D | 89 |
| 57 | Modified Bearing Capacity Ratio vs. d/D for Test Results Reported in Reference 13 | 90 |
| 58 | Shape of Deflection Basin for the 3CP Tests | 92 |
| 59 | Shape of Deflection Basin for the 6CP Tests | 93 |
| 60 | Shape of Deflection Basin for the PS Tests | 94 |
| 61 | Normalized Deflection Basin Measurements for the 3CP Tests | 96 |
| 62 | Normalized Deflection Basin Measurements for the PS Tests | 97 |

LIST OF TABLES

| Table | Title | Page |
|-------|--|------|
| 1 | Test Variables and Symbols | 32 |
| 2 | Tests Conducted and Their Symbols | 33 |
| 3 | Physical and Chemical Properties of Tensar® Geogrids | 43 |
| 4 | Location of DCDT for Each Test Configuration (See Also Figure 26) | 52 |
| 5 | Dry Densities as Determined by the Small Density Can Measurements | 60 |
| 6 | Test Results | 80 |
| 7 | Theoretical Ultimate Bearing Capacity Pounds -- Unreinforced Sections | 81 |

SECTION I

INTRODUCTION AND TECHNICAL BACKGROUND

Increased understanding of the fundamental behavior of certain mechanical reinforcing and stabilization techniques is necessary before significant improvements can be made in the load-carrying capacity and service life of reinforced earth structures. Substantial advancements would be expected in several aspects of airfield pavement systems, particularly in expedient or alternate launch and recovery surfaces and for rapid repair of bomb-damaged runways. The knowledge gained is also appropriate to other potential application areas such as retaining walls, embankments, and protective construction.

1. EARTH REINFORCING

Soils often require reinforcing to accommodate anticipated loadings. "Cor-duroy" roads, constructed on logs or timbers in colonial North America and Scandinavia, are a form of reinforced earth, as are bamboo fascines used under low embankments in southeast Asia. Embankments have often been constructed directly on the brush and small trees which are common on marshy lands. In recent years, a reinforcing system of two rows of short sheet piles or steel channel sections connected by steel anchor rods has been developed at the Swedish Geotechnical Institute to increase the stability of embankments constructed on soft foundations (Reference 1). Reinforcing has also been carried out using woven and nonwoven fabrics, plastic and steel nets, used automobile tire casings, ordinary landing mats, "Columbus" fascine mats (Reference 2), or reinforced plastic or rubber membranes. Reference 3 summarizes many of these recent developments for reinforcing both embankments and retaining walls.

The primary functional requirements of the reinforcement elements are that: (1) they must have a sufficiently high deformation modulus in tension; and (2) they must be able to develop sufficient frictional resistance with the subsoil and/or embankment materials. Many plastics and nonwoven fabrics have creep properties such that their effectiveness as reinforcement may decrease with time. Of course, in reinforced embankments the strength of the subsoil may increase faster than the corresponding creep in the reinforcement to neutralize the effect of creep. Or, in the case of reinforced sands or retaining wall backfills in which consolidation does not take place, creep deformations under high loads could be significant. However, for the relatively short-term loadings considered in this research, the creep of plastic reinforcement materials was thought to present no particular difficulty.

The use of woven and nonwoven fabric materials (ASTM: "geotextiles") is a relatively recent development in the U.S. With a few notable exceptions, most of the research and development work on these materials was done in Europe, and applications were primarily directed toward stabilizing temporary roads on soft foundations. During the past 10 years, many European nonwoven fabrics have become available in the U.S., and their use for certain specific situations is increasing.

With only a few exceptions, woven geotextile technology began in the U.S. and then moved to Europe. Initial applications in the U.S. were with woven monofilament fabrics used as "filter fabrics," that is, as an alternative to

granular filters under riprap and in other erosion control features. Recent developments in woven technology have included the slit film fabrics, which are much stronger and have a higher modulus than typical nonwovens, but cost about the same per unit area.

Considerable research using woven fabrics as reinforcing has been conducted at the Swedish Geotechnical Institute and at Purdue University. This work involved laboratory investigations (References 4 and 5) and three field installations using a woven polyester fabric (References 6 and 7). This same fabric was used in the present investigations.

Other U.S. research on woven fabrics has been carried out primarily by T. A. Haliburton and his associates. They were interested in the problem of embankments constructed on very soft foundations (References 8, 9, and 10). They have also conducted experimental research on the mechanical properties of geotextiles (Reference 11) and on soil-fabric interaction (Reference 12). Of considerable interest to the present research is Reference 13, in which the potential use of geotextiles for airfield runways is considered. The conclusions of Reference 13, which are appropriate to the present research, will be discussed in some detail later in this report.

To date, most of the theoretical research on earth reinforcing has been directed towards "classical" reinforced earth retaining walls (References 14 and 15). Noteworthy in this regard is the work described in References 16 and 17. Very little theoretical research has been carried out on the problem of reinforced embankments or pavements, with the exception of the work described in References 18, 19 and 20. For example, in Reference 20, it is shown that horizontally lying reinforcement layers may not be the optimum orientation for the reinforcement under embankments. It is not known whether a similar situation exists with respect to pavement systems, although practical construction requirements probably would control design.

Related theoretical analyses and model footing tests on horizontally reinforced foundation soils were conducted by Binquet and Lee (References 21 and 22). Their results indicated that the settlement behavior and ultimate bearing capacity were improved over unreinforced soils by factors of two to four. The actual improvement depended on the percentage of total area covered by the reinforcement and the thickness and spacing of the reinforcing layers. Increasing the amount of reinforcing definitely improved the ultimate bearing capacity and reduced the settlements, especially if the reinforcing began near the bottom of the footing. This result is similar to that found by Haliburton, et al. (References 12 and 13). Similar results were also obtained in some of the present theoretical analyses. Improvement in bearing capacity resulted even when the reinforcing was located significantly deeper than the lowest point on the theoretical bearing capacity failure surface, an observation which suggests that a different failure mechanism is operative when reinforcing is used. This result was not verified previously by Haliburton, et al. (References 12 and 13).

Finally, the results of the studies of Binquet and Lee (References 21 and 22) indicate that the greatest advantage of reinforcing foundations was for short-term construction involving heavy loads over inferior foundation conditions. To some extent, such conditions involve the function of separation

rather than reinforcement. However, the research by Binquet and Lee was limited to smooth noncontinuous metallic strips (rather than continuous sheets of other materials as tested by Haliburton and in the present study) and only one soil, a sand, was tested. Only static surface loadings were applied and no assessment was made of the possible effects of impact or vibratory loading on the behavior of the reinforced soil system.

2. RELATED WORK ON REINFORCED ROADS; MESL

Considerable related research has been conducted on thin but relatively strong tensile-resistant materials or membranes under small embankments (haul roads) constructed on very soft foundations. Much of this research has been sponsored by the manufacturers of nonwoven geotextiles, and unfortunately in most cases, the assumptions, theoretical analyses, and backup experimental data are not publicly available (References 23 and 24). The procedures developed by Barenberg and his students (References 25, 26, and 27), which are based on research which was initially privately sponsored, are an exception. Kinney (1979) has developed a "fabric tension model" by which the modulus of the geotextile, as well as subgrade strength, traffic loads, and rut geometry can be appropriately considered. Summaries of the various manufacturer-sponsored design methods are given in References 23, 24 and 28.

Giroud and Noiray (Reference 29) developed a method with a very sound theoretical basis that takes into account full-scale test data developed at the U.S. Army Engineer (U.S.A.E.) Waterways Experiment Station. The method offers design charts that allow the determination of aggregate thicknesses for unpaved roads when geotextiles are used as reinforcement and when traffic is taken into account. The rut depth considered in the design charts is approximately 1 foot (0.30 meter). Recently, Sivakugan (Reference 30) has prepared design charts for lesser rut depths. Important for the present research is the fact that the tire inflation pressures and axle loads presented in the charts developed by Giroud and Noiray are for typical construction equipment and not military aircraft. Their standard axle load is 80 kN (about 18,000 pounds) and maximum tire inflation pressure is 620 kPa (about 90 psi). Consequently, considerable extrapolation would be necessary to use their charts for design purposes for typical fighter aircraft loads which might be applied to alternate launch and recovery surfaces. Such an extrapolation could be dangerous without the results of full-scale tests such as outlined in Section V. For the purpose for which it was developed, the Giroud and Noiray method is simple to use, and according to Giroud (personal communication, 1982) the method has been used with considerable success in practice.

Hamilton and Pearce (Reference 31) developed guidelines for the design of flexible pavements using slit film woven fabrics. The method is specifically applicable to the Texas Gulf Coast region where very poor subsoils predominate and suitable construction aggregates are either nonexistent or of poor quality. Significant haulage distances can result in extremely high construction costs. Hamilton and Pearce found that high modulus geotextiles have the potential of solving many of the pavement problems in that region. They present a design method and suggest that the use of woven geotextiles offers: (1) a reasonable and cost-effective alternative to mechanical or chemical subgrade stabilization, (2) a reduction in required base thicknesses, and (3) an extended pavement life.

For about 15 years, the U.S.A.E. Waterways Experiment Station (WES) has been conducting research on membrane encapsulated soil layers (MESL). Both nonwoven geotextiles as well as military membranes such as the T-16, T-17 and WX-18 membrane mats have been used (References 32 and 33). WES has also conducted research on "sand bag" type structures for the expedient construction of bridge piers and abutments in a theater of operations (Reference 34). Recent research by the same group has involved very unconventional reinforcing materials such as small plastic cylinders and paper and aluminum grids, both hexagonal and rectangular in shape. Roadways were constructed of reinforced sand on both very soft clay and sand subgrades. These tests are described in References 35, 36 and 37.

3. HALIBURTON'S WORK AND CRITIQUE BY VAN DEN BERG

As mentioned above, the work by Haliburton, et al. (References 12 and 13), is particularly pertinent to the research reported herein. This section will summarize their research and show that, in some cases, their conclusions were verified, and in other cases, they were not. They determined, among other things, that the potential improvement of the performance of embankments and runways results from three different phenomena: (1) The geotextile appears to act as a separation medium which prevents the intrusion and deterioration of the aggregate materials in the embankment. This phenomena is especially pertinent when the subgrade is soft and cohesive. (2) There appears to be a degree of lateral restraint provided by the fabric to the cohesionless cover material. As the wheel load is applied, the embankment material tries to spread laterally and this expansion tends to be prevented by the friction developed between the fabric and the embankment material. The effect is to increase the deformation modulus of the material in the embankment. (3) The third mechanism or benefit provided by the geotextile is that of membrane-type support. For this mechanism to occur, relatively large deformations must occur in the subgrade to mobilize the full membrane resistance.

Because the presence of the fabric is the controlling factor, there is an optimum location of the fabric to provide for lateral restraint reinforcement in cohesionless soils. Haliburton and coworkers suggest that this location is approximately $0.5 B \tan \phi$ below the soil surface, where B is the effective width of the loaded area and ϕ is the angle of internal friction of the material above the fabric. Placement of the fabric at the optimum depth produces three main types of behavior: (1) Elastic deformation of the cohesionless soil mass above the fabric occurs, with considerably greater deformation resistance than exists for an unreinforced soil. A significantly greater resistance to initial shear failure is also developed. (2) After the initial shear strength of the reinforced soil is exceeded, rapid yielding occurs and the loaded area sinks into the subsoil. The yielding occurs as a result of plastic deformations in a modified radial shear zone around the loaded area. There is also a concurrent shear failure in the soil mass along some failure surface above the fabric. (3) The fabric begins to "reinterfere" with the plastic flow in these modified radial shear zones as sinkage of the loaded area takes place. The writers believe that these zones return to elastic equilibrium, which stops the "sinking" from continuing. This phenomenon, a "soil strain hardening," results in a significant second-phase strength gain.

Haliburton and coworkers found that if the fabric is placed below the optimum depth, only minimal improvement in the load deformation characteristics of the reinforced soil mass will be realized. However, if initial soil failure does occur, then the loaded area will sink to near the optimum depth and the strain-hardening phenomena will begin to take place. In practice, such sinkage would likely be seen as excessive rutting in the wheel paths and probably would not be tolerable. They found that if the fabric was placed at the optimum depth, only a small amount of loaded area sinkage was required to mobilize a very large part of the soil strength and deformation resistance due to "strain hardening." They concluded that if the fabric was placed on a "good subgrade," then the second-stage strength would likely be sufficient to carry very heavy imposed loads, although no data were presented to verify this belief. If a relatively soft subgrade soil is present under the fabric, then a failure in the soil under the fabric is likely to occur which would prevent full utilization of the total cover soil strength available from the fabric reinforcement.

In contrast, van den Berg (personal communication, 1981) is somewhat critical of the laboratory test procedures used by Haliburton and his associates. His primary complaint has to do with the fact that the fabric was clamped at the edge to a frame; that is, it was prestressed to some extent prior to burial in sand and the subsequent loading by the load plate. He points out that if the failure pattern occurs as a failure wedge in the classical sense as postulated by Haliburton, then there will be a movement outward of the soil mass on both sides of the failure wedge. The resulting shear forces will tend to increase the tension forces in the fabric. Thus, the effects of "lateral restraint" and membrane tension will be difficult to separate. Clamping the fabric results in a fixity that is almost perfect, and van den Berg is not sure that in practice the fabric would be "anchored in that perfect way." He is also critical of the use of the "low quality" base materials (sand) and the fact that the width of the fabric is only six to eight times the width of the loading plates. He concluded that there may be something like an "optimum depth" of fabric reinforcement in road construction but the concept is not clearly developed nor completely accepted by the profession.

4. MATERIALS FOR REINFORCING

Several materials have been suggested as being potentially useful as primary reinforcing elements in airfield runways and other similar construction. Excellent descriptions of engineering fabrics or geotextiles, as they are now called, are found in several references, particularly, References 23 and 38. Both these books describe geotextiles in some detail and give extensive reference lists.

New materials called "geogrids" have recently been developed which have some features similar to geotextiles. Geogrids look like nets of plastic, although the strength of these materials is significantly greater than typical plastic nets. An English manufacturing company, Netlon, produces the new material under the trade name of "Tensar®." Tensar® geogrids were utilized for a few of the tests in the present study, and their properties will be described in some detail later in this report. On a weight basis, Tensar® nets are stronger than steel but their costs are on the order of woven geotextile materials. They also have an added advantage over ordinary geotextiles of providing

"interlock," in addition to frictional resistance, if materials coarser than sands, e.g., fine gravel, are used in construction.

5. RELATED WORK ON RRR AND ALRS

Much of the research on rapid runway repair procedures has been summarized in References 39 and 40. In Reference 41, materials for "contingency runways" were evaluated by full-scale tests with the F-4 load cart. An open graded crushed stone base course with a sod surface was found to rut severely when subjected to the F-4 loadings. Some success has been reported with cement and lime stabilization, but almost any kind of unstabilized soil or sod surface (overlying the stabilized base) was found to rut excessively unless the top surface was less than 1-inch thick. With such thin surface layers, the topsoil might be subject to sliding on the base course due to the breaking action of aircraft tires. It is possible that geotextiles might improve the bonding of a thin topsoil surface to stabilized subbases. Furthermore, we suggested that the top layer of contingency runways and alternate launch and recovery surfaces might be stabilized economically and reinforced by geotextile-like materials. The use of geotextiles on ALRS sites in conjunction with vegetation established on the surface would enhance their multiple use and add considerably to the concealment of the site.

6. OBJECTIVES OF THE PRESENT RESEARCH

A major objective of the present research was to develop an improved theoretical model for the interaction of reinforcement in soil. Such a model would improve our understanding of the fundamental interaction of subgrade soils with various types of reinforcement and pavement materials when subjected to surface loadings. An additional objective was to develop reinforcement configurations for ALRS pavement systems and, if possible, optimize such systems. Finally, plans were to be developed for full-scale field tests to be carried out as "Phase II."

7. OUTLINE OF THIS REPORT

In Section II of this report, the analytical work carried out will be summarized. In Section III, the details of the experimental phase of the research will be given and the results of the experiments will be examined in terms of the theoretical developments and empirical physical behavior models. A brief section is also included on the implications of the present research for RRR and ALRS. Recommendations for Phase II research, field studies, are also outlined. Finally, some conclusions and recommendations are presented.

SECTION II

ANALYTICAL WORK

1. INTRODUCTION

It is the function of analysis in Civil Engineering to perform inexpensive experiments (generally on paper) that will help to predict the response of otherwise expensive prototype systems. Considering the number of possible permutations of soils, types and placement of fabrics, pavement types, and aircraft gear configurations and loading involved in this study, it is apparent that discovered truths must first be approached by means of analysis. On the other hand, the dominating factors in the analysis of an aircraft moving over a pavement system are extremely complex and are generally "wished away" or ignored in ordinary mechanics. Consider this: the pavement system presents itself as a number of layers; each one is thin in comparison to the contact dimensions of the load (the tire imprint). The layers, in turn, are composed of discrete particles that are, at best, cemented by a thermal-sensitive material. The system may exhibit varying degrees of saturation by liquids and/or gases. Loadings are known only in magnitude, not in their distribution. Contacts between layers vary with time, ambient conditions and loadings.

In spite of the noted complexities, the engineering system offers a methodology with a high potential for success; namely, (a) to offer simple analytical models that relate the pertinent factors believed to govern performance and (b) to conduct simple laboratory-scale model tests to examine the various offered analytical developments.

Analytical and experimental models may themselves be divided into three parts: (a) input, (b) transfer mechanism, and (c) output. If both types of models are subject to the same input, the test of the adequacy of an analytical model will be its ability to predict the observed response of its experimental counterpart. Several such models will be presented in this chapter. All models consider the loading to act normal to the plane of the surface.

2. HOMOGENEOUS MEDIUM

a. Plane Strain Case

This solution was presented by Harr (Reference 42)¹. The expected value of vertical stress (S_z) under a line load of intensity p , per unit run, (Figure 1) is given by

$$S_z = \frac{2p}{\pi} \left[\frac{z}{r} \right]$$

¹I. Harr (Reference 42, Chap. 7) demonstrated that the stress at a point in a particulate media is a Poisson variable. Consider that at such a point there may exist - a void - a solid - a liquid - a gas - ... - and, it is evident, that any measure of the distribution of boundary energy, such as stress, at a point is indeed a variable. The expected value, the mean value, is the best measure of this intensity at a point.

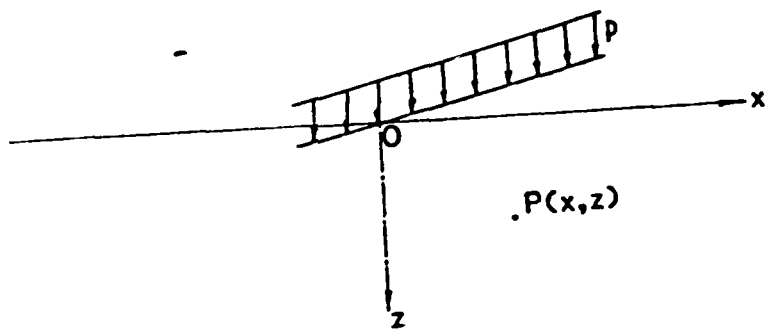


Figure 1. Load Geometry.

Harr called ν the "coefficient of lateral earth stress." He showed it to be related to the more common "coefficients of lateral earth pressure." The classical, two-dimensional, elastic solution (Flamant solution) requires no measure of the properties of the material. The attenuation of stress is assumed to be purely geometric.

For a uniform normal load, q , over an infinite strip, (Figure 2), of width a , the equivalent solution is

$$\bar{\sigma}_z = q \left[\nu \left(\frac{x+a}{z\sqrt{z^2 + (x+a)^2}} \right) - \nu \left(\frac{x-a}{z\sqrt{z^2 + (x-a)^2}} \right) \right] \quad (2)$$

where $\nu(\cdot)$ is the well-tabulated cumulative distribution (see Reference 42, p. 459).

b. Three-Dimensional Case

For a single concentrated force, P , normal to the plane of the surface, Reference 42 gave for the expected value of vertical stress

$$\bar{\sigma}_z(r,z) = \frac{P}{2\pi r z^3} \exp \left[-\frac{r^2}{2xz} \right] \quad (3)$$

This expression is in the same form of that given by Boussinesq. However, the above acknowledges the characteristics of the media (ν); whereas, the Boussinesq solution is devoid of any material properties characteristics.

For uniform normal load, q , over a circular area (Figure 3), Equation (3) generalized to

$$\bar{\sigma}_z(r,z) = \frac{q}{2xz} \int_0^a \int_0^{2\pi} \frac{\exp \left[-\frac{1}{2xz} (x^2 + r^2 - 2xr \cos \theta) \right]}{r^2} r dr d\theta \quad (4)$$

General solutions of Equation (4) can only be obtained by numerical means. Some results will be presented below.

For the special case, under the center of a uniformly distributed load, q , acting on a circular area of radius a , the expression reduces to

$$\bar{\sigma}_z(0,z) = q \left[1 - \exp \left(-\frac{a^2}{2xz} \right) \right] \quad (5)$$

3. MULTILAYER MEDIUM

Although many solutions exist in the literature for the transmission of stress through a layered system, none are unique, even with the constraints of the classical theory of elasticity. The calculated values of stress depend on

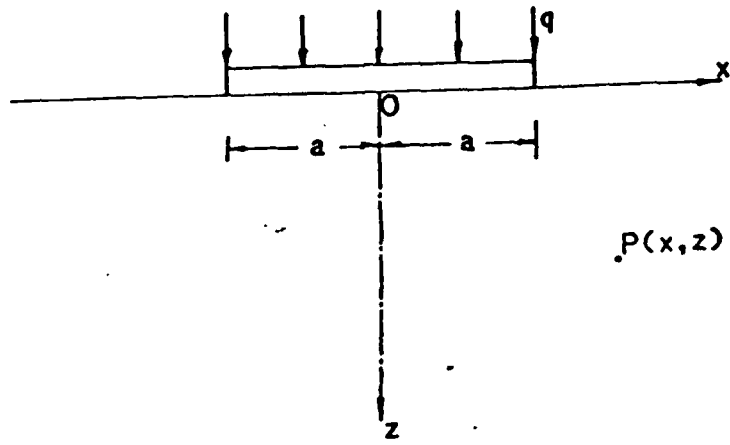


Figure 2. Infinite Strip Geometry.

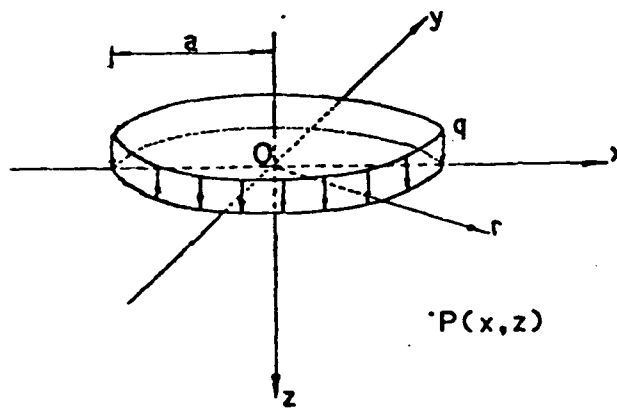


Figure 3. Uniform Load over Circular Area.

the assumptions invoked at the boundaries between the individual layers. All solutions assume continuity of displacements across interfaces; however, this assumption alone is not sufficient. Some statement must be offered as to the transformation of shearing stresses at the interfaces as this is not known a priori. Two such assumptions, commonly prescribed, are that (a) there is "no slip," and (b) there is "no friction" at the interface. Although, it is generally believed that these provide "upper" and "lower" bounds to the system; unfortunately, this is not the case. A boundary wherein one-half evidences "no slip" and the other half the "no friction" condition would be more severe than either. Harr (Reference 42) presented a solution that obviates the need to specify the shearing stresses at the interfaces of layered media. For the expected vertical stress due to a line load of intensity p (Figure 4), he gave

$$\sigma_z(x, z) = \frac{p}{2\pi} \sum_{n=1}^{\infty} \frac{2n\pi z}{(2n\pi z)^2 + x^2} \sqrt{\frac{2n\pi z}{(2n\pi z)^2 + x^2}} \quad (6a)$$

where

$$h_n = \frac{2n\pi z}{\sqrt{\frac{2n\pi z}{(2n\pi z)^2 + x^2}}} \quad (6b)$$

and z_n is the vertical distance into the N th layer.

As an example: **EXAMPLE** A three-layer system is subjected to a line load of 1000 lb/ft with the following information: $h_1 = 1$ ft, $\nu_1 = 0.4$; $h_2 = 2$ ft, $\nu_2 = 0.3$; $h_3 = 0.2$, $\nu_3 =$ unbounded. Find the expected value for the vertical normal stress 3 feet into the third layer immediately under the line load.

SOLUTION From Equation (6b), the equivalent thickness is

$$h_{eq} = \sqrt{\frac{2n\pi z}{(2n\pi z)^2 + x^2}} \cdot \sqrt{\frac{2n\pi z}{(2n\pi z)^2 + x^2}} \quad (6c)$$

Thus, from Equation (6a) we have for the expected vertical normal stress at a depth of 3 feet in the third layer, immediately under the line load ($x = 0$),

$$\sigma_z(0, z) = \frac{p}{2\pi} \sum_{n=1}^{\infty} \frac{2n\pi z}{(2n\pi z)^2 + x^2} \sqrt{\frac{2n\pi z}{(2n\pi z)^2 + x^2}} \quad (6d)$$

The theory of elasticity (Reference 43) would give for this case (assuming a homogeneous section), $\sigma_z = 954.9$ lb/ft².

For a uniformly distributed normal load q , acting over a circular area of radius a , the equivalent form of Equation (6) is

$$\sigma_z(x, z) = \frac{q}{2\pi} \sum_{n=1}^{\infty} \frac{2n\pi z}{(2n\pi z)^2 + x^2} \sqrt{\frac{2n\pi z}{(2n\pi z)^2 + x^2}} \quad (6e)$$

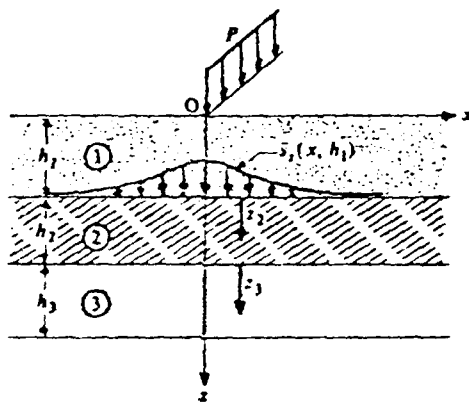


Figure 4. Layered Medium (After Reference 42).

Again, results can only be obtained by numerical methods. Examples will be developed subsequently.

4. SOIL-FABRIC MEDIUM

An analytical model was developed to simulate the action of a soil-fabric system. Briefly, the model assumed a particulate medium, as described by Equations (1) through (7), founded on a layer specified as a Winkler body. Between the two layers (at their interface) is a "geotextile" membrane. Solutions were obtained by numerical means for a range of values of soil and geotextile properties. The details of the model and some results were given in a paper by the authors and Mr. P. L. Bourdeau, which was presented at the Second International Conference on Geotextiles, August 1982 (Reference 44). A copy of the paper is in Appendix A. The results of the developed analysis indicated that very little improvement in the load-carrying capacity of the reinforced system would be achieved unless the subgrade was very soft. (This can be seen in Figures 9 and 10 in the paper in Appendix A.) Another interesting observation was that the effective length of the reinforcement was relatively short. In other words, at a rather short distance from the loaded area, the reinforcement would not "feel" any stressing due to the surface load. This result seemed anomalous at first, but recent evidence by Andrawes, et al. (Reference 45), showed very similar results for plain strain tests on reinforced sands. They found that the measured tensile force in the reinforcement was practically nonexistent at distances from the centerline as close as twice the diameter of width of the loaded area.

Although the model does not consider failure induced by insufficient bearing capacity, it does investigate two other important possible modes of distress: (1) that of the tensile force exceeding the tensile strength of the fabric, and (2) the slipping ("pull out") of the fabric if its length is less than that required for stability.

5. STRAIN DIFFUSION

The previous cases, as in continuum mechanics, presume that the stress distribution at the surface, the input into the system, is a known quantity. This is seldom the case. Contact pressures under tires are far from the idealized uniform values commonly assumed. In addition, the pressures change with time, temperature and ambient conditions (Reference 46).

The rationale of continuum mechanics is to determine the transmission of boundary energy through media as statements of stress intensities. Granted such measures, constitutive relationships are then introduced that relate stresses to commensurate strains. The vertical components of the strains are then integrated to obtain the surface deflections, which are examined relative to differential settlements and/or rutting.

When one considers the mechanism responsible for the deformations noted at the surface of a medium subject to induced loading, it is apparent that it is not caused by the deformation of the individual particles. Even a cursory examination will demonstrate that the registered displacements occur in response to the relative movements of the more mobile individual particles to form a denser matrix. Motivating this movement is the induced boundary energy. In principle,

when a rigid plate is impressed upon a soil surface, the medium, in effect, "diffuses" this displacement.

The question arises, if boundary strains (or displacements) are known precisely and if we seek their diffusion into media, why not do this directly? This suggests a "strain diffusion" process rather than the more conventional stress diffusion process. The investigation of this matter was considered to be germane to the present study and hence was conducted as an integral part of the work project. Its development follows.

Adopting the foregoing diffusion of stress as a strain process, as was done to obtain Equation (7), the expected vertical strain at any point, P, due to a surface strain of intensity q, acting over a circular area of radius a (Figure 5), is

$$\bar{\epsilon}_z(x, z) = \frac{q}{2\mu z^2} \int_0^a \int_0^{2\pi} \exp\left(-\frac{x^2 + r^2 - 2xr \cos \theta}{2uz^2}\right) r \, dr \, d\theta \quad (8)$$

where μ is a material parameter. Defining $v(x)$ as the deflection of the surface, we have

$$v(x) = \int_0^\infty \bar{\epsilon}_z(x, z) \, dz \quad (9)$$

Introducing the Bessel functions of the first kind, $J_0(x)$ and $J_1(x)$, Equation (8) takes the form

$$\bar{\epsilon}_z(x, z) = \frac{q}{z^2} \int_0^\infty J_0(xt) J_1(at) \exp\left(-\frac{u^2 t^2}{2}\right) t \, dt \quad (10)$$

where:

$$J_n(t) = \left(\frac{t}{2}\right)^n \sum_{k=0}^{\infty} \frac{(-1)^k t^{2k}}{k! (n+k)!}$$

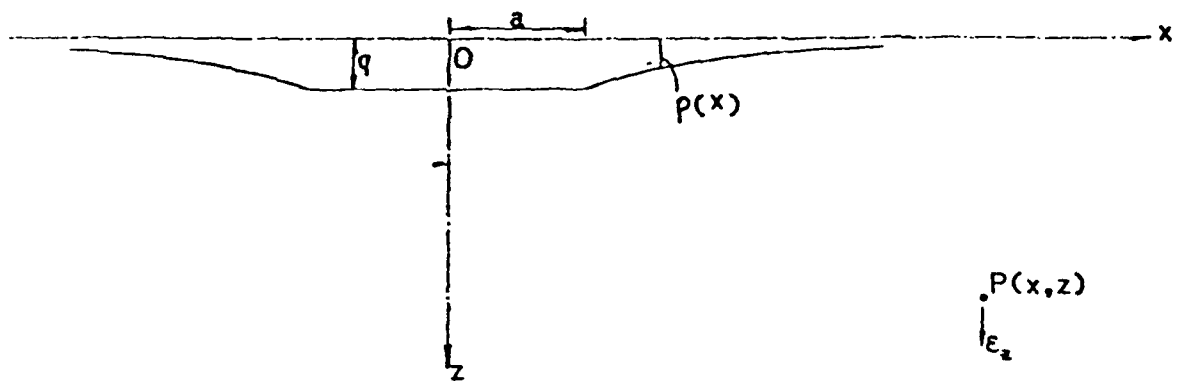
For large values of t,

$$J_n(t) = \sqrt{\frac{2}{\pi t}} \cos\left(t - \frac{\pi}{4} - \frac{n\pi}{2}\right)$$

Equations (9) and (10) were solved numerically. In Equation (10), t is a dummy variable introduced by the transformation $t = t(x, z)$. It should be evident that Equation (10) lends itself to simpler numerical solutions than does Equation (8). Examples will be given below.

Finally, a parallel situation to that in Section II.4 on "Soil-Fabric Medium" was investigated using "strain-diffusion." Equations (9) and (10) were

a. Profile



b. Plan

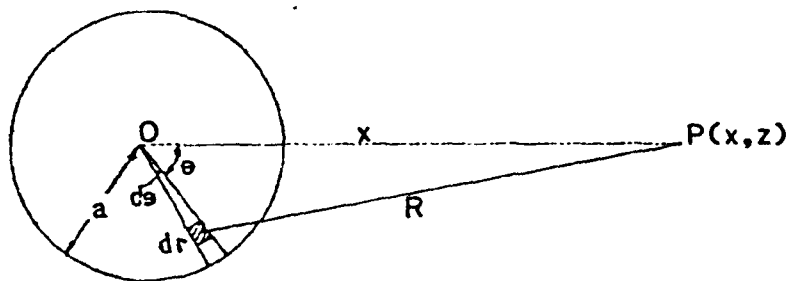


Figure 5. Strain Diffusion Under a Circularly Loaded Rigid Plate.

assumed to hold for each of the layers (Figure 6). For the **multilayer** case, that is of (h_1, μ_1) and (h_2, μ_2) , Equation (10) must be solved twice for each value of the parameter μ ; i.e.,

$$\bar{T}_{10}(x, z) = \bar{T}_{10}^1(x, z) \text{ for } \mu = \mu_1$$

$$\text{and } \bar{T}_{10}(x, z) = \bar{T}_{10}^2(x, z) \text{ for } \mu = \mu_2$$

Equation (9) then takes the form of

$$T(x, z) = \sum_{n=1}^{\infty} \bar{T}_{10}^1(x, z) e^{-\lambda_n z} + \sum_{n=1}^{\infty} \bar{T}_{10}^2(x, z) e^{-\lambda_n z}$$

b. EXAMPLES OF MODELS

a. Homogeneous Medium - Infinite Strip

Figure 7a shows a plot of the expected vertical stress for a unit distributed load on an infinite strip, Figure 2. Equation (2) governs this case. The depth is taken as one-half the width of the strip ($z = a$), the μ parameter is 0.25, and a unit load is applied.

b. Homogeneous Medium - Circular Area

Figure 7b provides a plot of the vertical stress under the center of a uniformly loaded area of radius a at a depth equal to the radius. Equation (5) applies for this case. The differences between Figures 7a and b are only minor. That is, only a small part of the energy available for the infinite strip is effective under the center (or centerline) of the loaded area.

c. Strain Diffusion

Recall in Section II.5 that a methodology was developed that invokes the diffusion of boundary displacements through a continuum rather than through the customary boundary stresses. Inherent in the new analysis is the μ parameter, Equation (8), which scales the transmission of the boundary energy. A number of numerical values were assumed for this parameter to examine the influence that it had on surface deflections. It was assumed that a uniform unit displacement acted over a circular area of radius a ; that is, Equation (4) applied with $q = 1$. The relative depth of the medium was $h = 7.7$ (the actual depth in the test box of 23 inches divided by a plate diameter of 3.0 inches). A computer program (Program STRAIN) for calculating the surface deflections was written and is given in Appendix B. Input to this program were the values of $q = 1$, $a = 1$, $h = 7.7$, and various values of μ , ranging from 3.0 to nearly that of zero (0.005). Output was in the form of normalized tabulated values of deflection (actually a deflection ratio equal to the deflection at any radius divided by the maximum deflection) and the relative radius, x/a . The results for a number of values of μ are plotted in Figures 8 to 14. As an example of how these plots were obtained, the output for cases $\mu = 0.3$ and $\mu = 0.2$ are tabulated below and plotted in Figures 11 and 12, respectively.

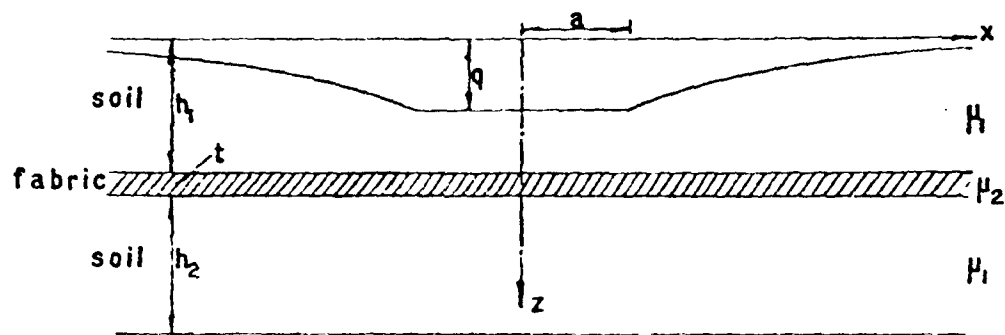


Figure 6. Strain Diffusion for a Layered Medium.

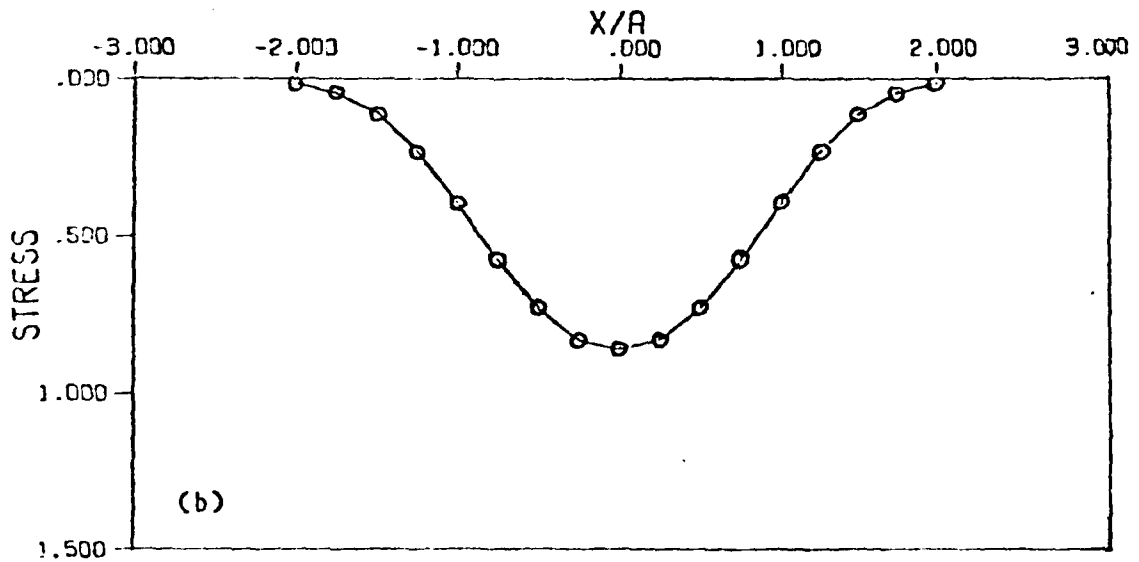
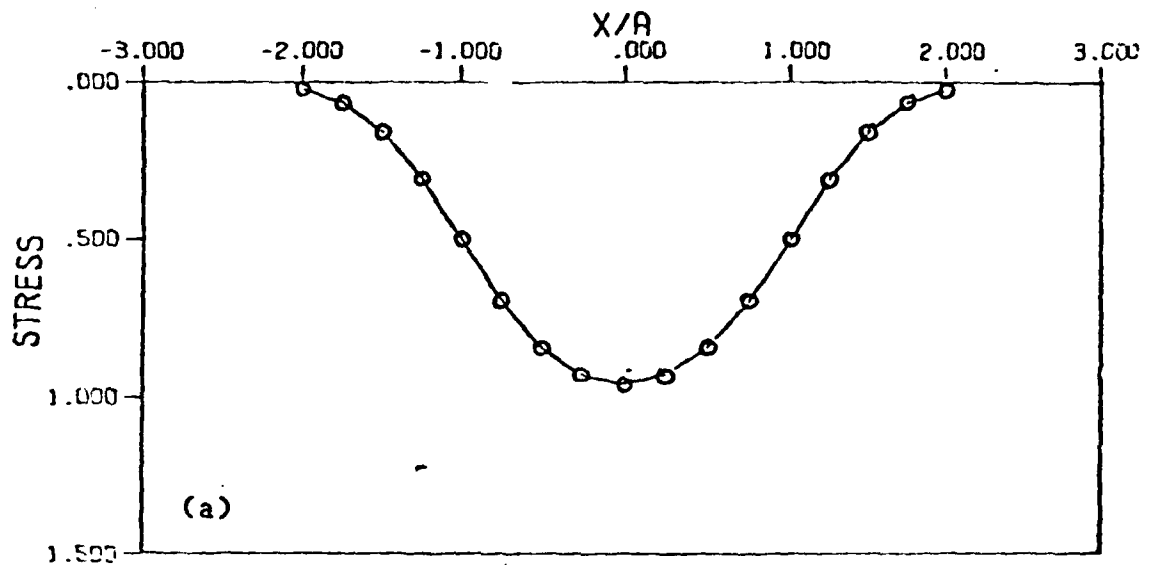


Figure 7. Expected Vertical Stress at Depth $z = a$ Under a Unit Load Distributed Over (a) an Infinite Strip, and (b) a Circular Area for $\nu = 0.25$ in a Homogeneous Medium.

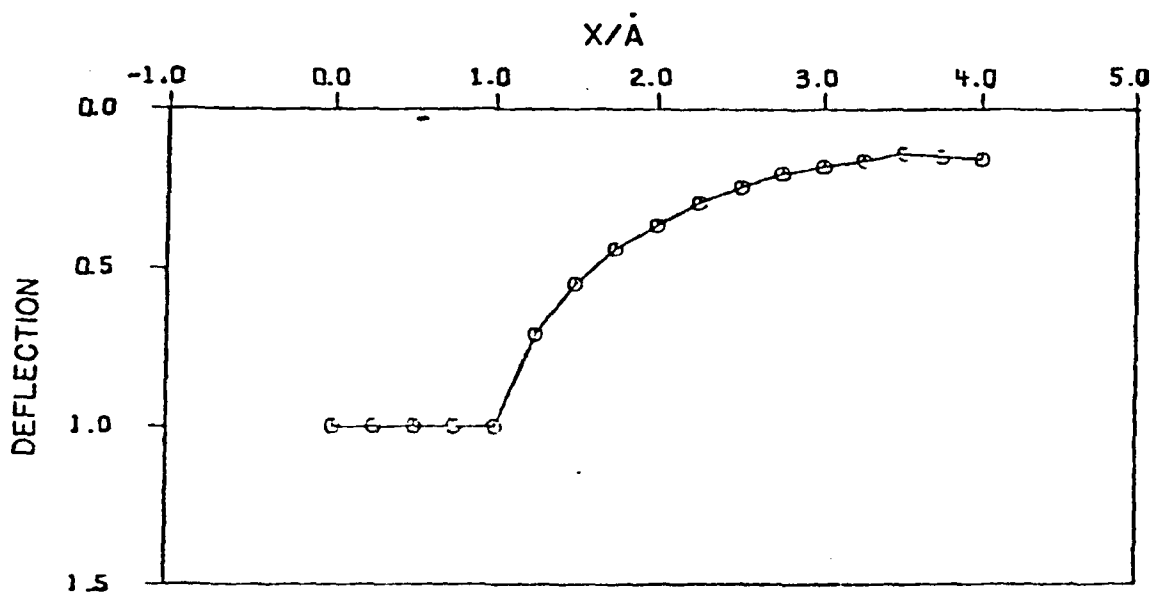


Figure 8. Relative Surface Deflections Given a Uniform Displacement over a Circular Area of Radius A , $\mu = 3.0$.

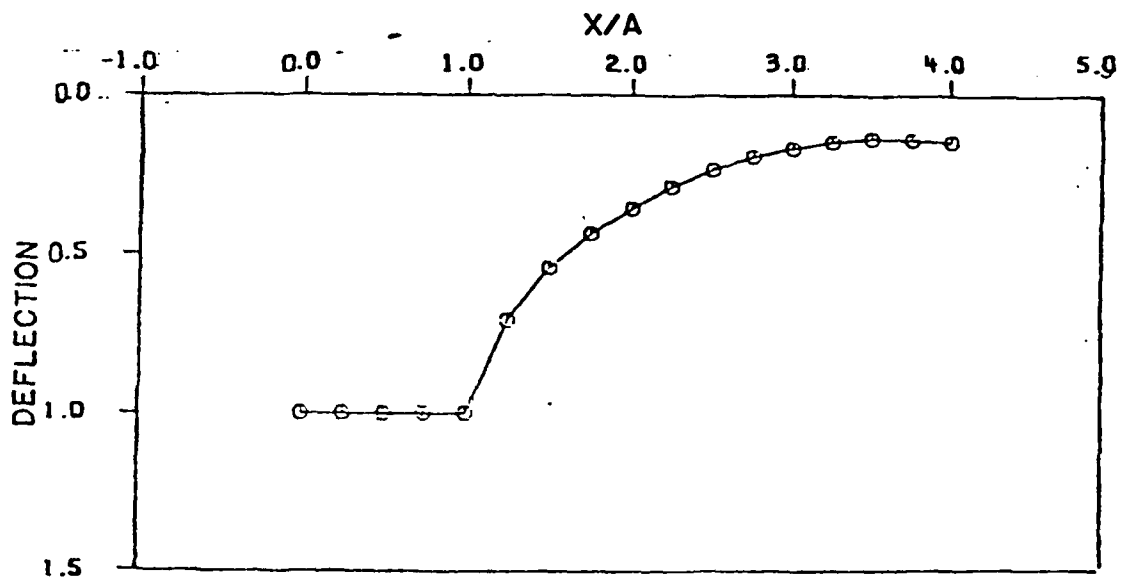


Figure 9. Relative Surface Deflections Given a Uniform Displacement over a Circular Area of Radius A , $\mu = 2.0$

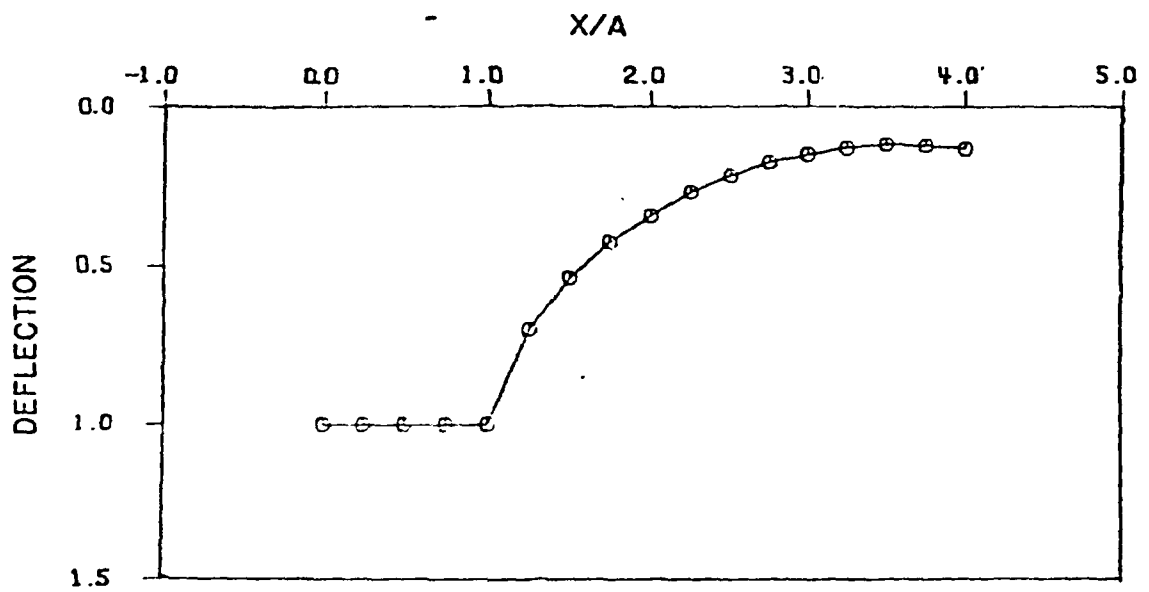


Figure 10. Relative Surface Deflections Given a Uniform Displacement over a Circular Area of Radius A , $\mu = 1.0$.

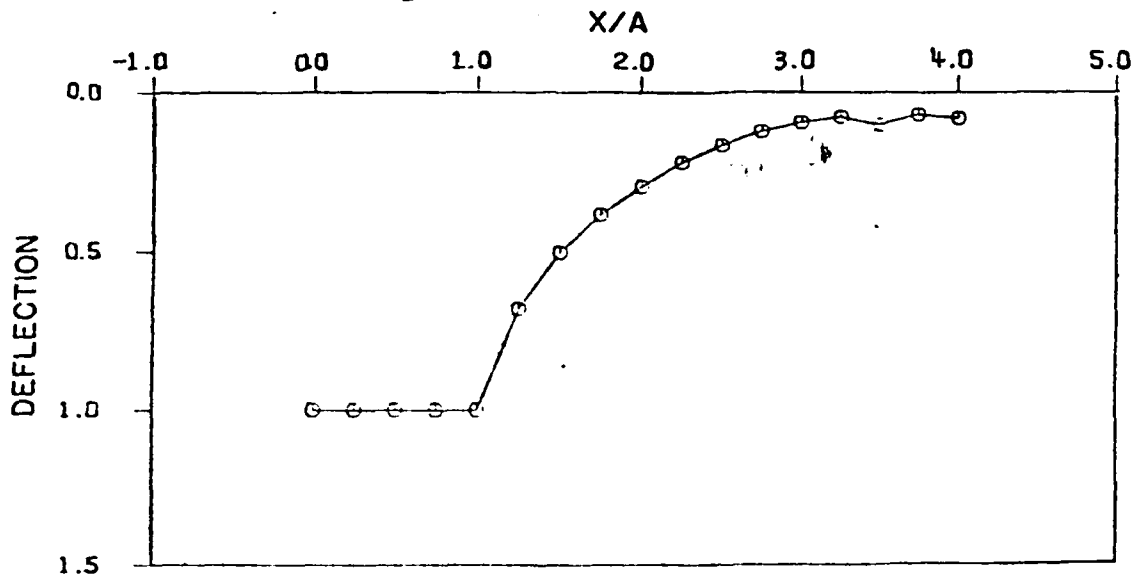


Figure 11. Relative Surface Deflections Given a Uniform Displacement over a Circular Area of Radius A , $\mu = 0.3$.

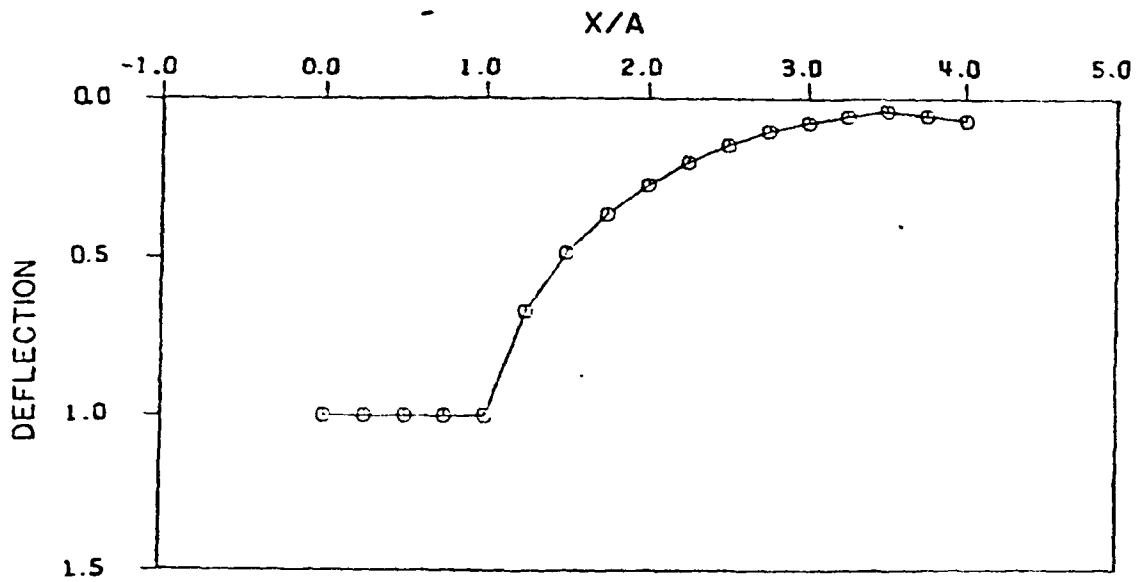


Figure 12. Relative Surface Deflections Given a Uniform Displacement over a Circular Area of Radius A , $\mu = 0.2$.

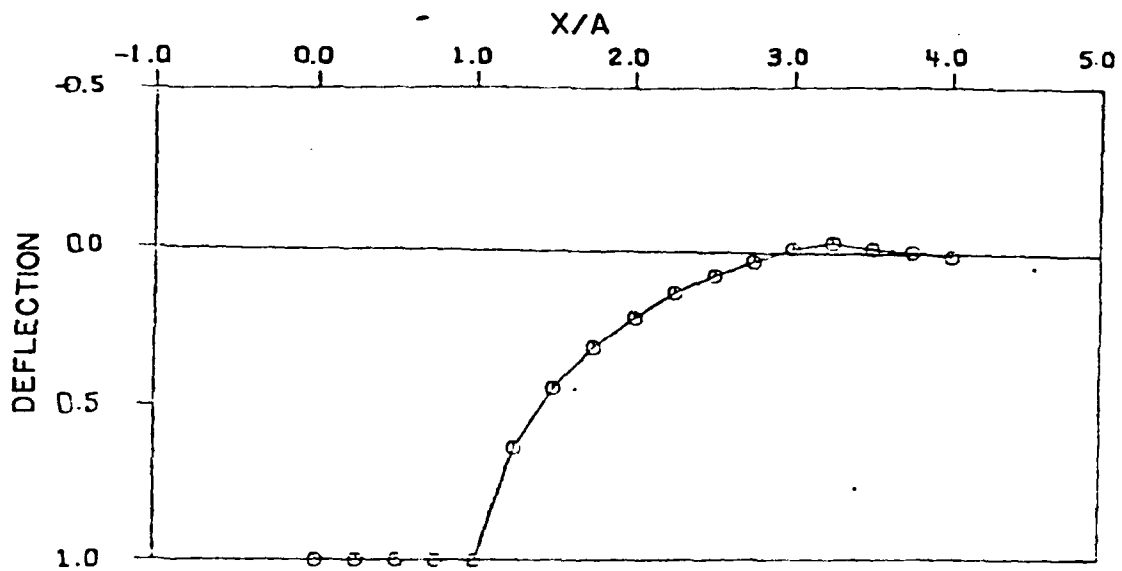


Figure 13. Relative Surface Deflections Given a Uniform Deflection over a Circular Area of Radius A , $\mu = 0.1$.

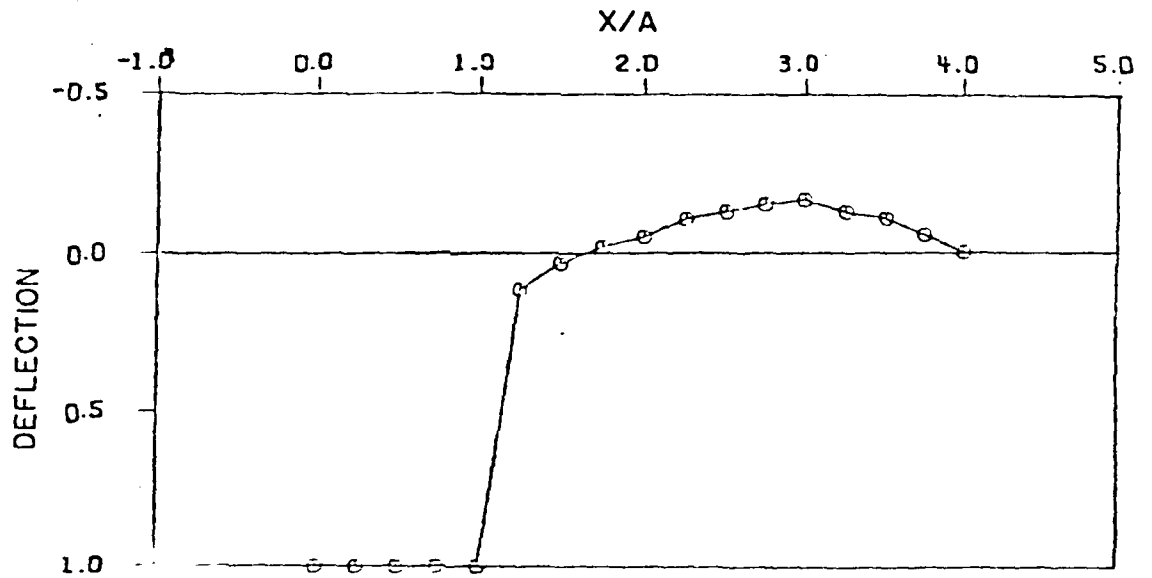


Figure 14. Relative Surface Deflections Given a Uniform Displacement over a Circular Area of Radius A , $\mu = 0$.

Deflection Ratio

| X/A | Deflection Ratio | |
|------|------------------|-------------|
| | $\mu = 0.3$ | $\mu = 0.2$ |
| 1.00 | 1.00 | 1.000 |
| 1.25 | 0.680 | 0.668 |
| 1.50 | 0.505 | 0.448 |
| 1.75 | 0.386 | 0.366 |
| 2.00 | 0.301 | 0.273 |
| 2.25 | 0.225 | 0.200 |
| 2.50 | 0.171 | 0.146 |
| 2.75 | 0.127 | 0.102 |
| 3.00 | 0.100 | 0.077 |
| 3.25 | 0.082 | 0.058 |
| 3.50 | 0.119 | 0.097 |
| 3.75 | 0.076 | 0.054 |
| 4.00 | 0.086 | 0.068 |

It was desired to obtain the value of the parameter μ that agreed with experimental observations of the deflected shape of the surface. Since this required a "back-calculation" of μ for the soil, no fabric was assumed to exist for this case. It is seen from Figures 8 to 14 that as μ decreases (figure numbers increasing), more heave is evident. The heaving of the soil is of considerable importance, as it was observed in all the laboratory tests (see Figures 61 and 62) to some degree. It should be emphasized, as shown in Figure 7, the classical theory of elasticity cannot account for the heaving of a homogeneous medium.

Figures 61 and 62 present normalized deflection basin measurements for a number of physical tests. It is seen that heaving on the order of 20 percent of the induced deflection is not out of order. Comparison with Figures 8 to 14 indicates that the μ -parameter is very close to zero. However, $\mu = 0$ introduces mathematical instability in Equation (8). Consequently, a value of 0.005 was used in subsequent work. The physical significance of this parameter is difficult to ascertain at this time. Apparently, it is somewhat analogous to Poisson's ratio.

Once the μ parameter for uniform soil (μ_1) is computed, it can also be used to obtain the μ parameter for the fabric (i.e., μ_2). Some calculations were made to determine the value of μ_2 using the experimental results for the circular plate (Figure 61). Then the calculated values of μ_1 and μ_2 were used in Equations (9) and (10) to predict the surface deflection pattern of a soil-fabric system when loaded in plane strain. The predictions did not agree well with the experimental results.

d. Displacements and Settlements

The objective of all the foregoing analyses is to predict the deflected shape of a surface when subjected to an imposed load. After this objective is achieved, determinations can be made as to whether the degree and nature of the deformations can be tolerated without impairing the intended use of the facility.

As noted in Section 5 and Figure 7, classical mechanics predict stress distributions. To translate these into surface displacements recourse must be had to constitutive relationships between stress and strain.

As is commonly the case, Hooke's law will be generalized to

$$\bar{\epsilon}_x = \frac{1}{E} (\bar{\sigma}_x - \nu \bar{\sigma}_y - \nu \bar{\sigma}_z) \quad (11a)$$

where $\bar{\sigma}_x$ and $\bar{\sigma}_y$ are normal stresses on planes parallel to the unloaded surface and E and ν are Young's modulus and Poisson's ratio, respectively (see Reference 43 for the derivation). For axisymmetric conditions, Equation (11a) reduces to

$$\bar{\epsilon}_r = \frac{1}{E} (\bar{\sigma}_r - \nu \bar{\sigma}_z) \quad (11b)$$

where $\bar{\sigma}_z$ and $\bar{\sigma}_r$ are the vertical and radial normal stresses, respectively.

Harr (Reference 42) found that the radial normal stress can be related to the vertical normal stress by

$$\bar{\sigma}_r = \bar{\sigma}_z \left(\frac{1 - \nu}{1 + \nu} \right) \quad (11c)$$

Substituting this expression with $\bar{\sigma}_z$ from Equation (5) into Equation (11b) produces an equation for the strain under the center of a circular load with a uniform normal intensity q , or

$$\bar{\epsilon}_r = \frac{1}{E} \left[q \left(\frac{1 - \nu}{1 + \nu} \right) - \nu q \right] \quad (12)$$

Equation (12) can be expressed in the form

$$\bar{\epsilon}_r = \frac{1}{E} q I(\nu, z) \quad (13)$$

where $I(\nu, z)$ is a "vertical strain influence factor" that is a function of the parameters ν and z , and z is the depth/radius ratio of a circular loaded area, $z = z/a$.

Equation (9) gives the displacement of the surface at the center of the circular load, which can be combined with Equation (13) to give

The stress approach could be extended to the plane strain condition by merely selecting the ϵ diagram under such conditions corresponding to the computed value for sand. Modulus plays an important role in the settlement computation, and because of the dependency of modulus on the degree of prestressing, an experimentally obtained modulus is required.

SECTION III
EXPERIMENTAL WORK

1. INTRODUCTION

The objectives of the experimental portion of the subject research were to:

- a. Obtain parametric data for the theoretical formulation developed in Section II.
- b. Test the theoretical formulation developed.
- c. Observe the empirical behavior of fabric-reinforced sands to obtain an indication of the relative improvements in system performance due to the presence of the geotextile.
- d. Verify, insofar as possible, previous research findings.

2. DESCRIPTION OF EXPERIMENTAL PROGRAM

A series of laboratory-scale model loading tests of reinforced and unreinforced sands was conducted and analyzed. A detailed description of this portion of the research follows.

a. Variables

As suggested previously, the number of possible permutations of the properties of soil, reinforcement, pavement types, and aircraft gear configurations and loadings is very large. Thus, to maintain the size of the experimental program within time and budget constraints, it was decided to hold constant a number of possible variables throughout the experimental program. For example, to minimize the effect of soil variability as much as possible, only one soil, a relatively uniform Ottawa sand, was tested at a constant relative density.

Sand was chosen for Phase I tests because it is easier than cohesive materials to handle in large volumes in the laboratory and to control densities. Furthermore, the beneficial effects of reinforcing sands is known from previous research, whereas reinforcement of cohesive soils with geotextiles has not often been done. A coarser material, e.g., a fine gravel, could have been used to model the granular surface materials, but it was felt that a better indication of the degree of improvement due to geotextile reinforcement would be shown with a poor quality surface material such as uniform sand. This was thought to provide a "lower bound" of granular soil performance. A single relative density (medium dense) was chosen as being typical of field densities obtainable with ordinary construction equipment.

Ideally, tests should have been conducted using elliptically shaped plates approximately 9 inches in average diameter, but the size of the test box, 32 inches square, was a constraining factor. Since the scale ratios were only 1.5

and 3, it was believed that the results of tests on 3- and 6-inch diameter circular plates could be extrapolated to provide reasonable estimates of the performance of a 9-inch diameter loaded area. Rigid plates were chosen not only for convenience, but with the knowledge that, as far as the soil was concerned, with aircraft tire pressures of the order of 250 to 300 psi, tire contact areas are effectively rigid. In addition to circular plates, a few tests were conducted with a rigid plate in a plane strain configuration. A loading plate 5 inches wide by 30 inches long (almost the entire width of the test box) was used. These tests were an attempt to provide experimental data to verify the plane strain theory described in Section II.

For the first series of tests, a woven polyester high-modulus fabric was chosen, primarily because considerable testing had already been carried out on this fabric at Purdue University and elsewhere. The second type of reinforcement tested was high-strength extruded plastic (polypropylene and polyethylene) geogrid nets. Geometric variables included the number of layers of reinforcement and the depth and spacing of those layers, as illustrated in Figure 15. To provide a "common denominator" against which to measure the degree of improvement of the reinforcement, several tests were run without any reinforcement.

Table 1 lists the test variables, the quantities assigned to those variables, and the symbol adopted for each variable.

b. Code

To facilitate identification of the individual tests, a coding system was adopted, using the symbols for the test variables listed in Table 1. For circular plate load tests, the code is

| (diameter) | (CP) | number of layers | type of reinf. | (depth) | (spacing) | edge cond. |
|------------|------|------------------|----------------|---------|-----------|------------|
| | | U | | | | -- |
| 3 | CP | 1 | W | d, in. | U | PF |
| 6 | CP | 2 | G | | s, in. | FF |

If an item is omitted for one reason or another, the symbol is left blank. For example, the symbols for the tests without reinforcement are 3CP and 6CP. Those with only one layer of reinforcement omit the symbol for s, and so forth.

For the plane strain tests without fabric, the test symbol is simply PS. For example, with one layer of geogrid reinforcement at 2 inches depth, the test designation is PS1G-2.

Table 2 lists the tests performed and their symbols.

3. DESCRIPTION OF APPARATUS AND EQUIPMENT

a. Loading Box and Reaction Frame

A test box of plywood and steel angle sections was constructed for this project. The inside dimensions of the box are 80 centimeters by 80 centimeters and about 70 centimeters high (31.5 x 31.5 x 27 inches). Because of clearance

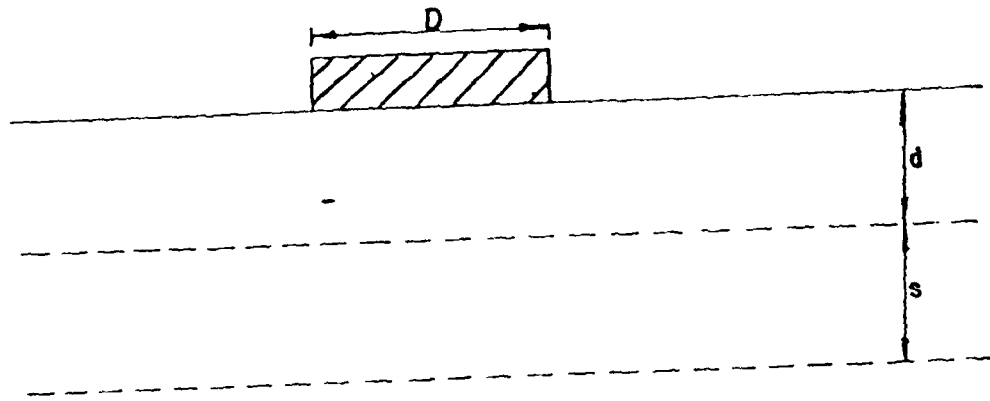


Figure 15. Illustration of Geometric Test Variables (Note:
D = B for PS tests).

TABLE 1. TEST VARIABLES AND SYMBOLS

| <u>Variable</u> | <u>Disposition</u> | <u>Symbol</u> |
|-------------------------|---|---------------------|
| 1. Soil Type | Ottawa "flint" sand | -- |
| 2. Relative Density | Medium dense ($D_r = 70\%$) | -- |
| 3. Loaded Area | | |
| Shape and size | Circular plate: 3 in. diameter 6 in. diameter | JCP 6CP |
| Plane strain: | 3 in. x 30 in. | PS |
| Type | Rigid | -- |
| Mode | Quasi-static (approx. constant rate of load) | -- |
| 4. Reinforcing | | |
| Type | None Woven polyester Geogrids | -- W G |
| Number of Layers, N | None One Two | -- 1 2 |
| Depth of reinforcing, d | Variable | (Depth in inches) |
| Spacing, s | Variable | (Spacing in inches) |
| Edge conditions | Free Partial fixity Full fixity | -- PF FF |

TABLE 2. TESTS CONDUCTED AND THEIR SYMBOLS

| <u>Code</u> | <u>Explanation</u> | <u>Total tests Conducted</u> | <u>Tests with Usable Data</u> |
|------------------|-----------------------------|----------------------------------|-----------------------------------|
| 3CP | without fabric | 2 | 2 |
| 3CP1W-0.5 | with one layer | 2 | 2 |
| 3CP1W-1.2 (or 1) | of fabric | 2 | 1 |
| 3CP1W-2 | | 1 | 1 |
| 3CP1G-1 | with one layer | 1 | 1 |
| 3CP1G-2 | of SS2 grids | | |
| 3CP1W-1-PF | with partial edge fixity | 2 | 1 |
| 3CP1W-1-FF | with full edge fixity | 1 | 1 |
| 6CP | without fabric | 8 | 4 |
| 6CP1W-1 | with one | 2 | 2 |
| 6CP1W-2 | layer of | 2 | 2 |
| 6CP1W-3 | fabric | 2 | 2 |
| 6CP2W-0.8-0.8 | with two layers | 1 | 1 |
| 6CP2W-1.6-1.6 | of fabric | 1 | 1 |
| PS | without fabric | 2 | 2 |
| PS1W-1 | with one | 1 | 1 |
| PS1W-2 | layer of fabric | 1 | 1 |
| PS1G-1 | with one layer | 1 | 1 |
| PS1G-2 | of SR2 grids | 1 | 1 |

requirements for the load cell and the loading plate, the depth of sand tested was always about 45 or 50 centimeters (18 to 20 inches). Two 0.5-inch thick plywood sheets formed the sides of the box, which was reinforced by steel angle sections held together with long threaded tie rods. Figure 16 is a photograph of the test box.

A heavy steel test frame was available in our laboratories from previous research on model asphalt pavements (Reference 47). The reaction frame supported the hydraulic load actuator and other parts of the loading system, as shown at the top of Figure 16. Figure 17 is a photograph of the test frame.

b. MTS "Closed Loop" Hydraulic Loading System

The MTS loading system used in this research was manufactured by Research, Inc., of Minneapolis, Minnesota. Figure 18 is a photograph of the controlling system (in background); the loading actuator and accumulator were shown on the top of the load frame in Figure 16. The entire MTS loading system consists of the following components:

Servoram Hydraulic Actuator, Model 204.13, 5 kip,
6-inch stroke

Servoram Hydraulic Actuator, Model 202.03, 30 kip,
6-inch stroke

Hydraulic Power Supply (3000 psi), Model 502.03

Electronic Control System:

Function Generator, Model 410.21

Counter Panel, Model 417.01

Control Panel, Model 413.04

"Servac" Control, Model 401.02

Recorder Input Selector, Model 414.02

Transducer Conditioner Panel, Model 425.41

The MTS loading system is a "closed loop" system because transducers and electronics in the system control the pressures and deformations, so that, within system capability, the desired load-deformation time history can be applied to the specimen. The system can be used in a "stroke" control mode, wherein the deformation of the actuator piston is controlled electronically; or in a "load" control mode, wherein the rate and/or magnitude of load are controlled electronically. The stroke mode was used for the test setup when "zeroing" the load plate, etc.; the load mode was used when applying the load to the test specimen.

c. Sand

The test soil selected for study was an Ottawa "flint" silica sand obtained from the Ottawa Silica Co. of Ottawa, Illinois. This sand had been used in previous research at Purdue University on fabric-reinforced sands (e.g., Reference 5), and its properties were well known. The grain size distribution of the sand is shown in Figure 19. Other classification parameters are:



Figure 17. Test Box.

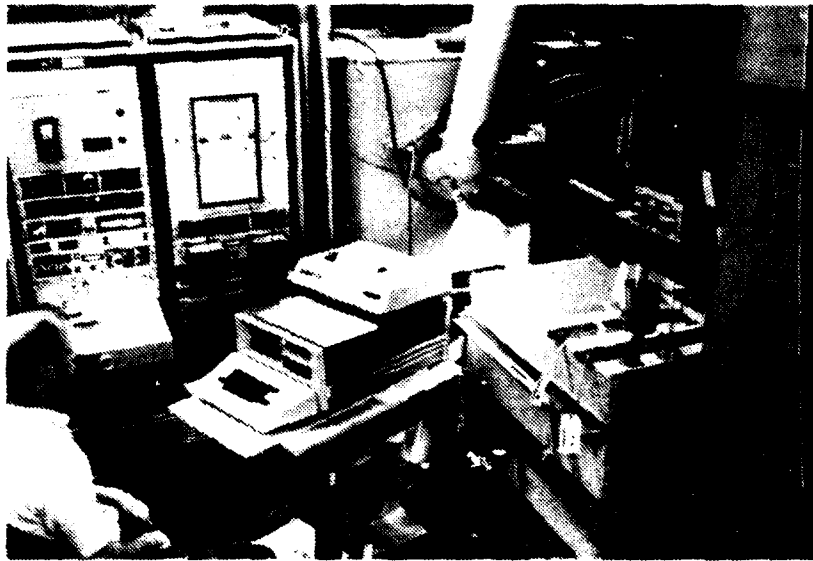


Figure 18. General View of Test Box, Data Acquisition System, and Controls for the MTS Loading System.

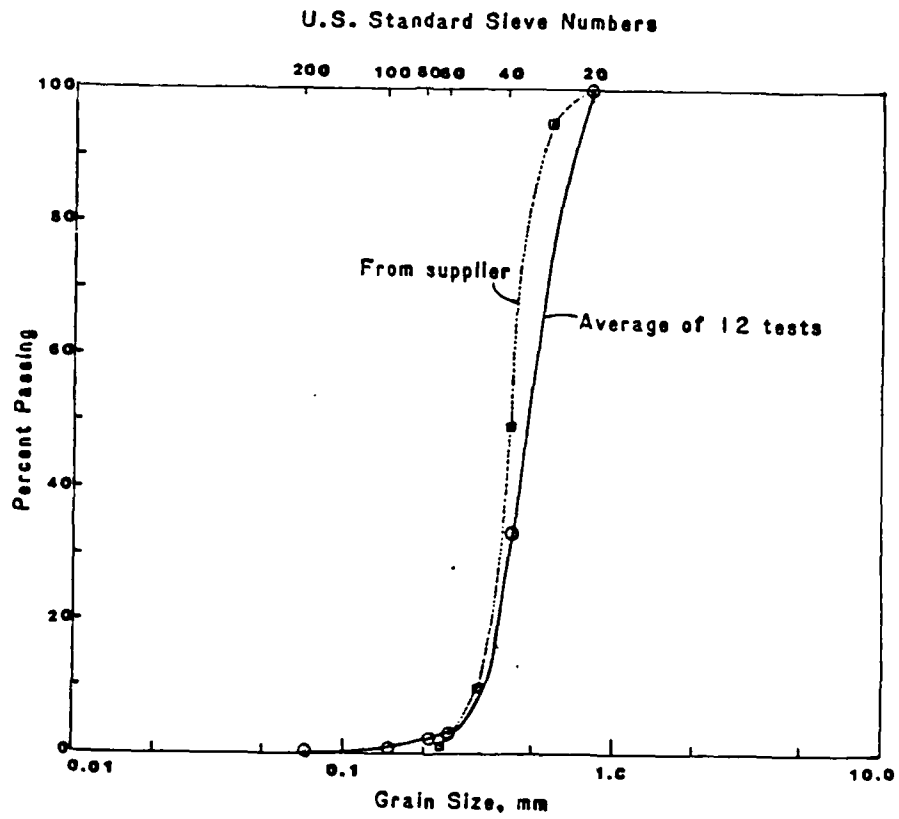


Figure 19. Grain Size Distribution of Ottawa Flint Sand.

$$\begin{aligned}
 C_u &= 1.6 \\
 C_c &= 0.94 \\
 U_{60} &= 0.34 \text{ mm} \\
 G_s &= 2.65 \\
 \gamma_{d \max} &= 114.9 \text{ pcf}; e_{\min} = 0.44 \\
 \gamma_{d \min} &= 93.3 \text{ pcf}; e_{\max} = 0.77
 \end{aligned}$$

The grain size distribution shown in Figure 19 is the average of 12 separate determinations, which varied only about 1 percent at each sieve size. These determinations were made in order to verify that the sand stored in several containers in the laboratory was the same as that used previously. Also shown in Figure 19 is the gradation supplied by the Ottawa Silica Co.

The angle of internal friction of the sand was determined from both direct shear and triaxial compression tests. Direct shear test results are shown in Figure 20. The tests were multistage; that is, only one test specimen was set up for each run. When the peak of the shear stress deformation curve was reached, the next increment of normal stress was applied. As shown in Figure 20, the failure envelopes are curved, as expected for sands under low normal stresses. Multistage tests may also contribute to envelope curvature. The direct shear test specimens were initially set up at a dry density of 100 pcf, which is very close to the average density of the sand in the test (97 pcf or a relative density of about 70 percent).

The normal stress existing at the elevation of the failure plane in the specimens is only on the order of 10 to 30 psf, or significantly less than the lowest normal pressure at which the direct shear tests were conducted (100 psf). Attempts to obtain friction angles at even lower normal stresses were unsuccessful, apparently due to the "internal" friction of the shear machine itself. A precision direct shear apparatus (Karol-warner) was used for these tests, and the sliding parts were specially remachined to make them as smooth as possible. Then a teflon[®]-based antifriction material was sprayed on each moving part. At a normal stress of 100 psf, the friction of the apparatus itself was about 15 psf, but the net observed shear resistance of the sand (machine friction subtracted) ranged from 80 psf to 145 psf. The two data points shown on Figure 20 are average values. Additional direct shear tests at normal stresses lower than 100 psf were not attempted because of the undesirably large experimental scatter.

If the extrapolation of the Mohr failure envelopes to the origin (as shown as dashed lines in Figure 20) is correct, then the friction angle at the relative density of 70 percent for the confining pressures operative in the test specimens would approach 45 degrees. At higher normal pressures, the average friction angle was around 35 degrees, a value more typical for the poorly graded rounded grain Ottawa sand. The direct shear results in Figure 20, at normal stresses greater than 200 psf, were verified by triaxial tests conducted earlier on this same sand as part of ongoing academic work at Purdue University. From plate tests on unreinforced sands described later in this report, it is possible to calculate a friction angle from classical bearing capacity theory. Using the Terzaghi-Meyerhoff bearing capacity factors and appropriate empirical corrections for the shape of the footing, an average friction angle of 42 degrees was calculated for all three loading plates tested. These results confirm that the angle of the failure plane was indeed approximately 40 degrees at the test dry densities.

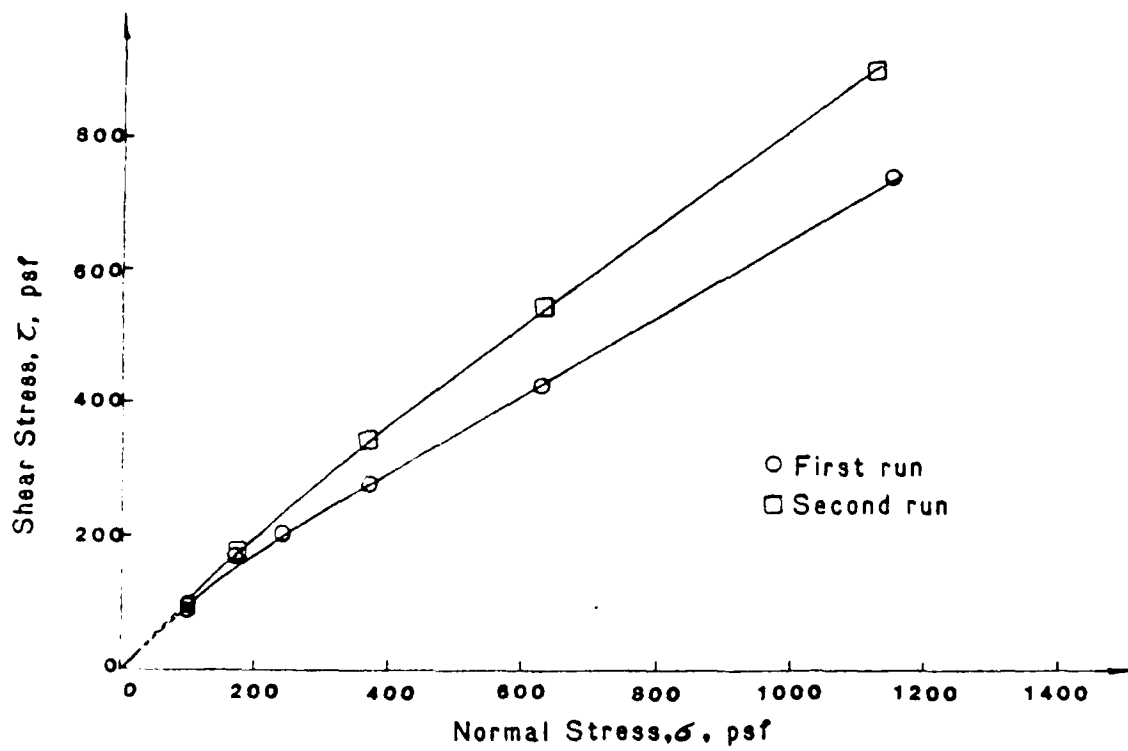


Figure 20. Results of Direct Shear Tests on Ottawa Flint Sand.

d. Reinforcement

Two types of reinforcement were used in this study. The first was a high-strength, high-modulus, woven polyester fabric which has been used in the past for other studies at Purdue University on geotextiles (see References 4, 5, 7, and 48). The fabric is typical of woven multifilament geotextiles (as produced, for example, by Nicolen, Carthage Mills, etc., although this fabric actually was obtained from AB Fodervavnader, of Boras, Sweden). The fabric is an industrial grade, woven multifilament manufactured from polyester fibers obtained from either Hoechst (Irevira No. 710) or ICI ("Terelin"). The basic fiber is a 1100 dtex (990-Denier) polyester with a 20/260 yarn structure. Wide strip tensile tests conducted as part of this study gave an ultimate tensile strength of about 160 lbs/inch. Typical tensile load-strain curves are shown in Figure 21. In this figure, strain was determined in two ways, (1) as the ratio of the crosshead movement to the crosshead spacing before the start of loading; or (2) from frequent measurements with a micrometer of two marks originally 2.5 inches apart near the center of the test specimen. If crosshead strain is used as the criterion, then elongation at failure is about 12 percent. The secant tensile modulus at 10-percent strain is about 800 pounds/inch. It should be noted that the data shown in Figure 21 were obtained from a modified wide strip tensile test. Although the test is not yet an official ASTM standard, it is currently under review by ASTM Committee D13.61/D18.19 on Geotextiles. Approval is expected shortly. The draft standard calls for a specimen width of 8 inches. Test specimens were 7 inches wide. This difference is considered negligible for a woven fabric. From previous studies (Reference 4), the stress-strain behavior is almost identical for both the warp and filling directions.

In addition to high tensile strength and favorable modulus, the fabric has several other important properties. It has excellent creep resistance. Tests conducted in Sweden (Reference 48) indicated that the extrapolated creep strength after more than 1 year was about 80 percent of its short-term strength. After 1 year, the creep was found to increase about 0.18 percent per log cycle of time. The fiber has excellent resistance to aging, sunlight, weathering, rotting, bacteria, and rodents. It is very resistant to acids, relatively resistant to bases and is, in general, insoluble in most inorganic solvents, including jet and diesel fuels.

The other reinforcing materials used in this study were "geogrids". Basically geogrids are extruded plastic sheets which have high tensile strength and modulus. They are made from a high-density polyethylene or polypropylene in which the polymer is strongly oriented to obtain high tensile strengths. On a weight basis, the grids are stronger than steel. The basic polymers are highly resistant to chemical, biological, and ultraviolet radiation. The geogrids used in this research are manufactured in England by the Netlon Corporation under the trade name Tensar. Samples were obtained from Gulf Canada, Ltd., who is the current North American licensee and who will soon be manufacturing the grids in Canada. Data provided by the manufacturer are given in Table 3 and Figures 22, 23 and 24. For reference purposes, physical and mechanical data for all of the available grids are shown, although only types SR2 and SS2 were tested. The tensile strength of SR2 is slightly more than 450 pounds/inch at a maximum strain of 12 percent compared to 160 pounds/inch for the woven polyester. The tensile strength of SS2 is somewhat greater than that of the polyester, or 206 pounds/inch at about the same ultimate strain. For the SS2, note that the

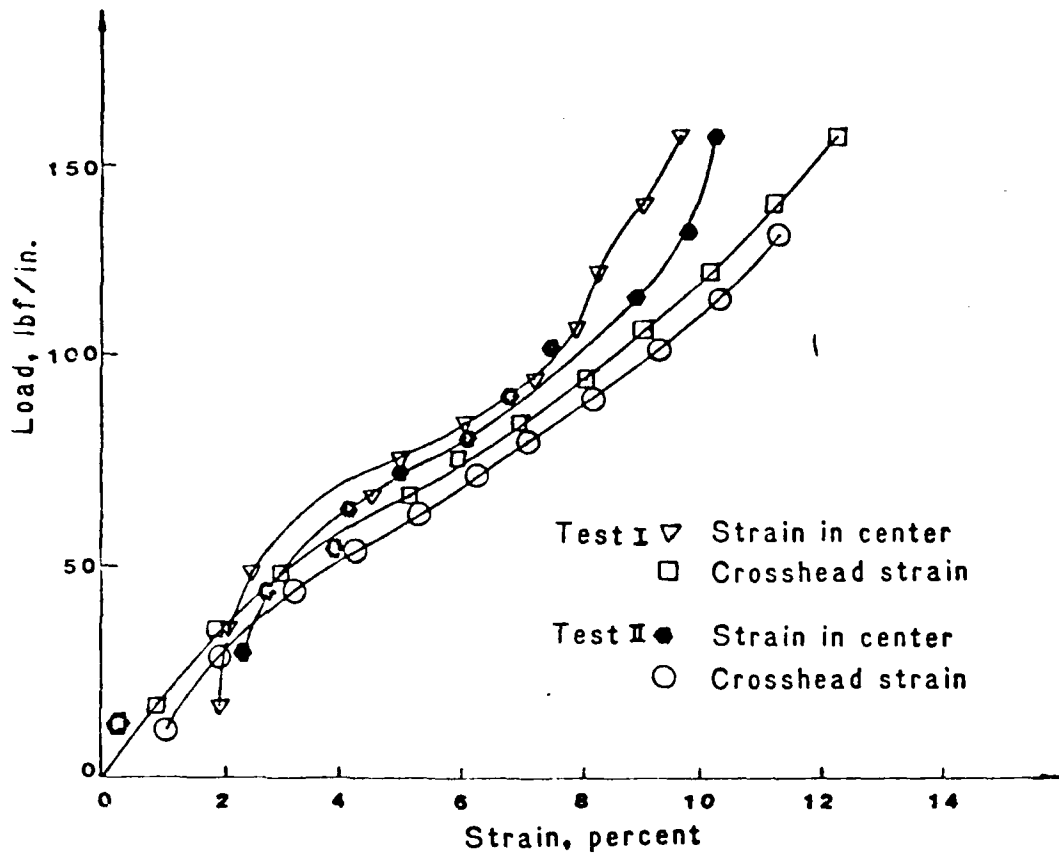


Figure 21. Results of Wide Strip Tensile Tests on Woven Polyester, Warp Direction.

TABLE 3. PHYSICAL AND CHEMICAL PROPERTIES OF TENSAR[®] GEOGRIDS

A. Polymer Characteristics

| Polymer | <u>SR1 and SR2</u> | <u>SS1 and SS2</u> |
|--|---|--------------------|
| | High-density polyethylene | Polypropylene |
| Shore hardness D (Din 53505) | 67 | 74 |
| Vicat softening point (Din 53460)(°C) | 127 | 148 |
| Impact Strength (Din 53453)(kJ/m ²) | 13.2 | 4.5 |
| Abrasion resistance (Dig 53754E) (mm ³ /100 revs) | 10 | 14.0 |
| Chemical resistance | Resistant to all naturally occurring alkaline and acidic conditions | |
| Biological resistance | Resistant to attack by bacteria, fungi and vermin | |
| Sunlight resistance | Resistant to UV attack | |

TABLE 3. PHYSICAL AND CHEMICAL PROPERTIES OF TENSAR®
GEOGRIDS (CONTINUED)

B. Mechanical Properties

| | <u>SR1</u> | | <u>SR2</u> | |
|--|---|-------------------------|-------------------------|-------------------------|
| Tensile strength - maximum (kN/m) | 84.0 | | 79.0 | |
| Extension at maximum load (%) | 12.3 | | 12.0 | |
| Extension at 40% load (%) | 3.5 | | 3.0 | |
| Modulus in tension (N/m ²) | 5.2 x 10 ⁹ | | 4.1 x 10 ⁹ | |
| Thermal stability | Stable over temperature range of -60 ^o to 80 ^o C | | | |
| | <u>SS1</u> | | <u>SS2</u> | |
| | Across Roll width | Along Roll length | Across Roll width | Along Roll length |
| "Characteristic" tensile strength per metre width (kN/m) | 20.9 | 12.6 | 32.0 | 18.0 |

(Samples, 3 junctions long and 1 rib wide were extended at a constant rate of 50mm/min, at a temperature of 20 ± 1°C.)

TABLE 5. PHYSICAL AND CHEMICAL PROPERTIES OF TENSAR®
GEOGRIDS (CONCLUDED)

C. Physical Properties

| | <u>SR1</u> | <u>SR2</u> | <u>SS1</u> | <u>SS2</u> |
|-----------------------------|------------|------------|------------|-------------|
| Roll length (m) | - | - | 50 | 50 |
| Roll width (m) | 1.0 | 1.0 | 3.0 | 3.0 |
| Weight (gm/m ²) | 872 | 938 | 203 | 320 |
| Grid pitch (mm) | 11 x 54 | 23 x 108 | 31 x 39.5 | 27.5 x 39.4 |
| Color | black | black | black | black |

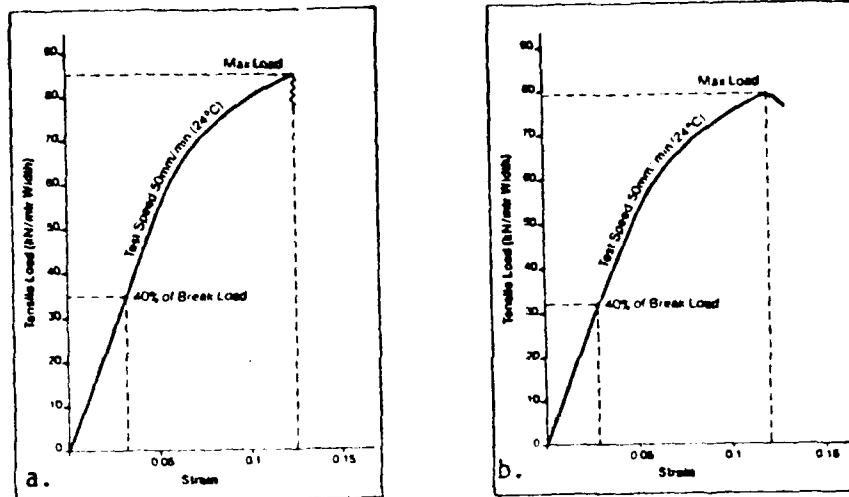


Figure 22. Tensile Stress-Strain Relationship for (a) SR1 and (b) SR2 Geogrids.

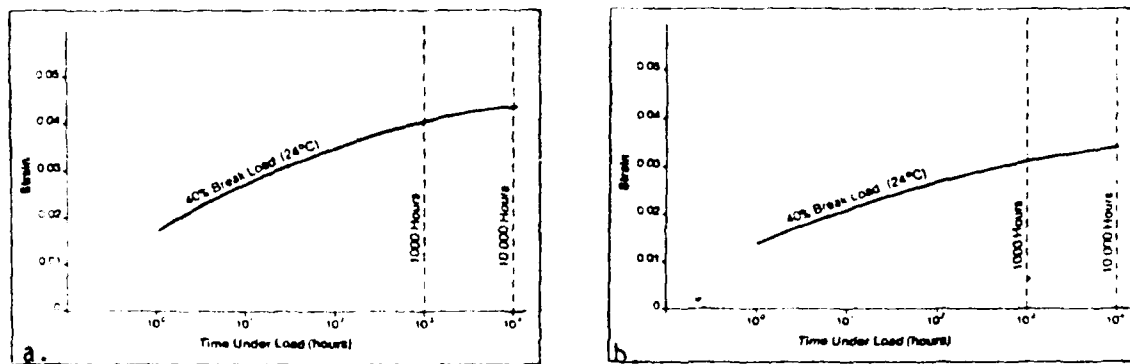


Figure 23. Results of Creep Tensile Tests on (a) SR1 and (b) SR2 Geogrids.

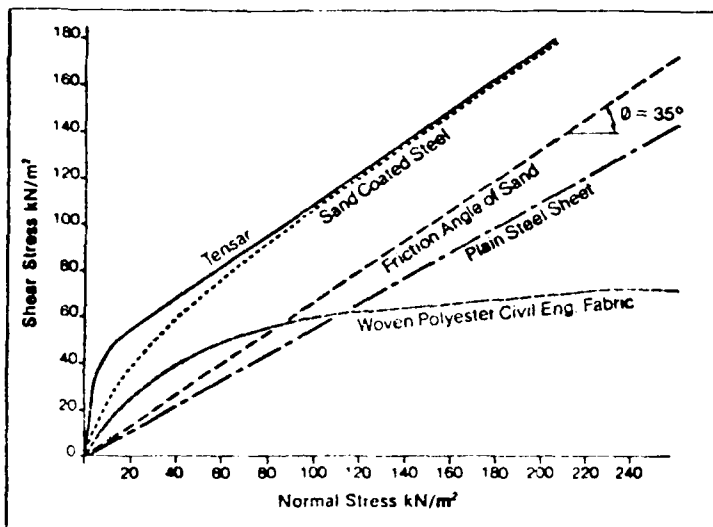


Figure 24. Results of Pullout and Shear Box Tests on Various Materials Including Geogrids ("Tensor"®) and Geotextiles (after References 4 and 48).

strength in the direction of the roll length is about 60 percent of the polyester, or about 97 pounds/inch.

The data given in Figure 24 are from Reference 49, and they compare the frictional resistance of Tensar® grids with that of other materials including a "woven polyester civil engineering fabric" (Reference 4) which is the same fabric used in the present research.

Geogrids could be called "second generation" geotextiles, because they are in general much stronger than most geotextiles, yet their cost is about the same for the same weight per unit area. Because of the large openings in the grids which can provide considerable interlock resistance, geogrids have an advantage in terms of frictional resistance (Figure 24).

e. Loading Plates

The loading plates used were rigid steel plates. Rigid plates were chosen because, at aircraft tire pressures, the tire appears to be essentially rigid to the soil. The two circular loading plates were 3 inches and 6 inches in diameter. The 3-inch plate was 0.75 inches thick while the 6-inch plate was 1 inch thick. The plane strain plate was 3 inches wide by 30 inches long by 1 inch thick and was stiffened along its entire length to minimize the possibility of bending during the test. The plates were attached to the load cell with reducing couplings and threaded studs.

Photographs of the loading plates will be shown later.

f. Instrumentation and Data Acquisition System

In this paragraph, only a brief description will be given of the instrumentation utilized in the test program. More detailed descriptions will be given later in this chapter when describing the test procedure.

The deformation of the load plates was measured either by an external deformation transducer (DCDT, direct current differential transducer) or by the LVDT (linear variable differential transformer) in the MTS system. The external instrument was a Hewlett-Packard Model 7DCDT 3.000, with a linear stroke range of 0.00 inches.

The load applied by the actuator ram was measured either by a Sensotec Model 41 load cell with a capacity of 50,000 pounds or a Lebow Model 16.103 load cell with a 5,000-pound capacity. Both these load cells are strain gage type.

Deflections of the sand surface were measured by several DCDTs mounted in a beam holder and running radially from the edge of the loading plate to one side of the box. All DCDTs were powered by a Hewlett-Packard Model 6205B power supply. Figure 25 shows the mounting beam for the DCDTs as well as the load cell and plate for a 6-inch CP test. The 3-inch DCDT can be seen just to the left of the load cell. As shown in the photograph, the DCDT support beam was held by long threaded bolts to "box girders" supporting it to facilitate leveling of the DCDT support beam.



Figure 25. DCDT Support Beam, Load Cell, and 6-inch Diameter Load Plate.

The location (radial distance) of the DCDTs for each test varied somewhat, depending on the test series and the size and geometry of the loading plate. Figure 26 and Table 4 show the plan and location of the DCDT for each test series.

An Analog Devices Inc. MACSYM 2 data acquisition system (DAS) was used to facilitate rapid data acquisition and reduction. The system is a "smart data logger." It uses software (a variation of the computer language BASIC) to both acquire and operate on the data. To obtain hard copy output from the MACSYM, a Heathkit printer, Model H-14 was connected to the DAS. Figure 27 is a photograph of the data acquisition system and printer unit. Figure 28 shows a schematic diagram for connecting the instrumentation to the MACSYM.

Additional instrumentation included a number of Micromeritics type large strain SR4 strain gages. It was originally intended that the strain gages would be attached to the fabric at several locations on the test specimen. However, considerable technical difficulties arose during some initial pilot tests with the strain gages attached to fabric tensile test specimens. Because the test results appeared so erratic and unreliable, it was decided not to pursue this line of research further. Tests results indicated that the stress-strain properties of the fabric were altered significantly by the presence of the gage on the fabric, probably because of the epoxy type adhesive used. (Coincidentally, the problem of large strain measurements on geotextiles is considered a No. 1 Priority Research Need by the Committee on Soil and Rock Instrumentation of the Transportation Research Board.) Unfortunately, we were not able to make a significant step toward solving that problem.

A Bison strain indicator and soil strain gage proved unsatisfactory within the constraints of the study. Some difficulty was encountered in calibrating these strain gages until very late in the research. Furthermore, it was not technically possible to read several soil strain gages at once during a test and avoid the interference between gages in the test box.

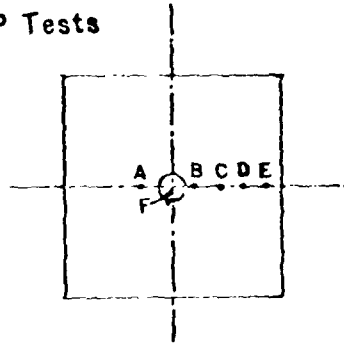
The only other measurement made during the test was the movement of the side wall of the box. This deformation was measured by an ordinary dial indicator, accurate to 0.01 millimeters. These measurements will be reported later in this chapter.

4. FABRICATION AND CONSTRUCTION OF TEST SPECIMENS

a. Sand Placement and Density Control

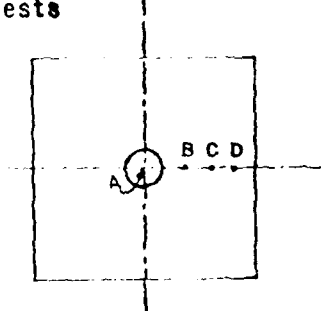
There was considerable initial concern about being able to place the large volume of sand in the test box at a reasonably uniform density. It was desirable that the sand be on the dense side, that is, not loose. Several systems were considered for both sand placement and density control. It was originally anticipated that the sand could be rained in the box, and by keeping the height of fall constant as the thickness of the sand built up, the resulting density could be maintained constant. Also considered was the air-activated sand spreader system described by Butterfield and Andrawes (Reference 50), and the scheme used previously at Purdue University by Brummond and Leonards (Reference 51). All these schemes were rejected because of the presence of the

(a) 3CP Tests

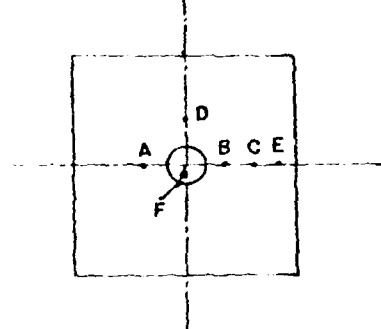


(b) 6CP Tests

Series I



Series II



(c) PS Tests

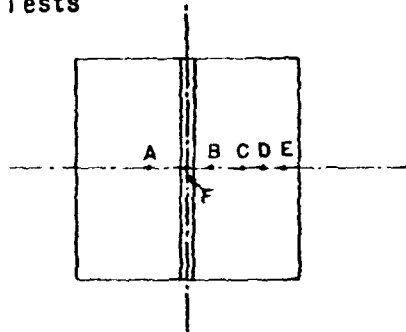


Figure 26. Location of DCDTs for Each Test Configuration (see also Table 4).

TABLE 4. LOCATION OF DCDT FOR EACH TEST CONFIGURATION
(SEE ALSO FIGURE 26)

| 3CP Tests | | | |
|-----------|----------------|----------------|--|
| DCDT | Range (inches) | Dist. (inches) | |
| A | ±3.0 | 3.9 | |
| B | ±0.5 | 5.7 | |
| C | ±0.25 | 8.5 | |
| D | ±0.25 | 11.2 | |
| E | ±0.125 | 14.4 | |
| F | MTS | | |

| 6CP Tests | | | |
|-----------|----------------|---------------------|-----------|
| DCDT | Range (inches) | Dist. from (inches) | |
| | | Series I | Series II |
| A | ±3.0 | 7.5 | 3.7 |
| B | ±0.5 | 10.6 | 4.5 |
| C | ±0.25 | 13.8 | 7.7 |
| D | ±0.25 | - | 5.9 |
| E | ±0.125 | - | 10.4 |
| F | MTS | | |

| PS Tests | | | |
|----------|----------------|---------------------|--|
| DCDT | Range (inches) | Dist. from (inches) | |
| A | ±3.0 | 3.1 | |
| B | ±0.5 | 5.1 | |
| C | ±0.25 | 7.9 | |
| D | ±0.25 | 10.6 | |
| E | ±0.125 | 13.8 | |
| F | MTS | | |

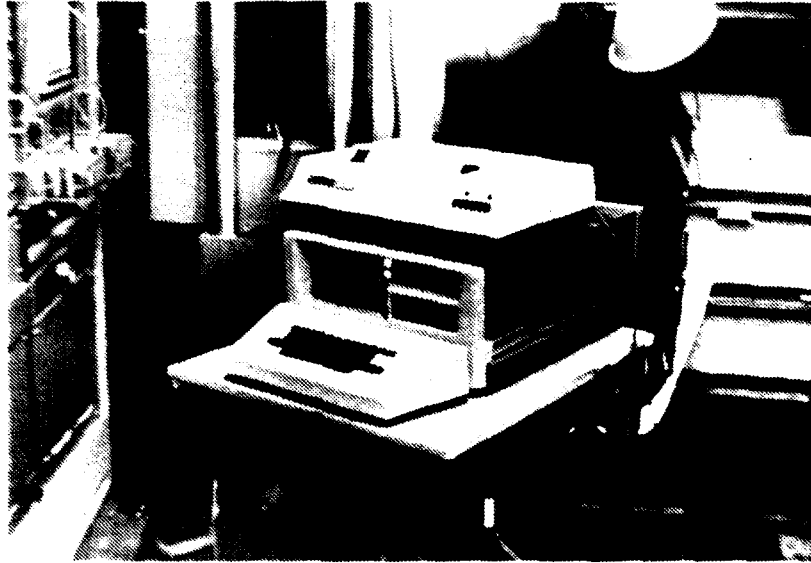


Figure 27. MACSYM 2 Data Acquisition System and Heatn Printer.

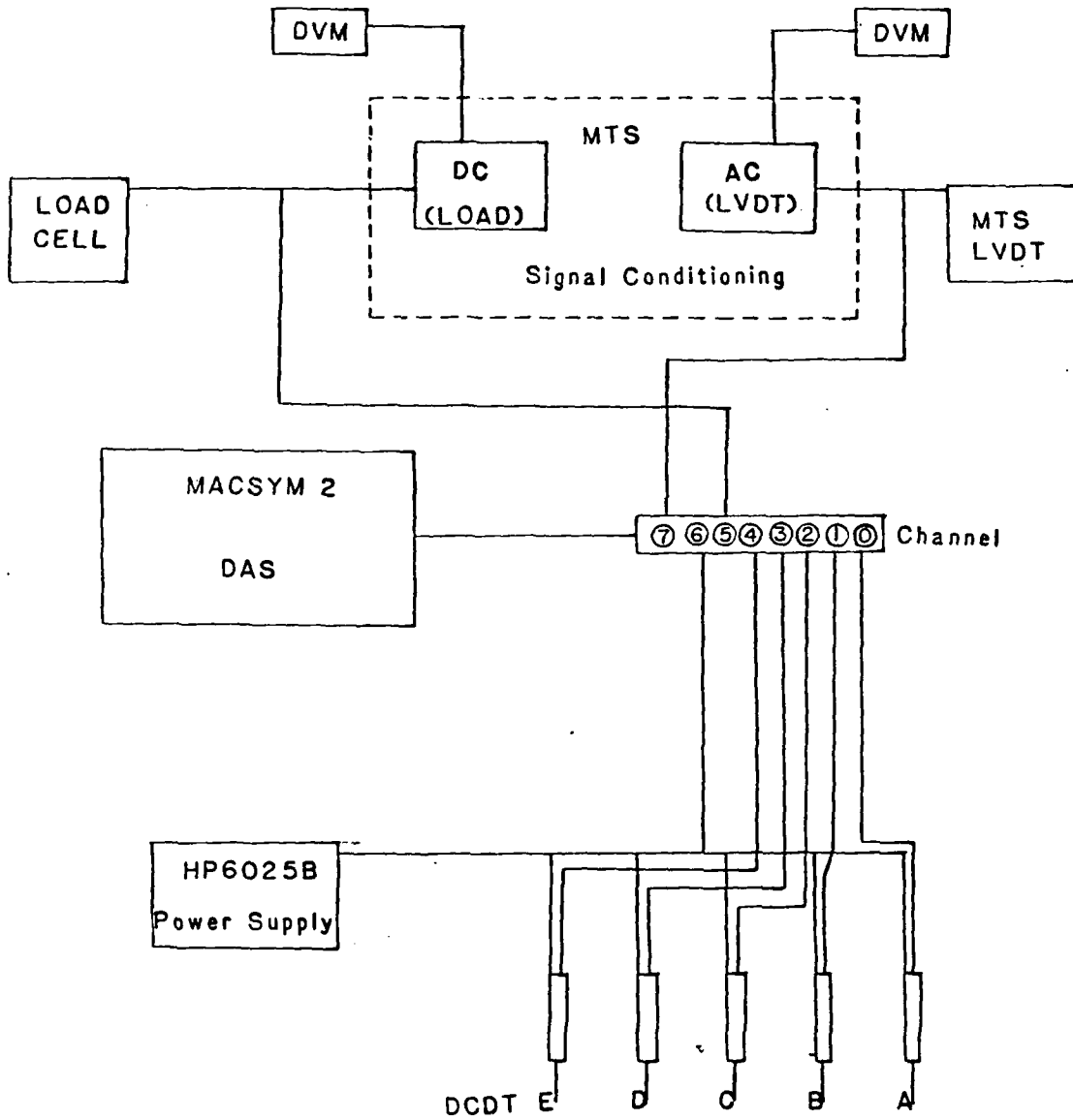


Figure 28. Schematic Diagram of Test Instrumentation and Data Acquisition System.

reaction frame (Figure 16). Either the reaction frame would have to be moved before each test, or the loading box, once it was filled with sand, would be moved back onto the base of the loading frame for testing. Both schemes were deemed impractical. The weight of the reaction frame was several hundred pounds and was securely bolted to the base plate. It seemed impractical to repeatedly bolt and unbolt the frame prior to a test. The weight of the sand plus box was in excess of 1200 pounds. Consequently, the placement scheme which was finally adopted is as follows:

The sand was placed in three layers, each approximately 6 inches thick and vibrated after each layer. The vibration was carried out with an FMC Syntron Magnetic Vibrator Model V51C1, controlled by a Syntron Electronic Controller Model SCR-18. The vibrator was attached to a 20-inch by 20-inch by 1/4-inch thick steel plate. Figure 29 shows the plate vibrator in position prior to compaction of the first layer of sand. The ropes which were attached to the rubber pads were used to facilitate moving the vibrator and plate to the four positions in the box. The frequency of vibration was 60 Hertz. The control was set on "maximum" at all times, and the measured amplitude of the plate vibration was 0.055 inch. The vibration pattern is shown in Figure 30. The area of the vibratory plate was such that there was about a 9-inch overlap in the center section. The initial loose lift heights were approximately 6.5 inches. After vibration, each layer ended up about 6 inches thick. Thickness control was maintained by a scale on the inside of the box.

The same pattern of vibration was followed for the tests in which reinforcement was used. In these cases, however, an extra pass of vibration was applied to the layer of sand on top of the fabric. As will be shown later, average densities of the test where fabric reinforcement was used tended to be slightly greater than the densities of the tests without fabric reinforcement, probably due to this extra time of vibration.

Density measurement and control were originally attempted with a nuclear density gage, but the readings were too erratic, probably due to all the high density material (steel) in the area of the test box and load reaction frame. To obtain accurate results with nuclear density meters, no other materials other than the specimen under test should be in the vicinity.

The two approaches that were finally used were to measure (1) the average overall density of the sand in the box, and (2) the density of individual small cans placed in several locations in the box. First, the overall density was obtained by carefully weighing all the sand placed in the box. This procedure was done twice and the average density was found to be 107.8 pounds/cubic foot. This is equivalent to a relative density of slightly more than 70 percent. The second procedure was followed in 23 tests. Small metal (water content) cans were placed in several locations in the test box (Figure 31). To determine the volume of these density cans, each was filled with distilled water of known temperature and the can was carefully weighed. The measurement was repeated five or six times and the average volume used. All weights were determined on a precision laboratory balance. Placement of the cans in the box was according to the following scheme:

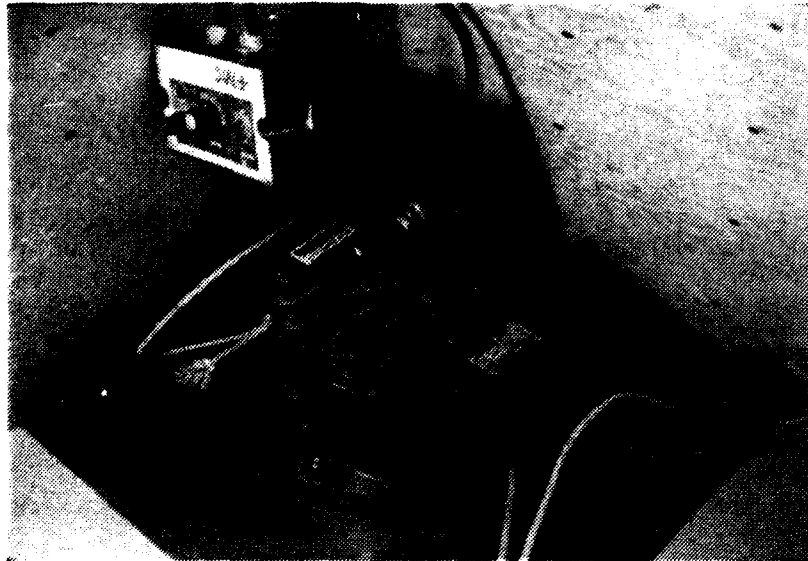


Figure 29. Vibrator and Plate.

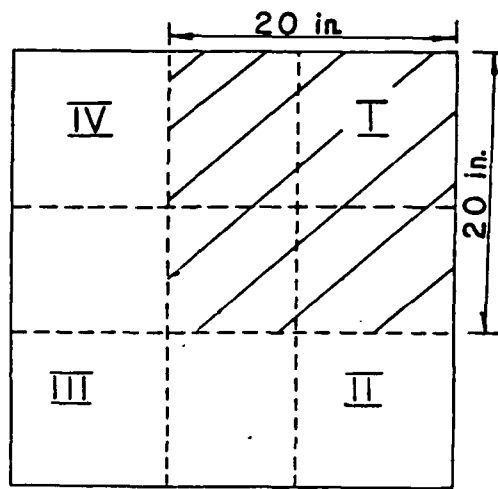


Figure 30. Vibration Pattern.

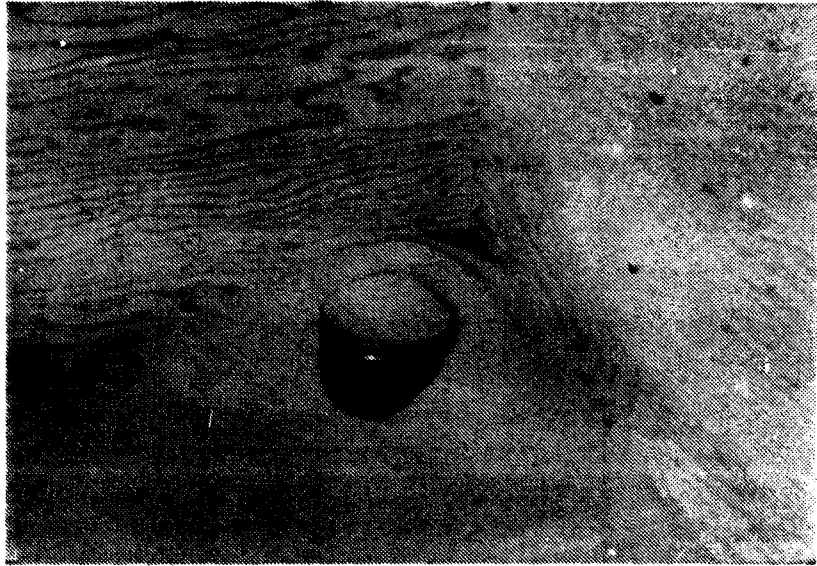


Figure 31. Density can in corner of Test Box.

| Layer | Location | |
|--------|-----------|------------|
| top | E wall | NW corner* |
| middle | SW corner | NE corner |
| bottom | | SE corner |

* Exception: for PS tests; this can was positioned near the south wall.

The cans were placed about 4 inches from the wall, except for the can under the centerline.

At the conclusion of the loading test, the cans were carefully excavated, struck off level, weighed, and the density of the sand in each can was calculated. The results of these measurements are given in Table 5. The average value of all the measurements by this scheme was slightly less than the overall average density in the box of 107.9 pcf. The range of densities measured in each test was between about 1 and 4 pcf. There seemed to be no definitive pattern of the densities, although, with a few exceptions, the two bottom cans tended to be lower than those on the middle and the top layers. Occasionally, the middle layer cans appeared to have the higher density (as might be expected from work with field vibratory rollers). The surface of the sand after compaction appeared to be very dense to the touch.

After the last layer was compacted on the reinforcement, a small-diameter wire probe was used to verify the depth to the fabric layer.

At the conclusion of a test, all but 2 to 4 inches of the sand was removed and placed in storage cans. The sand left in the bottom of the box was stirred repeatedly. For preparation of the next test, the sand from storage was loosely dumped into the box so that the initial loose-lift thickness was around 6.5 inches. Then the compaction process proceeded as described above in preparation for the next test.

b. Fabric and Geogrid Placement

The fabric or geogrids were placed at depths and in layers as described previously (see Table 1 for the test code). The reinforcement was placed on the compacted sand surface and smoothed by hand so that it was in full contact with the densified surface. Figure 32 shows the sand being loosely dumped on top of a fabric layer. Then this final layer of sand was compacted as described above. In the majority of the tests, the fabric or geogrid reinforcement was not attached to the walls or pretensioned as was done by Haliburton, Lawmaster and King (Reference 13). It was felt that tests of the loosely placed fabric under the low confining pressures applied by the thin layer of sand would provide a lower bound for the effect of the reinforcement. For comparison purposes, however, a few tests were carried out with (1) partial fixity, and (2) total fixity. The results of these tests will be described later.

TABLE 5. DRY DENSITIES AS DETERMINED BY THE SMALL DENSITY CAN MEASUREMENTS

| Test | ρ_d avg | Range |
|---------------|--------------|--------------|
| 3CP | 103.8 | 102.6-105.3 |
| 3CP1W-0.5 | 105.8 | 105.1-106.3 |
| 3CP1W-1.2 | 104.6 | 103.1-106.2 |
| 3CP1W-2 | 104.3 | 103.2-105.3 |
| 3CP1G-1 | 105.3 | 104.7-106.4 |
| 3CP1G-2 | 105.3 | 104.5*-106.1 |
| 6CP | 106.0 | 104.6-106.8 |
| 6CP | 105.6 | 104.6-107.0 |
| 6CP | 105.7 | 104.6-106.8 |
| 6CP | 105.5 | 105.1-106.1 |
| 6CP1W-1 | 106.4 | 104.9-108.3 |
| 6CP1W-1 | 104.8 | 104.4-105.8 |
| 6CP1W-2 | 107.0 | 105.4-109.4 |
| 6CP1W-2 | 105.4 | 104.3-106.1 |
| 6CP1W-3 | 108.8 | 104.9-109.6 |
| 6CP2W-0.8-0.8 | 106.4 | 105.1-107.1 |
| 6CP2W-1.6-1.6 | 104.1 | 103.1-105.5 |
| PS | 104.3 | 102.8-104.9 |
| PS | 104.6 | 103.5-105.7 |
| PS1W-1 | 105.1 | 103.2-106.1 |
| PS1W-2 | 105.4 | 105.2-105.6 |
| PS1G-1 | 104.7 | 104.0-105.2 |
| PS1G-2 | 106.3 | 104.8-108.0 |

*Appeared disturbed



Figure 32. Sand Loosely Dumped on Fabric Layer.

c. Mounting of the Load Plate and Load Cell

After the fabric and final layer were placed and densified, the load cell and appropriate loading plate were attached to the actuator piston by threaded studs. The cable from the load cell was then attached to the MTS system. Figure 33 is a closeup of the load cell and 6-inch diameter load plate.

d. Instrumentation

As described before, the DCDTs were set up according to the pattern shown previously in Figure 26 and Table 4. In the closeup view of Figure 33, the 3-inch DCDT is positioned just prior to loading of the 6CP tests (Series II of Figure 26[b]). Figure 34 is a closeup of the DCDT support beam. The cores of the DCDT rest directly on small cardboard discs on the surface of the sand to record the upward and downward movements of the sand surface as the loading plate is pressed into the surface.

After all the instrumentation was mounted and appropriate connections made to the MTS and the data acquisition system, the positions of the DCDTs were adjusted so that the cores were within the linear range of the expected movement during the test. A MACSYM program was written to assist in this positioning.

All connections were checked to make sure everything was ready for the loading test. The DAS was turned on, and, after a brief warmup period, the piston of the MTS was lowered to apply a very small seating load (1 to 2 pounds) on the surface of the sand. Now the test was ready to begin.

e. Loading Test

Loading was accomplished with the MTS system in "load mode." The hydraulic pressure range was set so that sufficient load can be applied by the actuator. The load range on the MTS was set to an estimated value of the maximum load so that maximum sensitivity of the load cell can be achieved. The load cell and the MTS LDVT were "zeroed" as close as possible with digital voltmeters (DVM, Figure 28). To apply the load, the "set point" on the MTS Servac control unit was turned slowly. The DAS was programmed to take readings of all channels at a specified frequency. For the present tests, readings were made every 0.25 or 0.5 seconds. Thus, for each test, about 1000 readings were taken of all channels and stored in the memory of the DAS. The load was applied at approximately a constant rate by monitoring the output from the load cell on the DVM. The load was applied so that failure was reached in 7 to 8 minutes.

Failure occurred suddenly in most cases, and sometimes additional load was applied to see if there was a work-hardening effect. At the end of each test, the loading piston was retracted, the plate raised, instrumentation removed, and photos and or sketches made as appropriate. After excavation, appearance of the fabric and/or grids was noted. For the fabric tests, there was no obvious physical evidence of disturbance or abrasion on any test specimens on the fabric. On the plane strain specimens on the geogrids (Tensar SR2), a definite "permanent set" of a "dip" directly under the loading plate was shown. This can be seen in Figures 35 and 36.

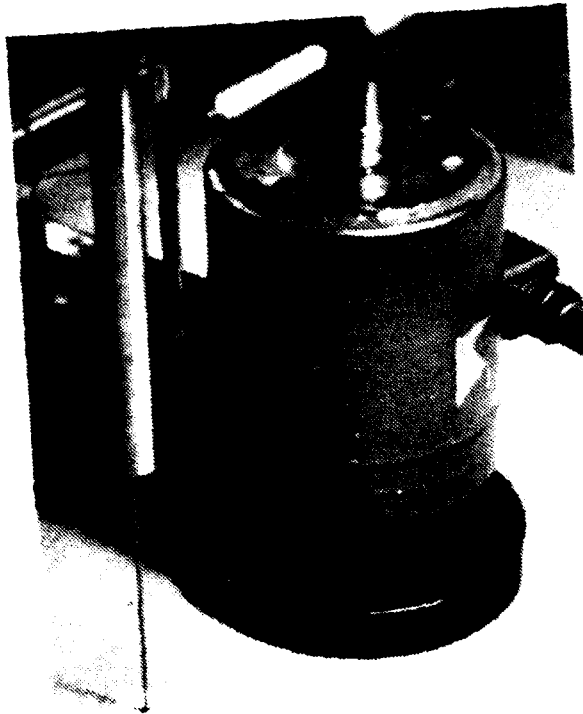


Figure 33. Closeup of Load Cell and Load Plate.

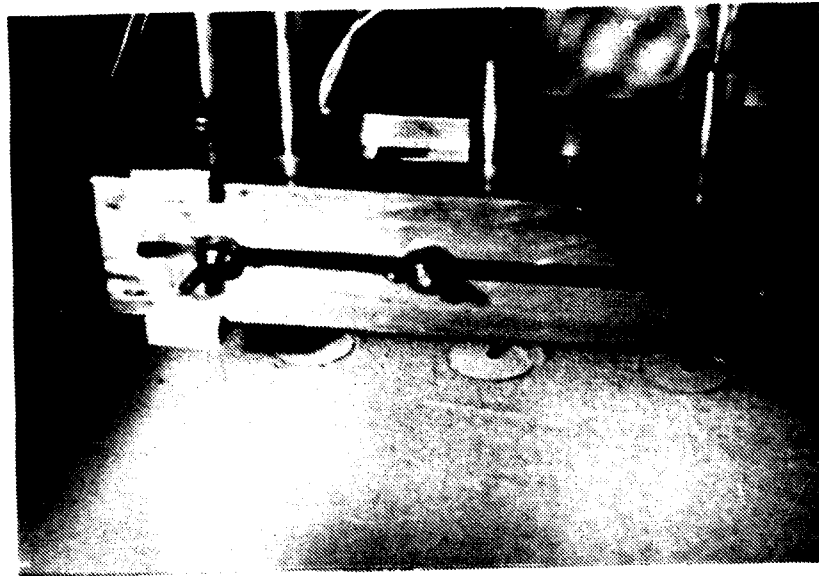


Figure 34. DCDT Support Beam.

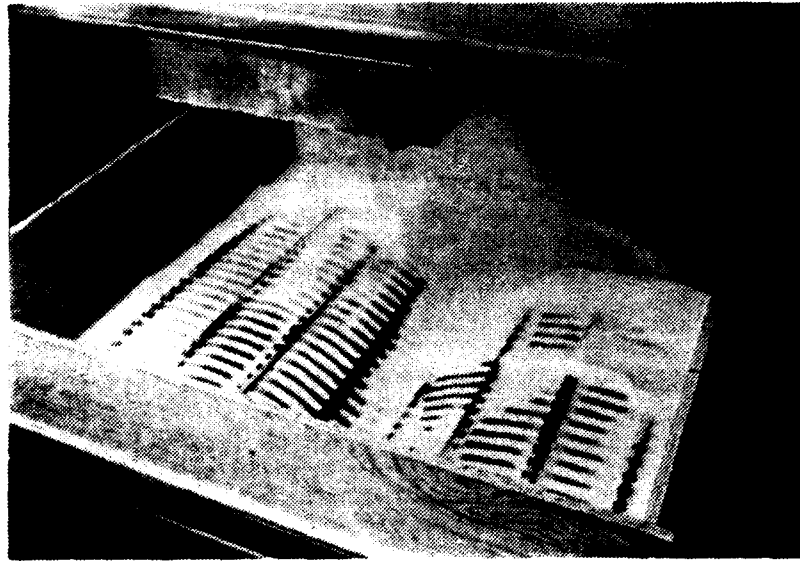


Figure 35. View of Geogrid (SR2) Specimen After a Plane Strain Test. (Loading Beam, Load Cell, and Top Sand Layer Have All Been Removed).



Figure 36. Close View showing "bulge" in Geogrid SR2 After a PT Test.

During the test, observations were made of the deformation of the side of the box by means of a mechanical dial indicator accurate to the nearest 0.01 millimeter. These measurements will be discussed in the next section.

5. EXPERIMENTAL RESULTS

The primary test variables were described earlier in this chapter (see Tables 1 and 2). It was originally planned to conduct tests with vibratory and impact as well as quasi-static type loadings. The analytical work (Section II) did not require other than quasi-static loading; consequently, other modes of loading were not utilized in these series of tests.

a. Photographs of Tests After Failure

Figure 37 shows a test with fabric reinforcement using a 3-inch diameter loaded plate after failure. Figure 38 is a closeup view of the same test. Note the uniform and symmetrical appearance of the failure surface. The next photograph, Figure 39, shows the failure surface after the piston has been withdrawn. Again, note the uniformity of the surface. These observations tend to verify that the sand density in the vicinity of the piston was sensibly uniform.

The next three photographs show plane strain tests. Figure 40 shows the plane strain test setup prior to loading. The next photograph (Figure 41) shows the same test after failure. At the "north" side of the box, that is, under the far end of the DCDT support beam, it can be seen that the fabric has pulled away from the edge of the box, leaving a depression in the sand at the edge. This was typical behavior of both the circular and plane strain tests at failure. The amount of "pull" away from the edge of the box depended on the total deformation of the loading plate. Figure 42 shows a plane strain test with a view from above. Note that the beam appears to be slightly off-center, an occurrence typical of the plane strain tests. The beam was set perpendicular to the sides of the box at the start of the test. When failure occurred, some slight rotation of the beam, either to the left or to the right, was usually observed.

For the partial and full fixity tests, the geotextile was held by means of wood slats bolted to the box sides. Figure 43 shows the fabric clamped in place prior to placement of the final sand layer. Figure 44 shows how the sand and fabric have pulled away from the right side wall and clamp in a circular plate test with partial fixity. In Figure 45, after failure, the sand has been removed, and an arrow drawn on the fabric to indicate how much the fabric has moved (in this case, about 1 inch). Again, this was a test with the fabric partially fixed; that is, the fabric was folded under about 1 inch all around prior to placement of the final sand layer. No photographs were taken of the test with full edge fixity because its appearance was so similar to the tests with partial fixity.

b. Load vs. Settlement of Plates

Test results are shown in the form of the load-settlement response of the loading plate size and shape, both with and without reinforcement. The effect of the several variables on the test result will now be discussed.

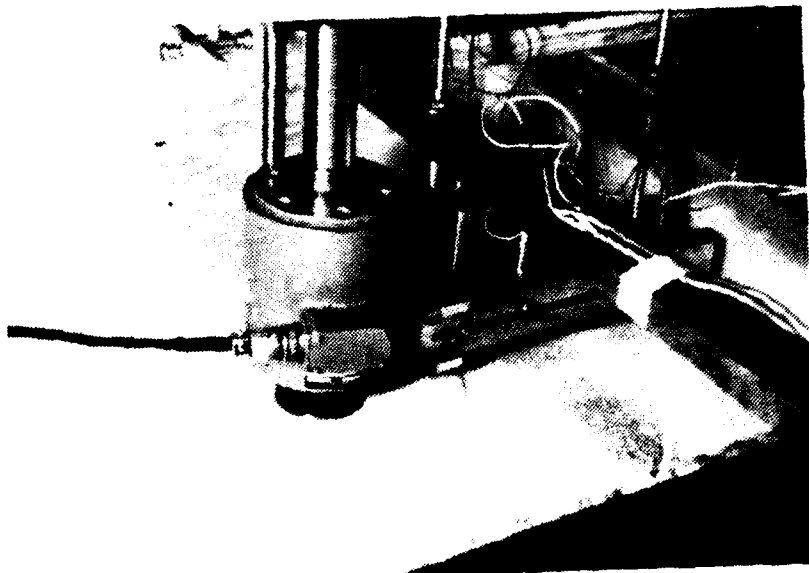


Figure 27. Test After Failure with Param. 5000 Element Using a 2-inch Diameter Electrode.



Figure 28. Close-up View of Figure 27.

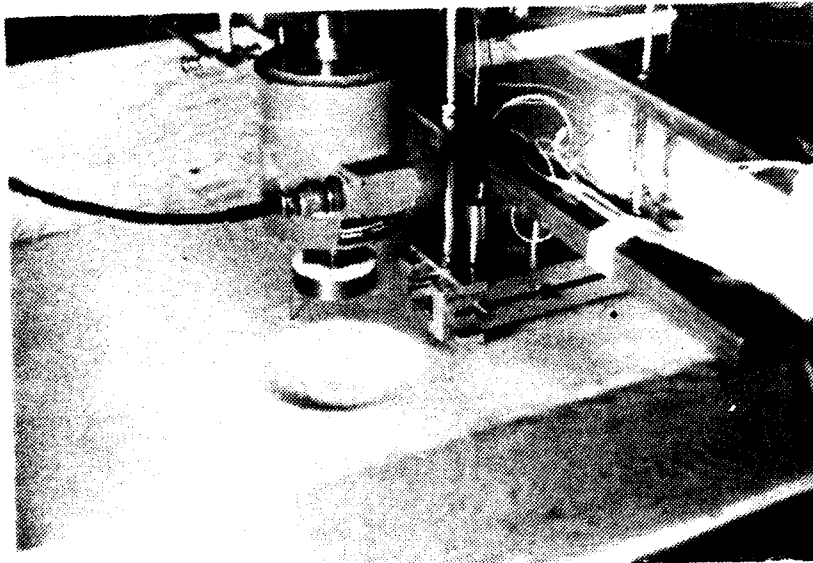


Figure 19. Tests shown in Figure 37 and 38 After Raising of the Plate.

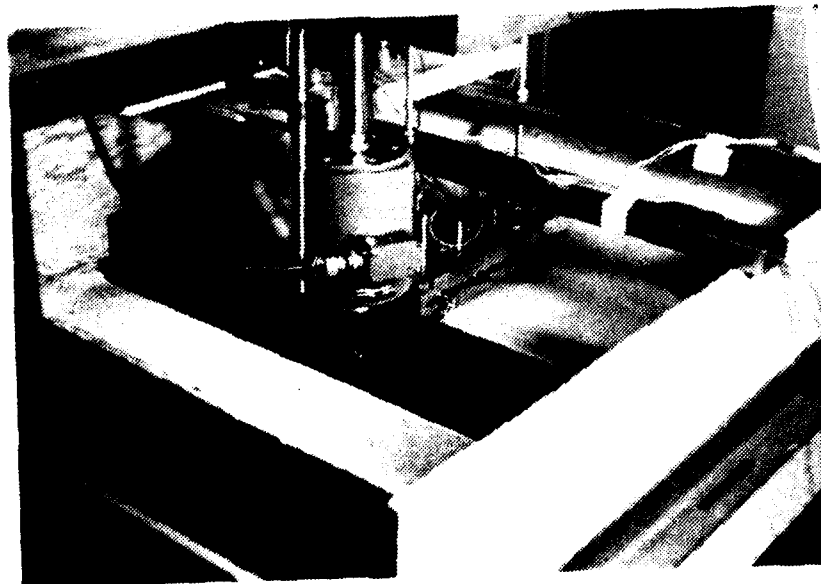


Figure 20. Large Drain Port After Raising of Plate.

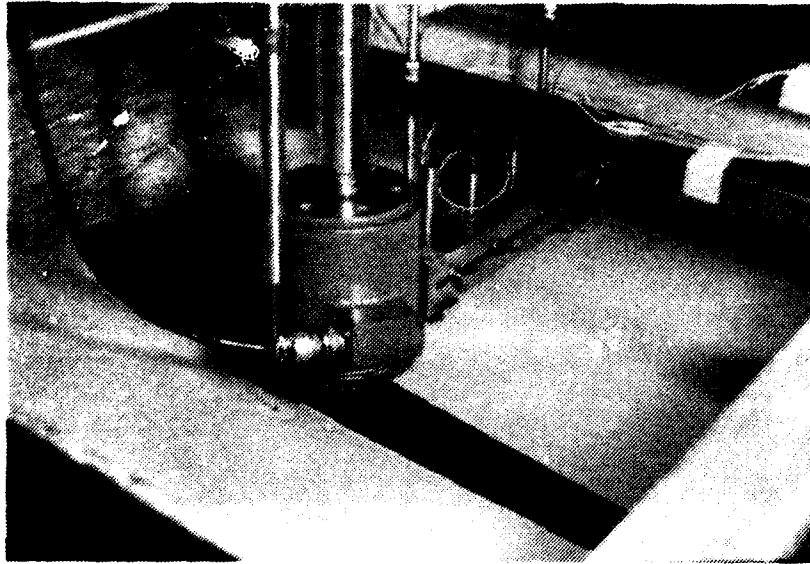


Figure 41. Plane Strain Test After Failure.

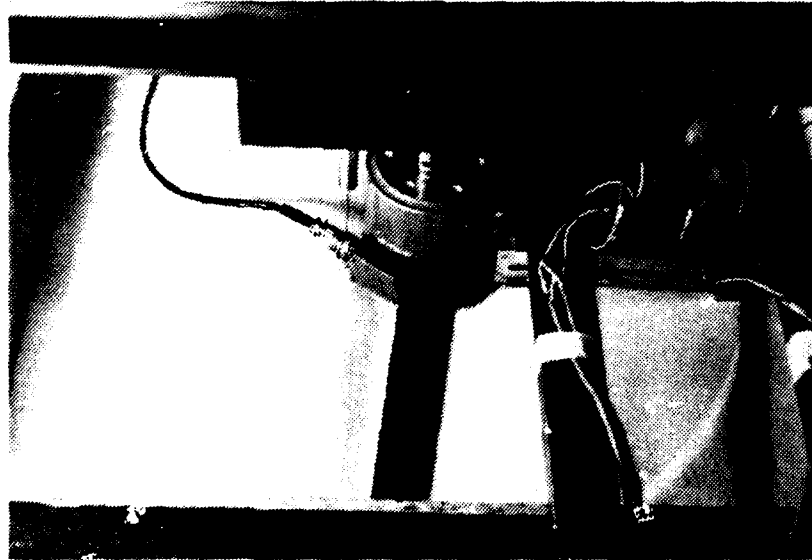


Figure 42. View from Above of Plane Strain Test After Failure.

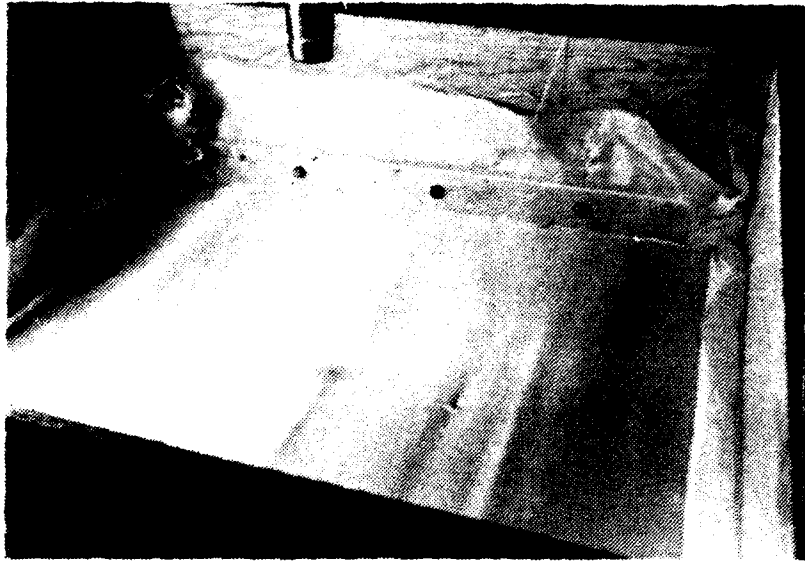


Figure 43. Tests with Fabric Partially Clamped, Prior to Placement of the Final Sand Layer.

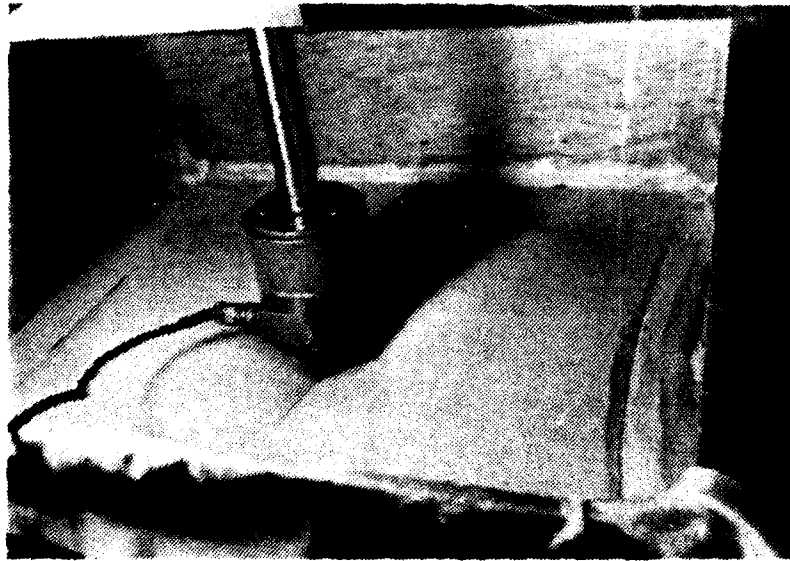


Figure 44. After Failure of a Test with Partial Fixity.



Figure 45. Same Tests as in Figures 43 and 44, After Top Sand Layer Was Removed. The Black Arrow Drawn on the Fabric Points to a Dashed Line Which Indicates How Much the Fabric has Moved from Its Initial Position (About 1 Inch).

Figure 46 shows the load vs. settlement behavior for the 3-inch diameter and the 6-inch diameter plate tests.

The increase in the bearing capacity due to the larger plate size is obvious. Note, too, the increase in bearing capacity due to the presence of the reinforcement. The amount of this increase as a function of depth, type and number of layers will be discussed later. Also, there was a significant work-hardening effect in the reinforced sands as the load continued to be applied to the plate after first yielding had occurred. In almost every test, a fall-off of load was observed as deformation continued; then, if the test was carried far enough, the reinforced soil system began to take up load again. In most cases, the range of the actuation LVDT was exceeded, so that measured settlements were not obtained beyond about 1.5 to 2.0 inches. The work-hardening effect was not so apparent for the unreinforced sands, although a peak in the load-settlement curves can be seen. Such behavior is not unexpected for dense sands.

The load-settlement results of Haliburton, et al. (References 12 and 13) indicated a much greater work-hardening effect than the present tests show, probably because of differences in the edge fixity conditions. This point will be further discussed later.

It is encouraging from Figure 46 to note that the test results are reasonably repeatable, both with respect to modulus and to maximum load. This effect is apparent in Figure 47, where the deflection scale (ordinate) is very much expanded. The initial moduli (or more properly the coefficient of subgrade reaction, which might be determined from a plate loading test similar to those carried out here) as determined from the slopes of the load-settlement curves, are approximately the same. In Figure 48, where the effect of different types of reinforcement is shown, the initial moduli of the tests with the woven fabric reinforcement are seen to be about the same as their counterpart tests with the geogrids. The moduli for the 2-inch depth of burial are somewhat less than those for 1-inch depth of burial, independently, of the type of the reinforcement. The presence of the reinforcement at 1-inch depth clearly affected the initial modulus (or coefficient of subgrade reaction).

Figure 49 shows the effect of the number of layers of the fabric reinforcement. Tests on multiple layers were only conducted using the 6-inch CP. The difference in behavior between the two tests with two layers of reinforcement is quite apparent, but it is not obvious why that difference occurred. Because of time and other constraints, these experiments were not repeated; therefore, it is not known whether the effect is a test artifact or not. The work-hardening effect is not so apparent, probably because of lack of edge fixity, although some effect was shown on the two-layer test with fabric at 1.6 inches spacing. As expected, there was a significant increase in the load-carrying capacity of the two-layer system at a shallow depth of burial (the 6CP2W-0.8 test).

Figure 50 shows the load-settlement results for the plane strain tests. There was a work-hardening effect for both tests with the fabric reinforcement as well as with the geogrid reinforcement at 1-inch depth. There was not much difference in response between the two kinds of reinforcement, although both showed a significant improvement over unreinforced sand. The moduli of all tests with reinforcing were slightly greater than the unreinforced sand, although the difference is small.

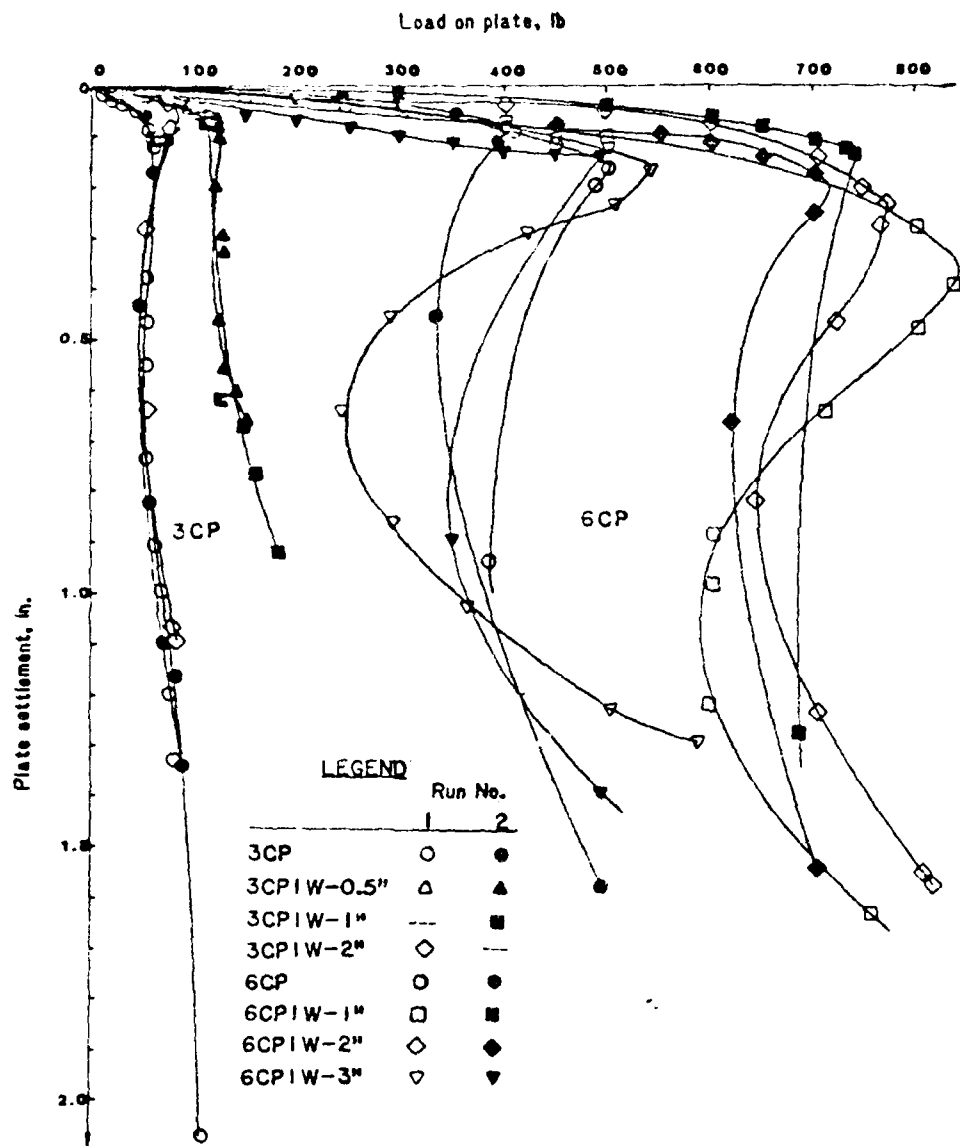


Figure 46. Load-Settlement Response of 3CP and 6CP Tests.

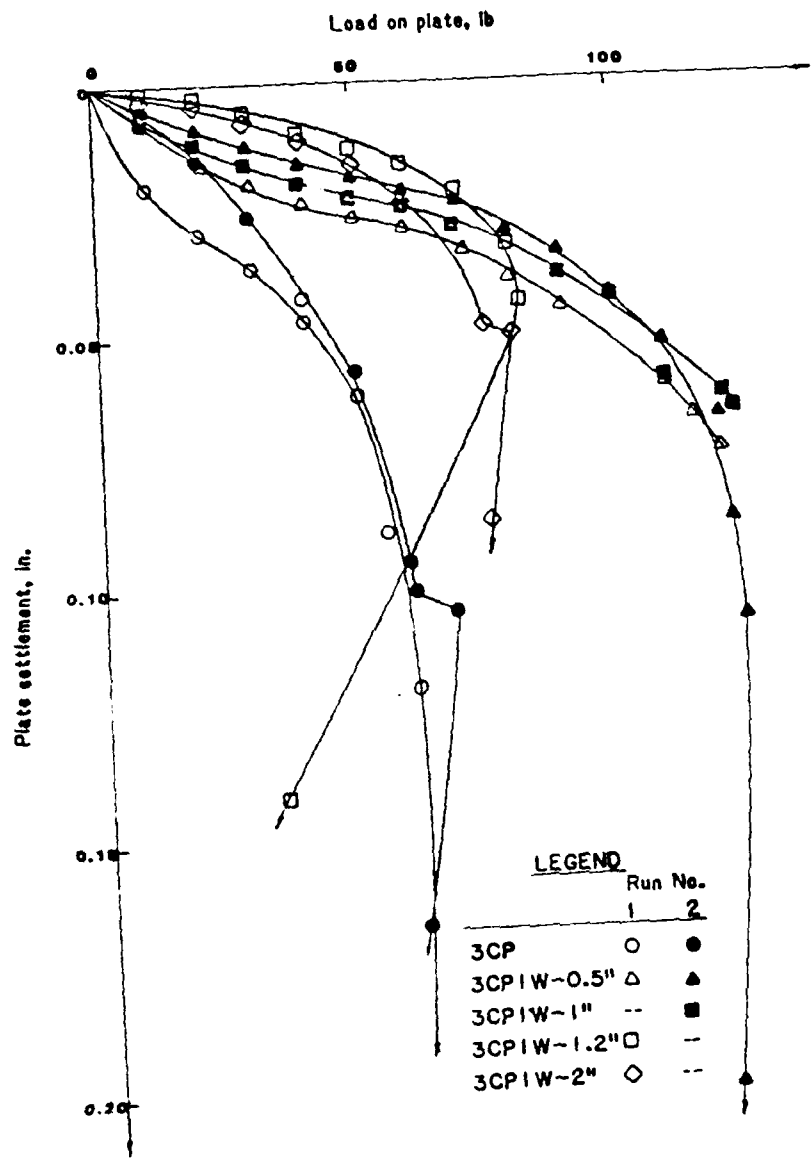


Figure 47. Load-Settlement Response of 3CP and 3CP1W Tests with Reinforcement at Three Depths (Expanded Settlement Scale).

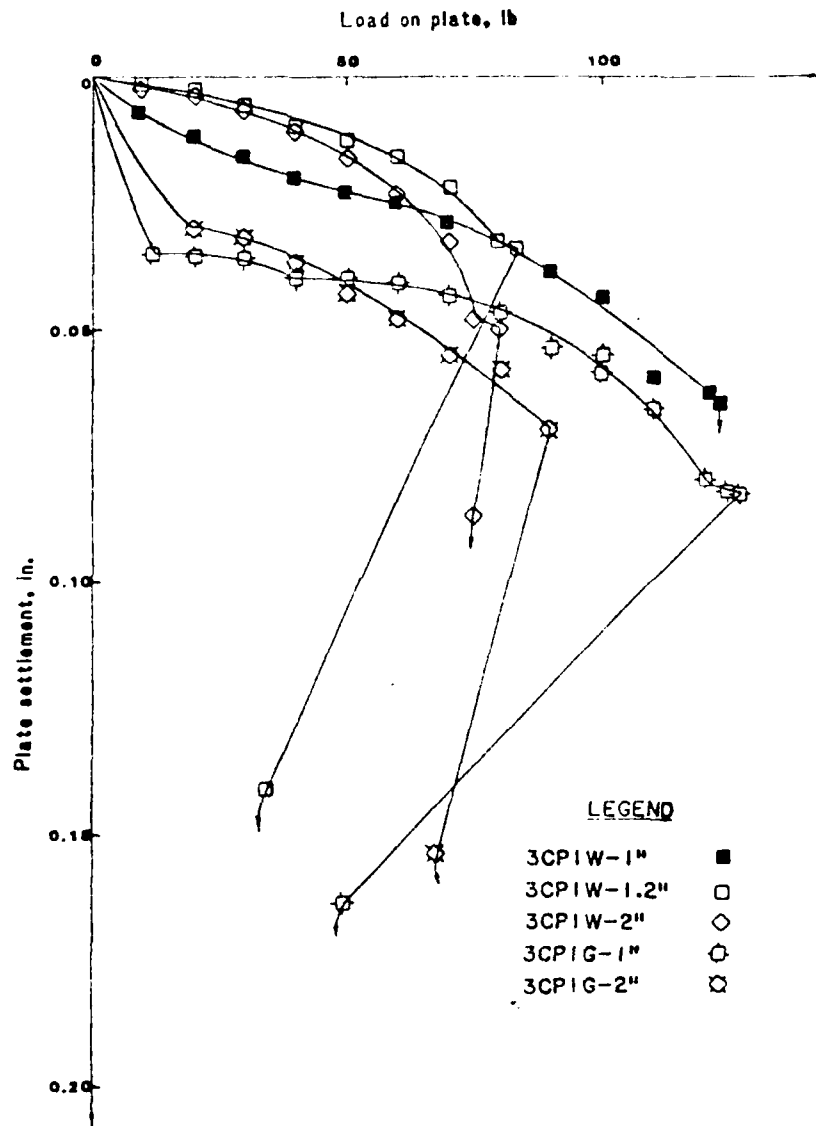


Figure 48. Load-Settlement of 3CP Tests, Grids vs. Fabric Reinforcement.

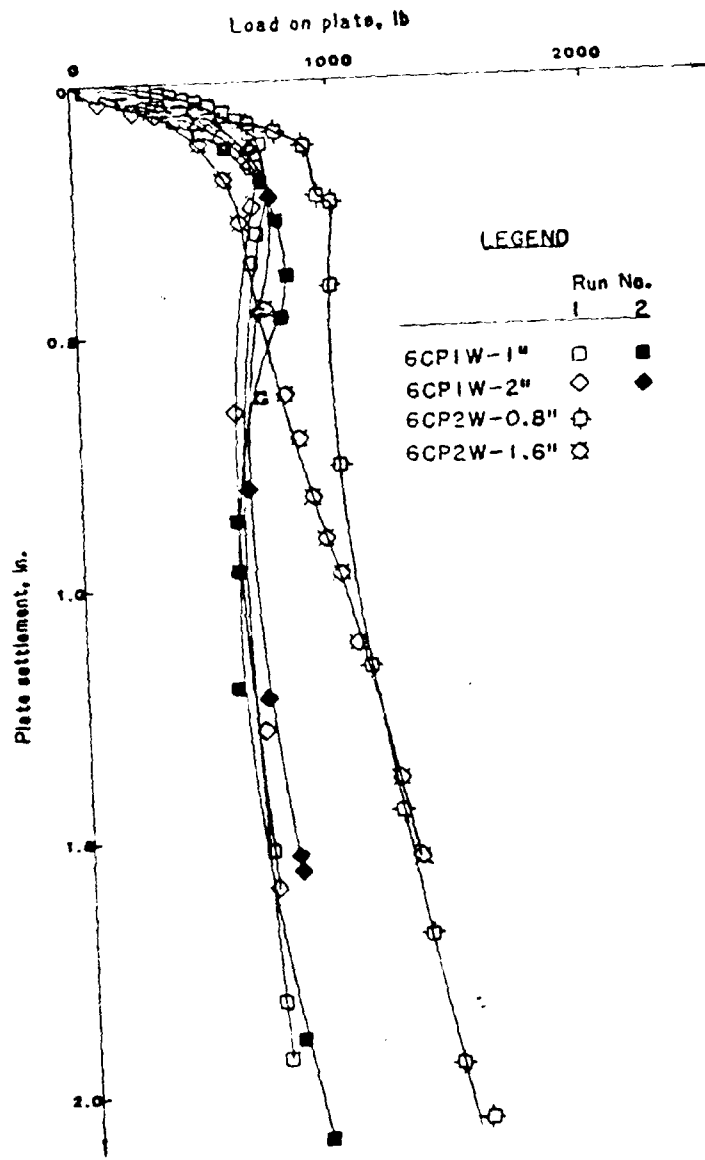


Figure 40. Load-Settlement Response of 6CP Tests, One vs. Two Layers of Fabric Reinforcement.

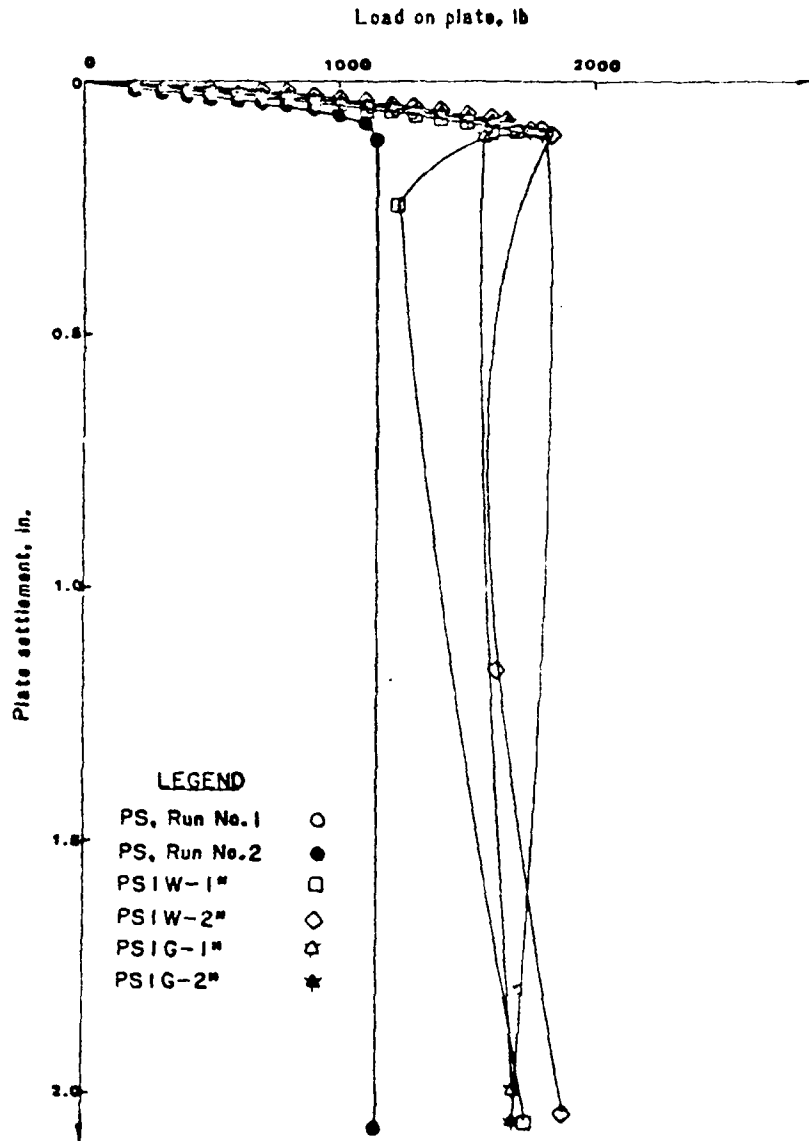


Figure 50. Load-Settlement Response of PS Tests with Fabric and Grids.

Figure 51 shows the effect of edge fixity. The second run of test 3CP1w-1-inch PF had a disturbed surface and consequently failed at a significantly less ultimate load than the first run of that test (102 pounds vs. 56 pounds). Surprisingly, there was very little difference between the tests with full fixity and those with partial fixity. Recall that in the full fixity test, the geotextile was attached by wooden slats bolted to the side of the box. For the partial fixity test, a fold of about 1 inch was made in the fabric all around the periphery. The full fixity test was expected to be an upper bound of the effect of reinforcement, while the test with partial fixity would show the intermediate value with respect to full fixity and no edge fixity. These results will be discussed in greater detail later in this section.

c. Ultimate Load and Stress

Table 6, an expansion of Table 2, describes the various tests, as well as some test results.

Table 6 gives ultimate load P at initial yield, P_{i} , and at a plate settlement of 1 inch for each test. The depths to the reinforcement layers are shown as a ratio of the plate diameter (or plate width in the case of the plate strain test), or d/b . The unit bearing stress at failure, q , is P_{i}/A . From the values in Table 6, it is apparent that reinforcement results in a significant increase in q for all plate sizes. Significant improvement also results with the addition of a second fabric layer, as shown in the 6CP2w tests. Full or partial edge fixity apparently has very little effect, and, surprisingly, the use of the higher strength geogrids did not increase the ultimate stress as much as expected.

Sinquet and Lee (Reference 22) expressed the degree of improvement due to reinforcement in terms of a bearing capacity ratio (BCR). They defined the BCR as q with reinforcement divided by q_0 without reinforcement, at the same vertical deformation. In the present test series, initial yield occurred at about the same settlement, and once failure occurred, the amount of vertical deformation occurring thereafter does not appear to make much difference in calculated BCR values (see the load-settlement curves, Figures 46 to 51). Therefore, present results were put in terms of a modified BCR, wherein the q/q_0 ratio was determined for the maximum observed values of each. The modified BCR values for the various tests with respect to the test on the unreinforced sand for the various plate sizes and shapes are also shown in Table 6.

It is of interest to compare the results of the tests on unreinforced sections with the theoretical bearing capacity. This was done using Terzaghi-Meyerhoff bearing capacity factors (References 52 and 53). Table 7 shows the theoretical ultimate bearing capacity in pounds for the three test configurations for a range of friction angles. Also shown in the table are the observed maximum values of load on the plate. For all of the tests, empirical corrections for the shape of the loaded area were made.

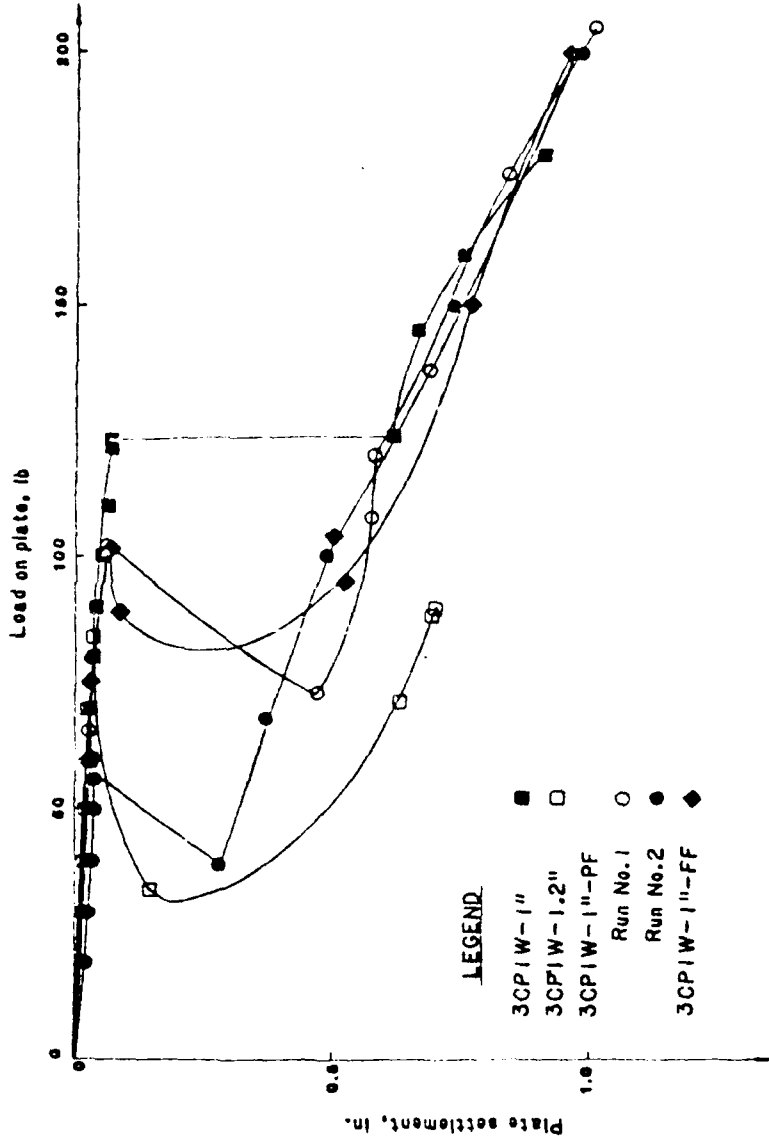


Figure 51. Load-Settlement Response of Tests with Partial Edge Fixity of the Fabric.

TABLE 6. TEST RESULTS

| Test | d/D | P _{max} , lb | P at s=1 in. | q, psi | BCR |
|----------------|------|-----------------------|-----------------|--------|------|
| 3CP | 0 | 60.5 | 67 | 8.52 | 1 |
| 3CP | 0 | 60. | 70 | 8.49 | 1 |
| 3CP1W-0.5 | 0.17 | 120 | 148(0.7") | 17.0 | 2.00 |
| 3CP1W-0.5 | 0.17 | 120 | | | |
| 3CP1W-1.0 | 0.33 | 123 | 180 | 17.4 | 2.05 |
| 3CP1W-1.2 | 0.39 | 84(?) | 89(0.9") | 11.9 | 1.40 |
| 3CP1W-2 | 0.67 | 80 | 79 | 11.3 | 1.33 |
| 3CP1G-1 | 0.33 | 127 | 130(0.7") | 18.0 | 2.12 |
| 3CP1G-2 | 0.67 | 90 | 91(0.8") | 12.7 | 1.50 |
| 3CP1W-1-PF | 0.33 | 100 | 205 | 14.2 | 1.67 |
| | 0.33 | 50(?) | 200 | | |
| 3CP1W-1-FF | 0.33 | 102 | 200 | 14.5 | 1.70 |
| 6CP | 0 | 500 | 384 | 17.7 | 1 |
| 6CP | 0 | 435 | 386 | 15.4 | 1 |
| 6CP | 0 | 444 | 465 | 15.7 | 1 |
| 6CP | 0 | 411 | 400 | 14.5 | 1 |
| | | | Avg | 15.4 | 1 |
| 6CP1W-1 | 0.17 | 832 | 600 | 29.4 | 1.91 |
| 6CP1W-1 | 0.17 | 736 | 700 | 26.0 | 1.69 |
| 6CP1W-2 | 0.33 | 767 | 700 | 27.1 | 1.70 |
| 6CP1W-2 | 0.33 | 763 | 650 | 24.9 | 1.62 |
| 6CP1W-2 | 0.67 | 640 | 300 | 19.1 | 1.24 |
| 6CP1W-3 | 0.67 | 492 | - | 17.4 | 1.13 |
| 6CP2W-0.5-0.2 | 0.13 | 943 | 1050 | 33.4 | 2.16 |
| 6CP2W-1.0-1.5 | 0.26 | 600 | 1020 | 21.2 | 1.38 |
| P ₅ | 0 | (no failure) | | | |
| P ₅ | 0 | 1123 | 1100 | 12.5 | 1 |
| PS1W-1 | 1.3 | 1708 | 1700 | 19.0 | 1.52 |
| PS1W-2 | 2.0 | 1835 | 1600 | 20.4 | 1.63 |
| PS1G-1 | 1.3 | 1656 | 1663 | 18.4 | 1.47 |
| PS1G-2 | 2.3 | 1800 | 1676 | 20.0 | 1.60 |

TABLE 7. THEORETICAL ULTIMATE BEARING CAPACITY, POUNDS - UNREINFORCED SECTIONS

| Test | $\phi = 35^{\circ}$ | 40° | 42° | 45° | Observed |
|------|---------------------|--------------|--------------|--------------|----------------------|
| SCP | 16.3 | 37.7 | 59.5 | 102 | 60; 60.5 |
| 6CP | 131 | 302 | 475 | 824 | 411 to 500; avg. 435 |
| FS | 304 | 704 | 1111 | 1927 | 1123 |

The agreement of the theoretical values for $\phi = 42^{\circ}$ with observed values is excellent. This value of ϕ also agrees with the results of the direct shear tests presented in Figure 20 and verifies the observation that the sands were relatively dense.

Comparison of present results for reinforced sands with previously published theoretical developments is not easy. Binquet and Lee (Reference 12) suggested that the theoretical bearing capacity ratio for one reinforcement layer should be about 1.2. Since their theory was for a strip footing and for strips of reinforcing rather than sheets, this comparison may lack validity. Present FS test results (Table 6) indicate bCR values significantly greater than 1.2. Binquet and Lee's results for two reinforcement layers suggest a theoretical bCR of about 1.5. Without any correction for strip vs. circular footings, present bCR values for two fabric layers were significantly greater. The only other theoretical model for bearing capacity of fabric reinforced sands has been presented by Maliburton, et al. (Reference 13). Their results will be discussed later.

Maliburton, et al. (Reference 13) report that an improvement on the order of 1.5 in fabric-soil load capacity can be inferred from the work of Sarenberg, Steward, and their coworkers (References 25, 26, 27 and 54). Our tests verify that 1.5 is a good average improvement value.

d. Effect of Reinforcement Depth and Spacing

Figure 52 shows the maximum load on the plates, P_{max} , vs. the depth, d , of the first reinforcement layer. It appears that depth has very little influence on the first reinforcement layer for both the SCP and 6CP tests if the depth of burial is less than 2 inches. For the 6CP test, when the depth reached 2 inches, there was a significant decrease in the P_{max} . On the ordinate of Figure 52, the theoretical bearing capacity values for the unreinforced sands for a ϕ of 42 degrees are shown ("Th. F.C.").

The use of two layers of woven fabric reinforcement with the 6CP tests shows a significant improvement. It is not known what would have happened if other reinforcement depths had been tested.

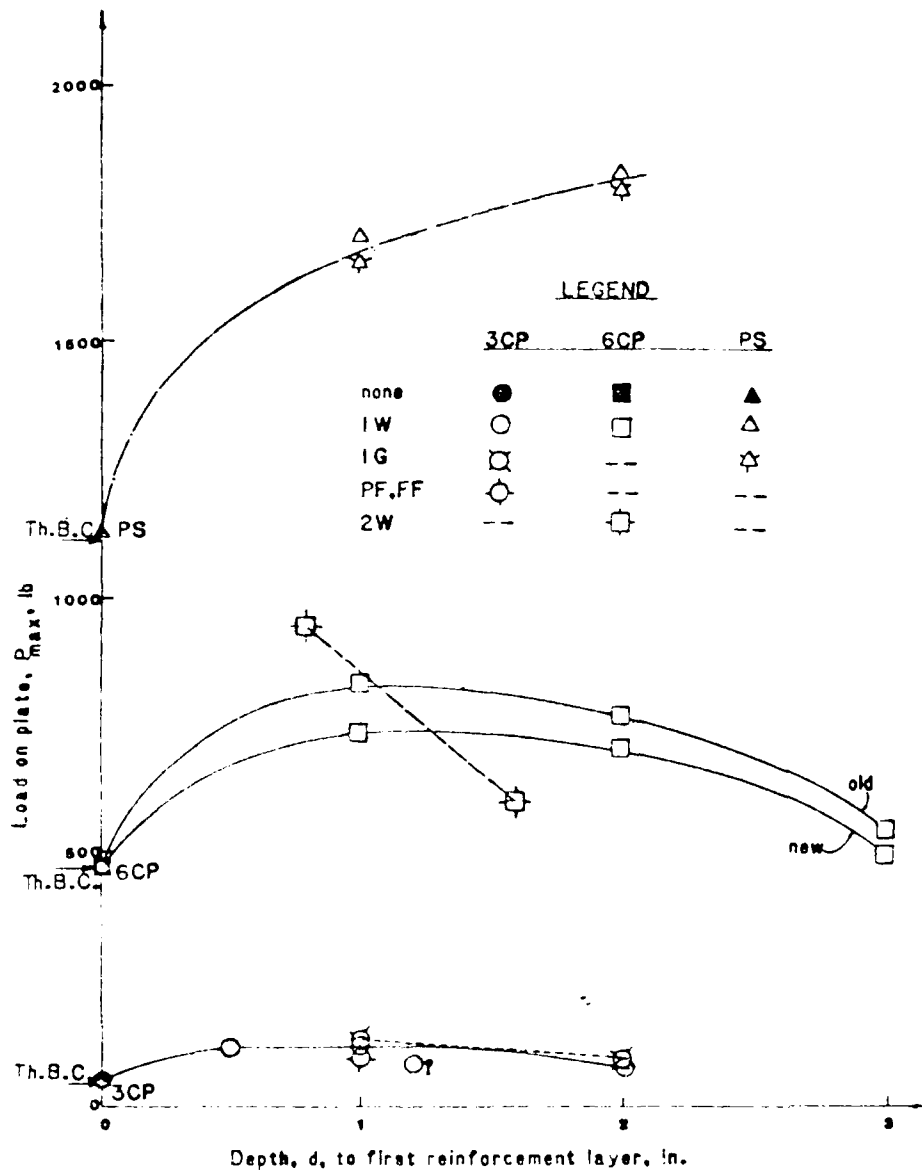
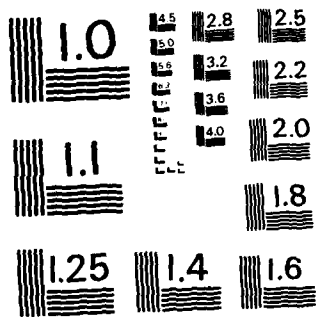


Figure 52. Maximum Load on the Plate vs. the Depth, d , to the First Reinforcement Layer.



MICROCOPY RESOLUTION TEST CHART
NATIONAL BUREAU OF STANDARDS-1963-A

With respect to increasing the depth to the first reinforcement layer, the results for the circular plates are exactly the opposite as with the plane strain tests. In the latter tests, the P_{max} increased significantly with an increase in the depth of the reinforcement layer, at least to the depths tested. It is likely that P_{max} would eventually decrease if the depth to the first layer was sufficiently large. The exact depth at which this decrease would begin to occur will require additional testing.

The effect of the geogrid reinforcement for both the CP and PS tests was surprising in view of the differences in modulus and ultimate tensile strength between the grids and fabric. Apparently the advantage of interlock, which the grids obviously have, was not realized with the relatively fine Ottawa sand (that is, "relatively fine" with respect to the dimension of the "threads" of the grids). With the fabric reinforcement, the diameter of the grains is of the same order of magnitude as the diameter of the threads, and therefore significant reinforcing effects occur (References 4, 48, 49), as indicated by the marked increase in bearing capacity of the reinforced vs. the unreinforced sands (Figure 52).

Similar effects are also shown in Figure 53, where the BCR is plotted vs. the depth in inches to the first reinforcement layer. The bearing capacity ratio, BCR, is defined herein as the bearing capacity of the reinforced section to the bearing capacity of the unreinforced section (after Reference 22). Figure 53 shows that the BCR is much greater for the reinforcement at shallower depths than for the reinforcement at greater depths. In both the 3CP and the 6CP tests, a general falling off of the BCR occurs as the depth of the first layer increases. The same trend is apparent for tests with two layers of reinforcement and for the grid reinforcement. In fact, for those two situations, the decrease of BCR with increasing depth is much greater than for the single layer of fabric. The only exception to these trends is with the PS tests, and as mentioned above, it is possible there would be a decrease in BCR if the depth to the first layer was increased sufficiently. In both cases, fabric and grids, the BCR increased from about 1.5 to slightly more than 1.6 as the depth was increased from 1 to 2 inches. When the effect of partial and full fixity of the fabric is considered, it is interesting that the BCR for those two tests was only about 1.7 as opposed to 2.0 or more for the "free" edge test. Why this decrease occurred is not obvious, but from the analysis of Haliburton's test data (References 12 and 13) presented later in this section, it appears that edge conditions and even partial fabric prestress do not significantly influence the bearing capacity at initial yield of the loaded plate.

Also shown in Figure 53 are the results of two series of 6CP tests, "old" and "new" series. The "old" series consisted of tests which were conducted with the 50-kip load cell, and, consequently, the sensitivity of the loads measured left something to be desired. Those tests with fabric at 1-, 2- and 3-inch depths were repeated, and although the observed strengths were somewhat less in terms of BCR, the trends were very similar, which gives one confidence in the overall validity of the data.

e. Effect of Number of Layers of Reinforcement

As shown in Figure 53, the 6CP test conducted with two layers of woven fabric reinforcement indicated somewhat greater BCRs with the spacing and depth

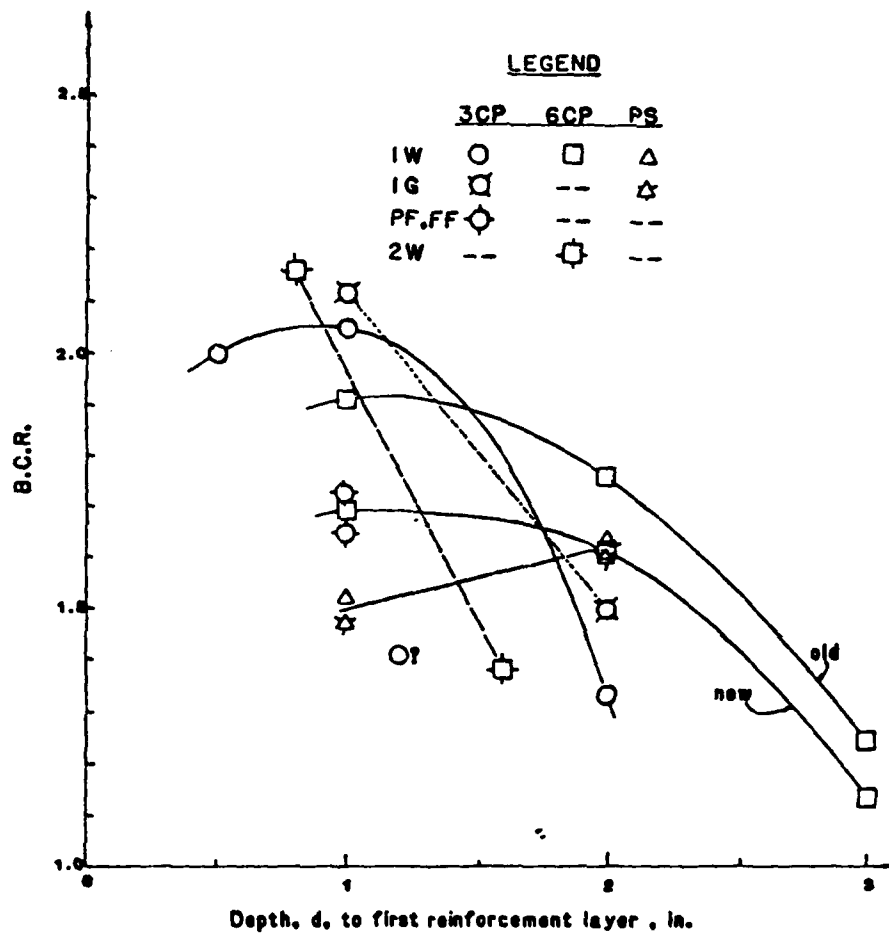


Figure 53. Modified Bearing Capacity Ratio(BCR)vs. Depth of the First Reinforcement Layer.

less than 1 inch, whereas the increase in BCR was about the same for the fabric layers at 4 centimeters or 1.6 inches depth and spacing. We conclude, therefore, that the benefit from two fabric layers is much greater if the depth and spacing of the reinforcement layers are relatively small compared to the diameter of the loaded area. The work by Binquet and Lee (References 21 and 22) suggests that the failure mode that would be observed because of the dimensions of the loaded area and the test box would be "ties pulling out." With short ties, i.e., a limited distance to the edge of the reinforcement, the ties do not mobilize sufficient frictional resistance to actually exceed their breaking strength in tension; rather the ties will simply pull out of the sand bed. This is the type of behavior that we observed, especially when we continued to push the loaded plate into the sand after the initial bearing capacity failure was observed. For evidence of the reinforcement pulling out, see Figure 41.

f. Function of Type of Material

The tests which contrasted the woven fabric with the geogrid reinforcement were the 3CP and PS tests. For the circular plate test, the BCR for the grids was about 3 percent greater than the fabric BCR at $d = 1$ inch, and about 13 percent greater for $d = 2$ inches. For the plane strain test, the reverse was true; that is, the grids actually had a lower bearing capacity than their woven counterparts at both depths, although the differences shown in Table 6 are small. For all practical purposes, the BCRs in plane strain for both types of reinforcement are the same.

g. Effect of Partial and Full-Edge Fixity of the Reinforcement

As shown in Figure 53, edge fixity actually decreased the BCR for the two tests conducted at $d = 1$ inch. This response is surprising because it is difficult to imagine how the edge conditions would influence the initial bearing capacity failure.

Present results will be contrasted with those obtained by Haliburton, et al. (References 12 and 13) later in this section.

h. Scaling Effects

As described earlier, one of the objectives of this research was to determine what the bearing capacity of fabric-reinforced sands would be under typical fighter aircraft loads and tire print sizes. For reasons explained previously, it was not practical to test circular plates of the same size as an aircraft tire print. It is interesting, therefore, to look at the tests in an attempt to "scale upwards" to the approximate 9-inch diameter print size of typical fighter aircraft tires.

Figure 54 shows the maximum load on the plate at failure vs. the ratio of the depth of burial of the reinforcement to the diameter of the loaded plate, or d/D . In the case of the plane strain tests, the ratio of the depth of burial to the width of the plate was used. For the sake of comparison, the theoretical bearing capacity values are indicated along the ordinate by small arrows. It will be recalled that these are the theoretical values calculated for $\phi = 42$ degrees. As in Figure 52, there is a marked increase in maximum load due to the

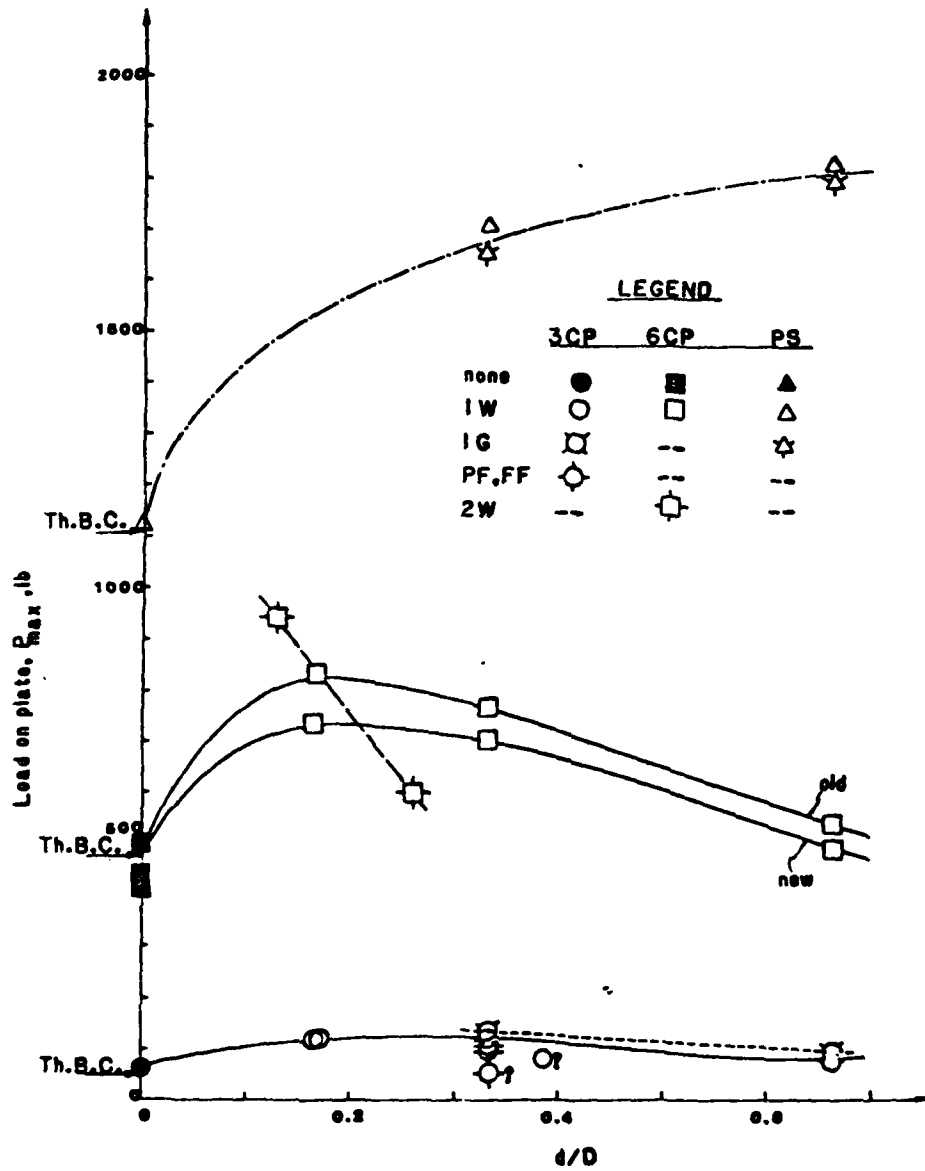


Figure 54. Maximum Load on the Plate at Failure vs. the Ratio of the Depth of Burial to the Reinforcement to the Diameter of the Loading Plate, d/D .

presence of the reinforcement. In every case of d/D , the presence of the reinforcement results in a greater ultimate load than for the unreinforced sand alone for the same size plate. For the case of the plane strain tests, the degree of improvement is significant. In Figure 55, the stress at maximum load, $P_{max}/A_{plate} = q$, is shown vs. d/D . The trends described with respect to Figure 54 are apparent here also.

For comparison purposes, data were extracted from Haliburton, et al. (References 12 and 13) and their data (for a 6-inch plate only) are shown in Figure 55. Shown on the ordinate is a small arrow labeled "Th.B.C." which indicates, as before, the theoretical (unreinforced) bearing capacity. This value is for $\phi = 35$ degrees, and it agrees very well with results in Reference 13. Actually, the trend towards increase in ultimate stress on the plate due to reinforcement is about the same as found in the present study, although there appears to be more scatter in their data.

In Figure 56, the BCR is shown vs. the normalized depth of the reinforcement, d/D . Obviously, for no reinforcement, the BCR is 1.0, so the points for $d/D = 0$ are not shown. The trends as suggested by Figures 54 and 55 are also indicated here. It was expected that the size effect for the circular plate tests would be small, but this is not the case, as shown in Figure 56. The 3CP tests have a higher ultimate BCR than the 6CP test, and from both tests, the BCR decreases as d/D increases. As noted previously, the plane strain test behavior is in the opposite direction. The responses for grids as well as multiple layers are also indicated here. With Figure 56, the benefit of the various reinforcement systems can be easily ascertained as a function of the ratio d/D .

A significant effect of the size of the plate on the BCR has been observed by others. For example, Jarrett (Reference 55) conducted several large-scale laboratory plate bearing tests on peats, and he found a significant difference between tests using a 6-inch diameter plate and those using a 12-inch diameter plate. Thus, using purely geometric scaling to predict the load-carrying capacity of geotextile-reinforced soils is not possible. Apparently other factors affect the results.

For comparison, the results from Haliburton, et al. (References 12 and 13) are shown in Figure 57. Several interesting phenomena are apparent. For one thing, there is a rather large scatter in the BCR for tests at $d/D = 0.5$. For the tests in which the BCR is greater than 1, those values are of the same order of magnitude as found in the present tests. When d/D increases to 1.0, there is actually a loss in efficiency due to the presence of the reinforcement, and this is true also for the 4-inch plates at $d/D = 0.5$. Why this effect occurs is not obvious. If the behavior hypothesis proposed by Haliburton and his colleagues is correct (Section I), then the deeper the initial level of the reinforcement, the less effective it should be. In other words, if the reinforcement is initially at a distance D or greater below the bottom of the footing, the reinforcement has essentially no effect on the deformation and failure pattern of the footing until the footing settles sufficiently, or well past the "ultimate." This effect is seen in the work-hardening of Haliburton's load-settlement curves and by our data in Figure 51. Haliburton's tests were conducted with edge fixity, whereas almost all of the present tests were not. However, Figure 56 shows that edge fixity was not a significant factor in increasing the BCR. For some unknown reason, it may actually cause a decrease in the

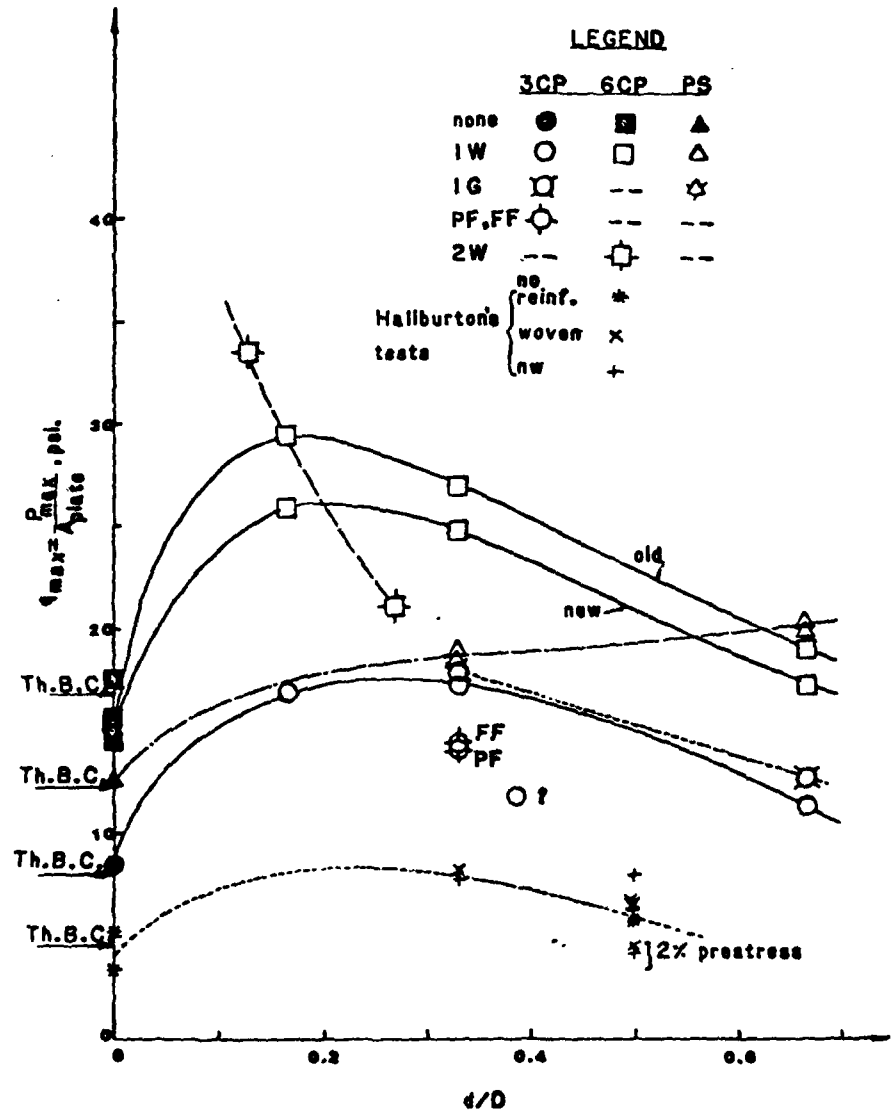


Figure 55. Stress at Maximum Load, q_{max} , vs. the Ratio d/D .

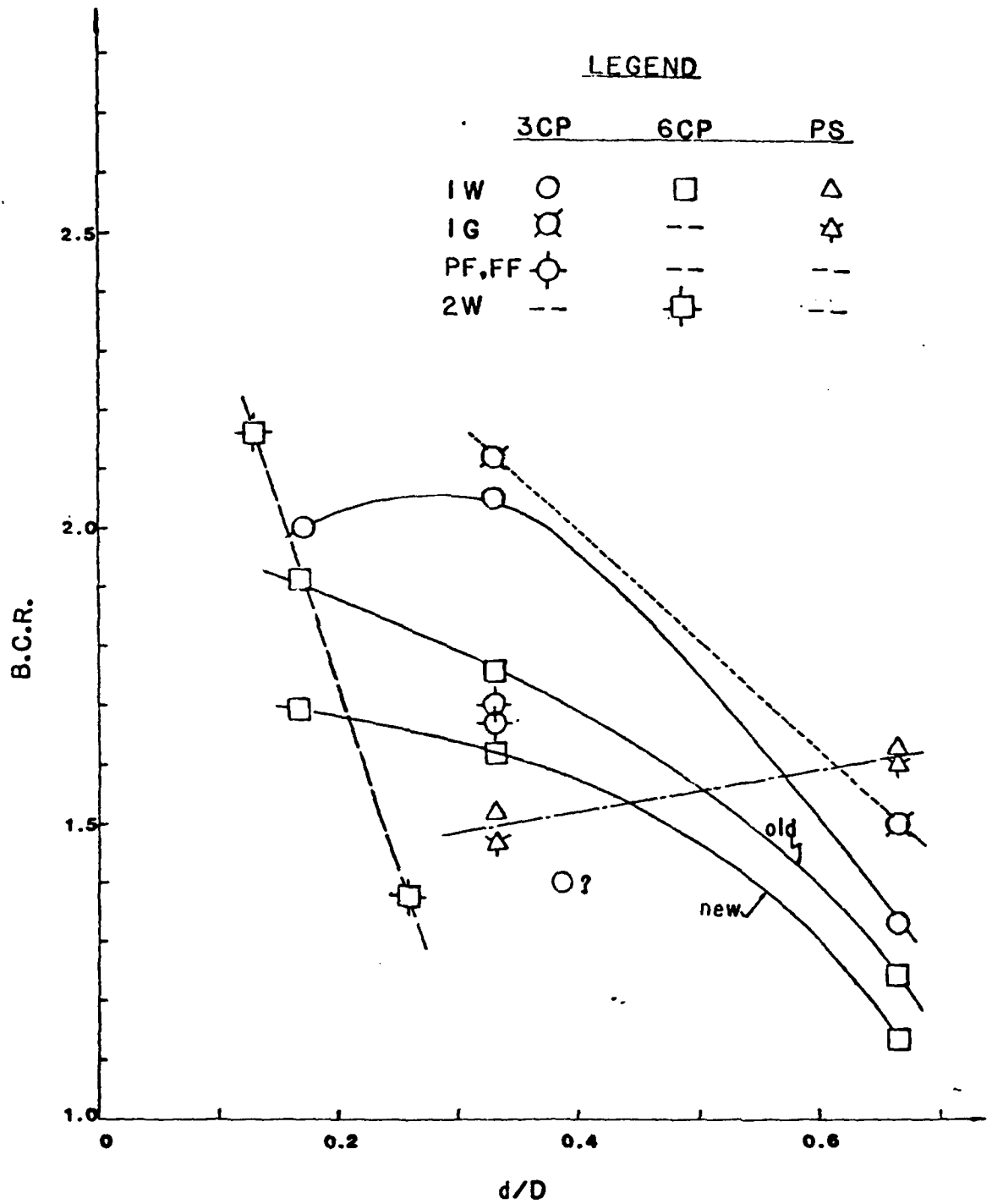


Figure 56. Modified Bearing Capacity Ratio BCR vs. the Ratio d/D.

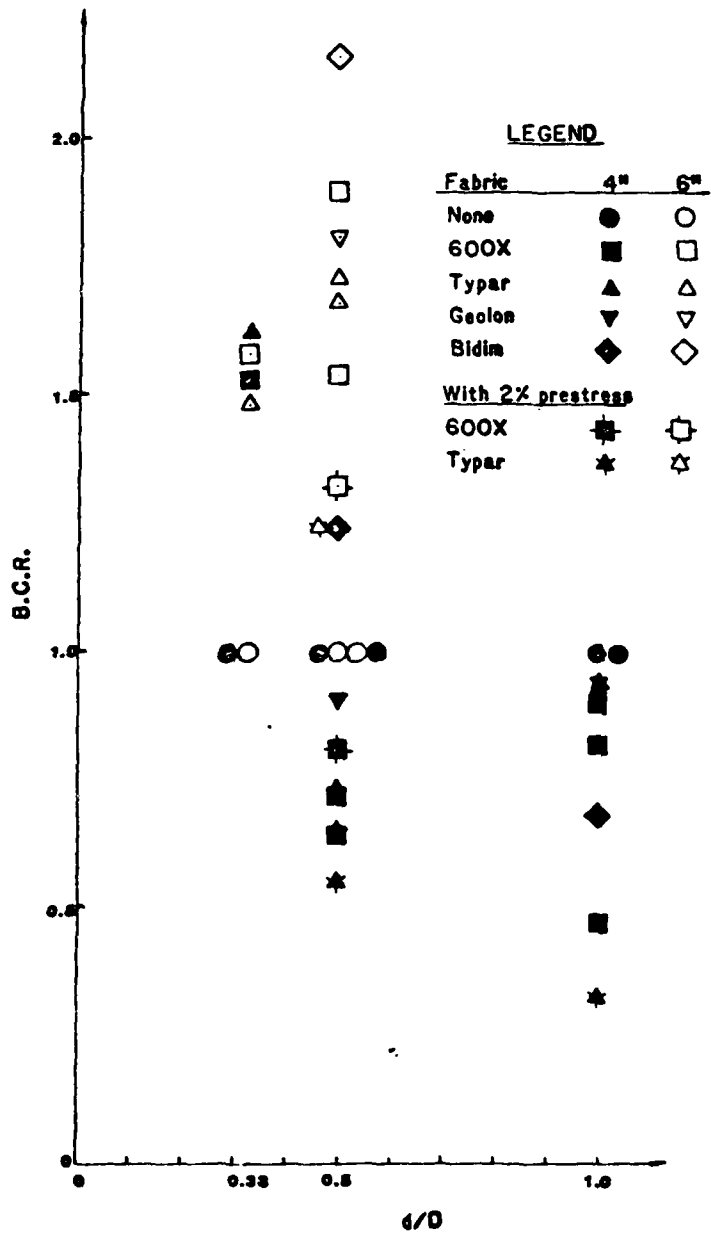


Figure 57. Modified Bearing Capacity Ratio vs. d/D for Test Results Reported in Reference 13.

BCR. It was originally anticipated that Haliburton's tests would provide an upper bound to the level of improvement due to the reinforcement. From the results in Figures 56 and 57, an upper bound is not apparent.

i. Box Size and Edge Effects

In the early stages of this research, the question was raised about the relationship between the size of our loaded plate, at that time 6 inches in diameter, to the width of the test box itself. For those tests, the ratio was about 5. Thus, the test series with the 3-inch diameter plate was planned to assist in scaling to larger plate sizes and to investigate possible edge effects.

During most of the tests, a mechanical dial indicator, accurate to 0.01 millimeters, was placed outside the box with its stem at the elevation of the reinforcement. During loading, the deflection of the wall of the box was noted. In the case of the 6CP and PS tests, the maximum observed deflection was between 0.2 and 0.35 millimeters. No wall movement was detected in any of the 3CP tests. It was apparent that the observed movements correlated directly with the loading. That is, as the load was increased, the deflection would increase until the maximum value was reached at approximately the time of initial bearing capacity failure.

Because the observed movements were so small, it is felt that any edge effects could be considered negligible.

j. Haliburton's "Optimum Depth" Concept

As described in Section I, Haliburton and his associates (References 12 and 13) proposed a concept of "optimum depth" for explaining the increase in bearing capacity due to the presence of the reinforcement. They suggested that the optimum depth of the fabric should be at $0.5 B \tan \phi$. For the present study, the most probable $\phi = 42$ degrees, so the "optimum depth" for the 3CP tests would be 1.35 inches and for the 6CP tests 2.7 inches. These values correspond to a d/D ratio of 0.45 for each case. The results in Figures 52 through 56 indicate that the "optimum depth," if it exists, is less than this value, perhaps even less than $1/3 D$. In a practical sense, however, there are severe limitations to the minimum depth of placement of the reinforcement, even if it could be shown that the "optimum depth" is $1/3 D$ or less. A practical minimum placement depth is probably about 1 inch or perhaps deeper, especially if ordinary construction equipment is employed for the placement of the top sand layer. Considering this limitation, then the "optimum depth" of placement that Haliburton found is not unreasonable for typical tire print sizes.

k. Deflection Basin Measurement and Rut Development

It was of some interest to determine the shape of the deflected surface of the sand. These results are shown in Figures 58, 59 and 60, for the 3CP, 6CP and PS tests, respectively. In these figures, the surface deflection in thousandths of an inch is shown vs. the distance from the center line of the plate. On the top of each figure, small arrows A through E are indicated. These positions correspond to the locations of the UCDTs described earlier (see

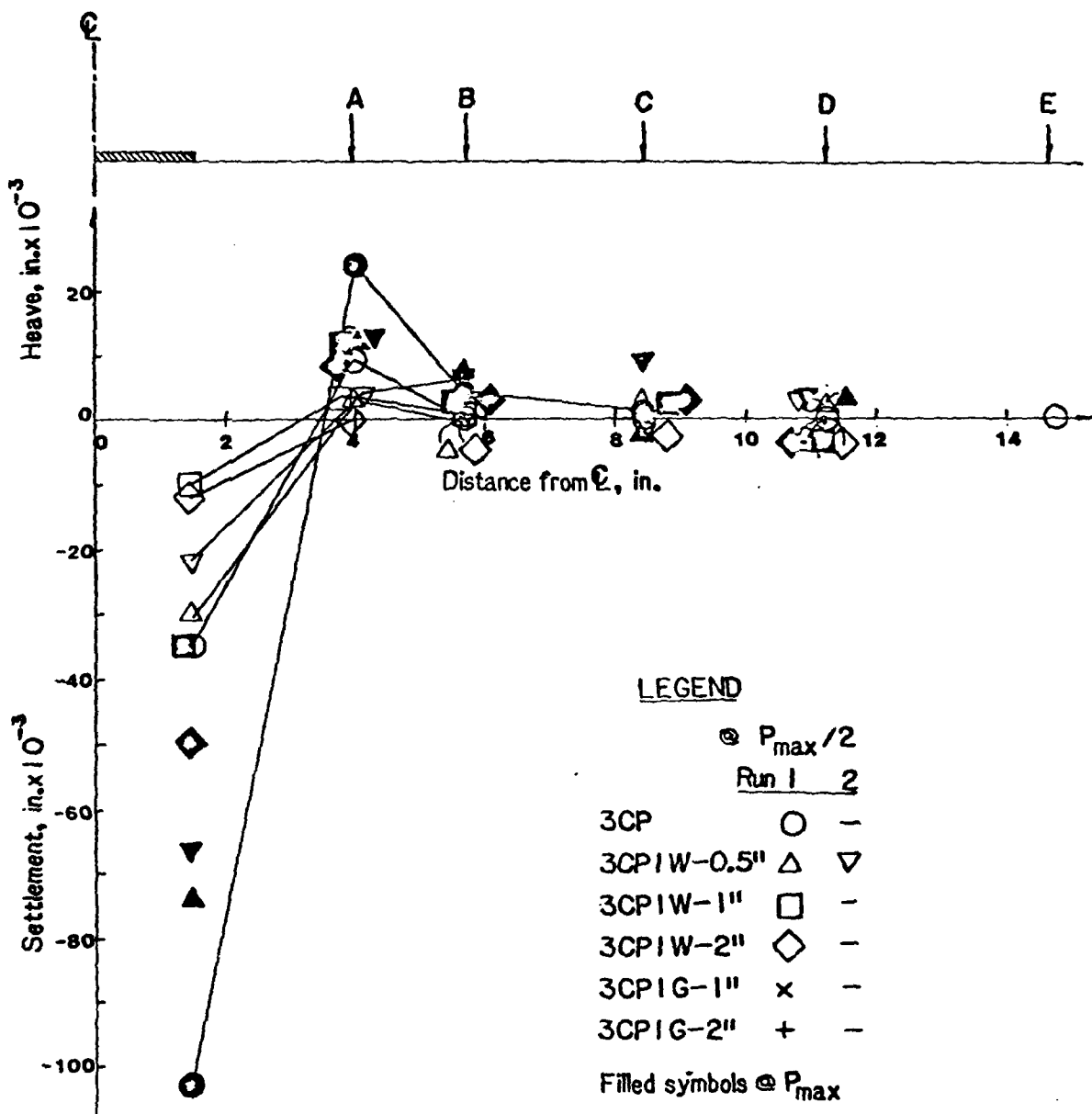


Figure 58. Shape of Deflection Basin for the 3CP Tests.

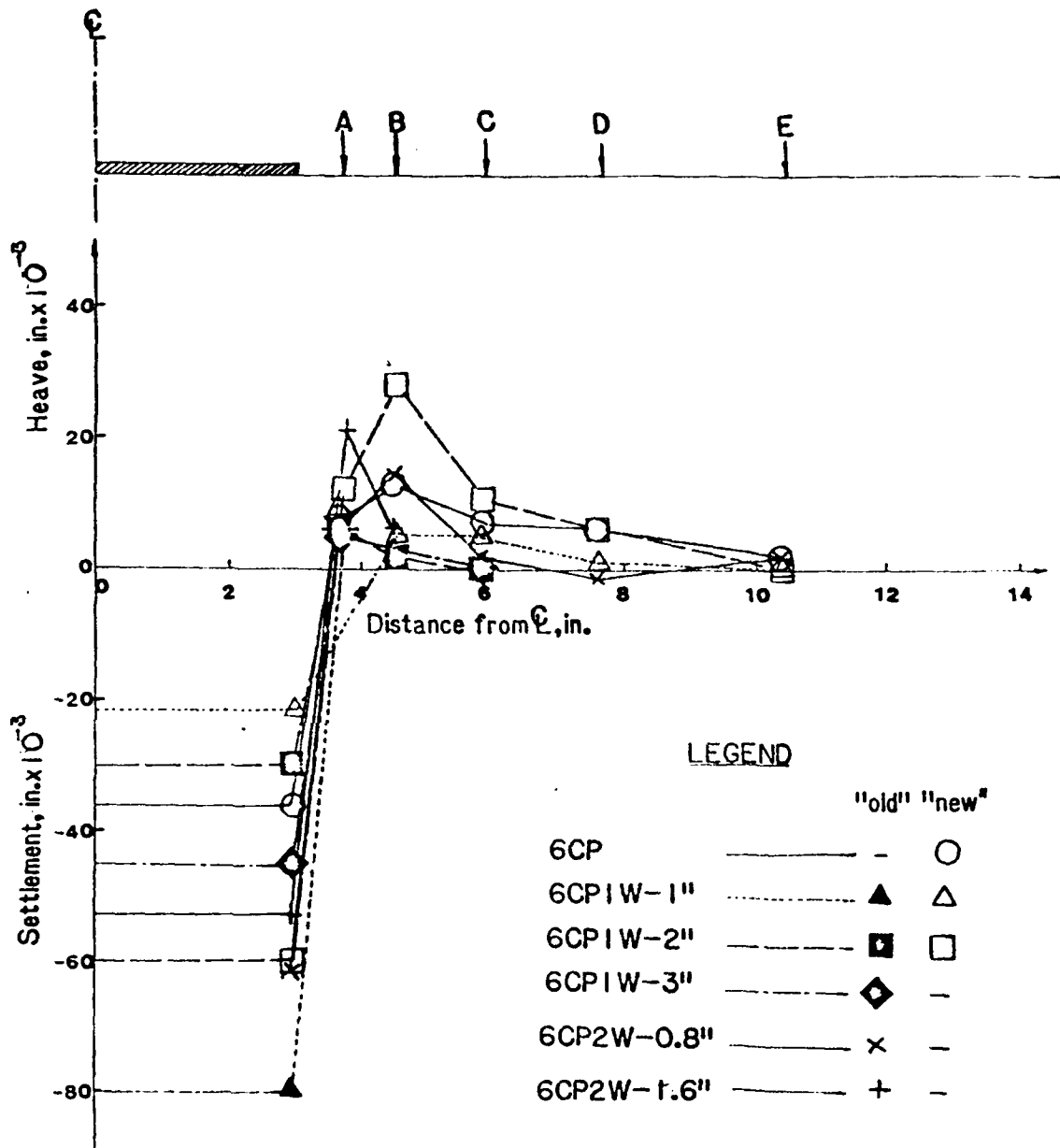


Figure 59. Shape of Deflection Basin for the 6CP Tests.

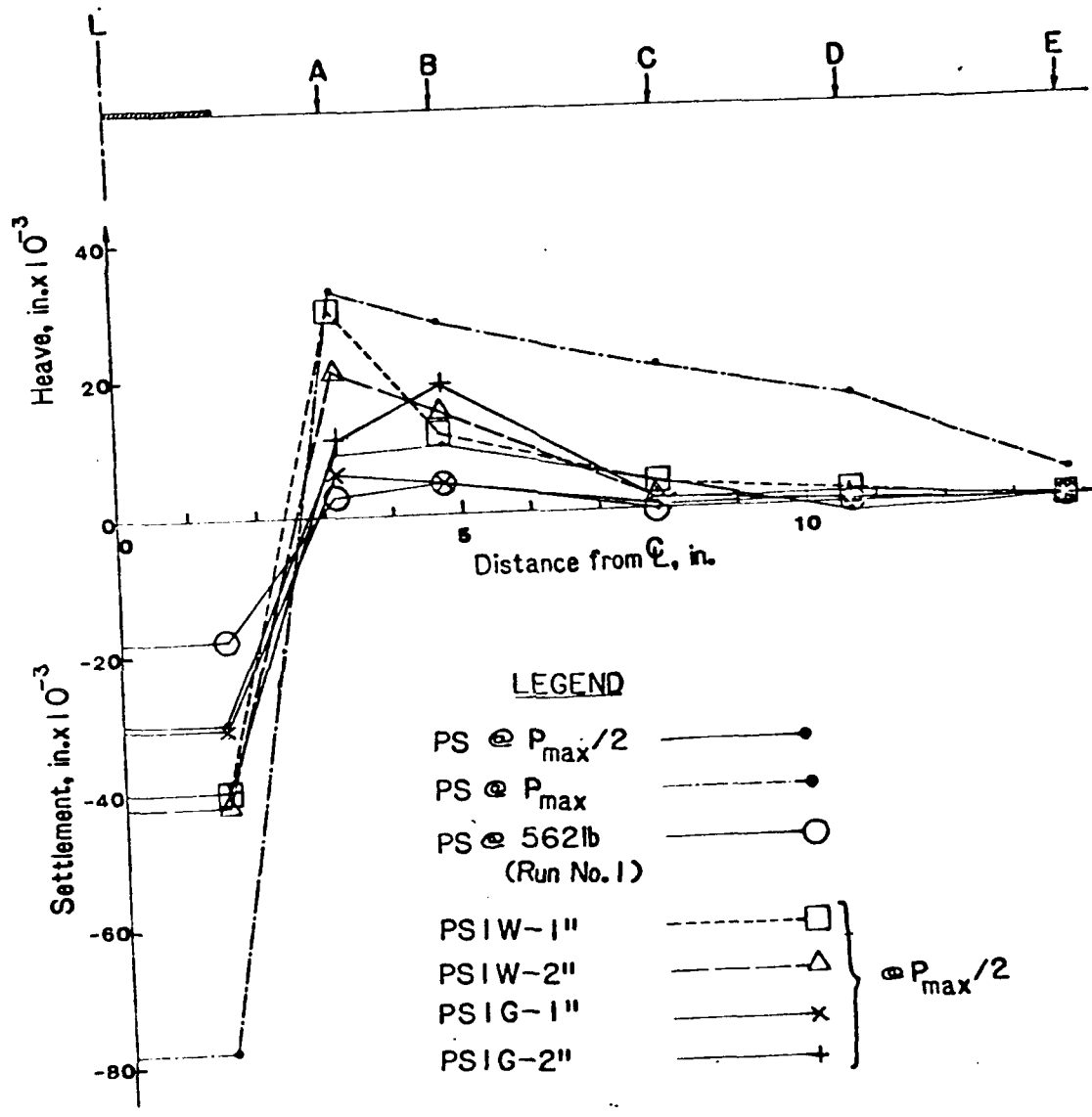


Figure 60. Shape of Deflection Basin for the PS Tests.

Figure 26). In all cases, the deflections were determined at one-half of the load on the plate at first yielding. Considering the rather small deflections measured (in many cases, only a few thousandths of an inch), the data are remarkably consistent. It is difficult, however, to see any significant effect of the different reinforcement configurations other than that there is some improvement, i.e., some decrease in deformation, because of the presence of the reinforcement. Apparently, the stress field is changed by the presence of the reinforcement well before yielding or "failure" occurs. This is consistent with the strain diffusion hypothesis presented in Section II.

Note that the shapes of the deflected surfaces are similar to those shown in Figures 8 through 14 for the strain diffusion hypothesis (Section II). However, deflection profiles in those figures are in terms of relative deflection (relative to the deflection of the rigid plate). Therefore, an attempt was made to normalize the deflection measurements in Figures 58 through 60. These data are shown in Figures 61 and 62. They correspond to the 3CP and PS deflection data given previously. (Because of the difficulty of interpreting the normalized 3CP deflection results for Figure 61, a similar normalization procedure was not attempted for the 6CP tests.) In these figures, the deflection at $P_{max}^2/2$ was normalized for the various reinforcement configurations with respect to the plate settlement at maximum load, which occurs just before the plate plunges into the subgrade sand. The data are remarkably consistent in the plane strain tests (Figure 62). However, this was not the case for the 3CP tests.

It can be determined from Figure 14 that the maximum theoretical heave is 0.2 at $x/a = 3$. Figure 61 shows that for the 3-inch diameter plate, a relative deflection (heave) of 0.2 occurs at $r/D = 1.3$, which is equivalent to $x/a = 2.6$, or very close to the theoretical maximum at $x/a = 3$. For the 6-inch diameter plate, the maximum relative deflection (heave) was 0.42, and it occurred at $x/a = 1.5$. The difference between the 3CP and 6CP behavior is probably related to some unknown scaling effect of plate diameter, as described earlier in this section.

As the operational criteria of some aircraft specifies ruts to be less than about 1 inch in depth, it was of interest to determine what the load would be at 1 inch depth for the various loading plate sizes and reinforcement configurations. In some cases, the nature of the load-settlement curves and the limitations of the instrumentation made it impossible to determine exactly what the load was at a settlement of 1 inch. But a few general conclusions can be drawn from the data that do exist (see Table 6).

In a large number of cases, there really was very little difference between P_{max} (load at initial yield) and P at $s = 1$ inch. This observation was true independently of whether the fabric or grid reinforcement was used. However, this was not true for the cases with partial and full fixity. The estimated P at $s = 1$ inch was at least twice that of P_{max} . These observations tend to verify the observations of Haliburton, et al. (References 12 and 13). They found a significant "work hardening" of the load-deflection relationship after substantial (0.3 to 0.5 D) sinkage of the loading plate took place. If the fabric is "fixed" at the edge and placed relatively close to the surface of the sand, then it could be expected that significant increase in bearing capacity and decrease in deformations before failure would occur (see Sections I.3, III.5.h, and III.5.j of this report).

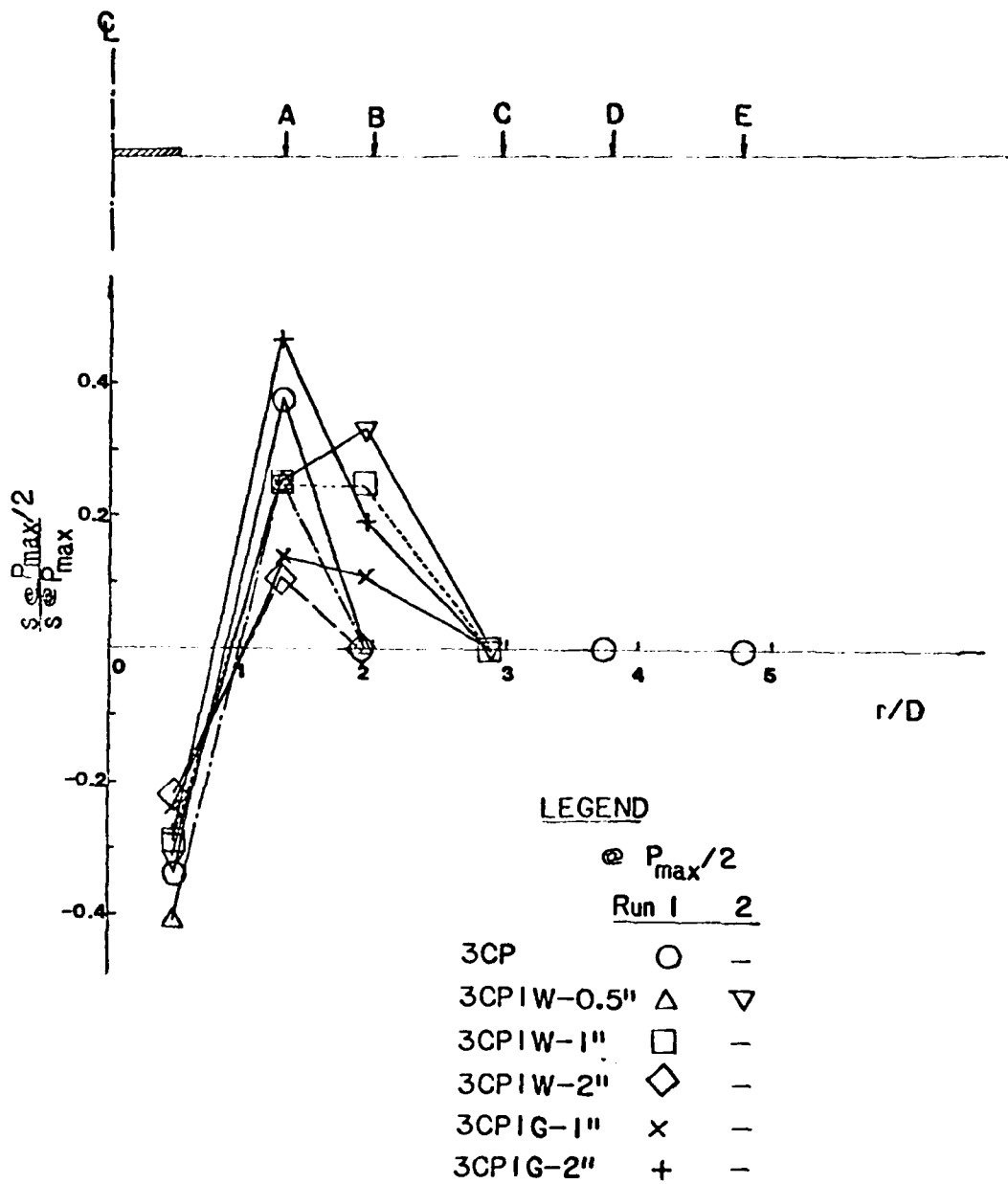


Figure 61. Normalized Deflection Basin Measurements for the 3CP Tests.

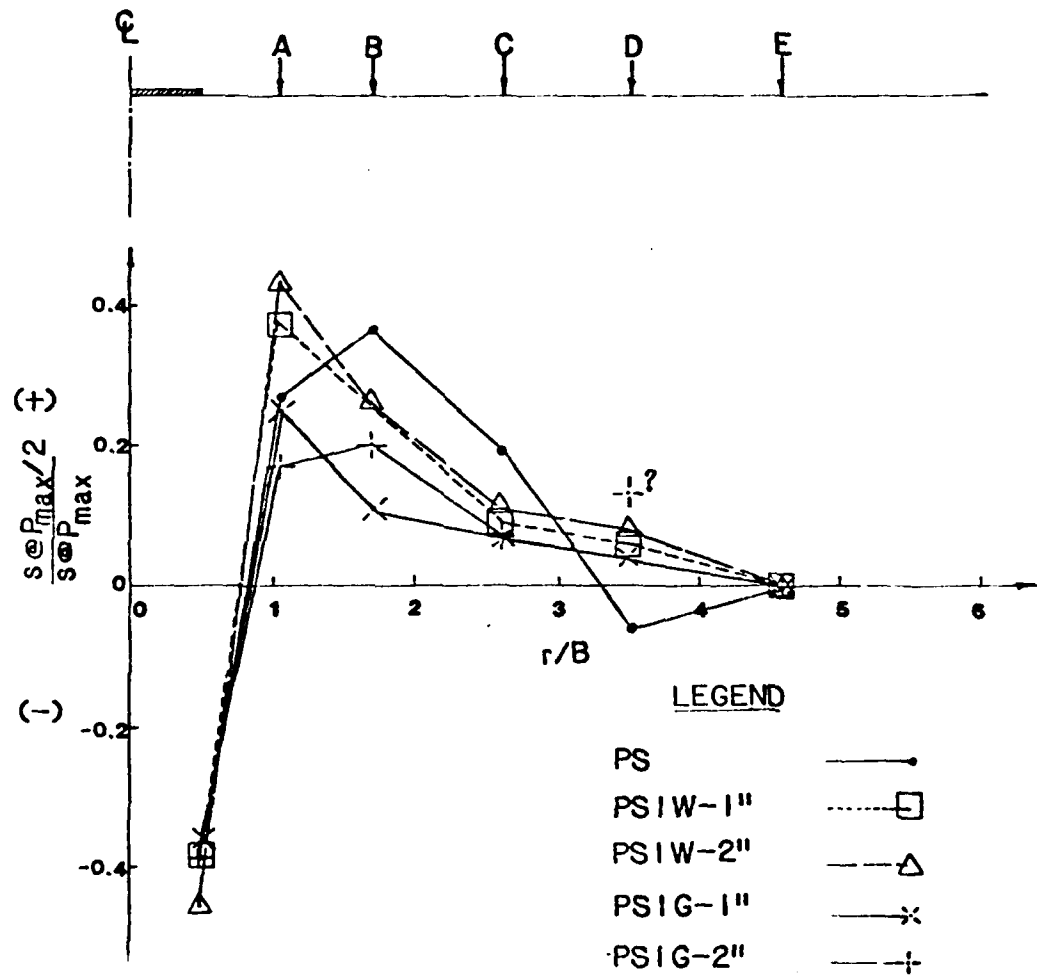


Figure 62. Normalized Deflection Basin Measurements for the PS Tests.

In several "reinforced" tests, loading was continued well past the initial failure so that the loading plate penetrated 2 inches or more into the subgrade. Then the top layer of sand was carefully excavated and the reinforcement removed. Significant depressions in the exposed sand surface were observed (see, for example, Figure 35). In contrast, Haliburton, et al. (References 13, p. 72) reported finding no such permanent deformation below the level of the reinforcement. The difference between present test observations and those by Haliburton was probably the result of the edge fixity in his tests, but this is only speculative.

SECTION IV

IMPLICATIONS FOR ALTERNATE LAUNCH AND RECOVERY SURFACES

The experimental and analytical investigations described in the previous two sections have rather important implications for the design and construction of alternate launch and recovery surfaces. This statement is made in spite of the fact that none of the reinforcement configurations actually tested would be able to support present military aircraft on unpaved but reinforced surfaces constructed of dense sands. The results, however, do point the way towards several practical techniques which could significantly enhance the bearing capacity of unpaved surfaces and may ultimately provide economic ALRS systems.

With the exceptions discussed in Section III, the test results presented herein tend to verify the conclusions of Haliburton, et al. (Reference 13) as to the effect of lateral restraint reinforcement where membrane-type support is not expected. However, if a very soft subgrade exists, then one would expect the greatest effect of the membrane to be realized. This was shown theoretically by Bourdeau, Harr and Holtz (Reference 44; see Section I and Appendix A), but it could not be verified experimentally in the present series of tests because only dense sands, not soft clays, were tested.

The important effect of geometry, that is, the depth of placement of the first layer of reinforcement, as well as the effect of multiple layers of reinforcement, was shown. However, the concept of a "critical depth" of reinforcement at $0.5 B \tan \phi$, was not verified, although the data are not sufficiently precise to recommend an alternate numerical value of "critical depth." If it exists, it probably is less than $0.5 B \tan \phi$ or about $1/3 B$.

The requirement of sufficient depth of cover for proper fabric anchorage is apparently not as critical as had been originally thought. From the tests reported in Section III, even shallow depths of cover are sufficient to develop fabric frictional resistance. This result is shown even with the "lower bound" tests with no edge fixity in comparison with the results of partial and full fixity at the same depth of fabric. This observation has important practical implications. In the field, the depth of cover to the first reinforcement layer can be relatively shallow, depending on the depth required to develop sufficient bearing capacity versus the practical consideration of how to actually construct a thin layer of sand over a geotextile. This means that the fabric can be placed at a relatively shallow depth, contingent only upon practical construction constraints, and not contingent upon the requirement of a sufficient depth of burial to develop fabric frictional resistance. The value of the geotextile reinforcement is apparently much greater for ALRS installations, which are only required to support a relatively few operations before excessive surface deformation or rutting may occur. Excessive surface deformation indicates that a bearing capacity "failure" has occurred and that the soil exists in a state of plastic equilibrium. Thereafter, there will be little or no increase in bearing capacity, even with very large deformations.

Based on the results presented herein, the system most likely to be successful as a reinforcement system for ALRS would be multiple layers of a heavy geotextile or geogrid with the depth to the top layer as small as can be practically constructed. The minimum depth should be on the order of 1 inch or less

if it is possible to construct such a thin layer, although scaling upward to aircraft tire sizes may alter this recommendation. Construction problems will exist also with the requirement for multiple layers of reinforcement. Specific design rules for ALRS systems as well as specification of the desired fabric properties are not possible at this time without the results of experiments similar to those proposed for Phase II of this effort (Section V).

SECTION V

OUTLINE OF PLANS FOR PHASE II RESEARCH

It was originally envisioned that the laboratory and analytical portions of the research would allow a program of full-scale field tests to be planned and carried out as a second phase of the research. The program would assess the validity of the analytical relationships developed in Phase I and would gather additional experimental evidence on the performance and economics of selected soil reinforcement systems.

1. FIELD TESTS

Full-scale model tests of a limited number of fabric-reinforced runway systems would be constructed. These test sections would be constructed to simulate actual field installation procedures. The size of the test sections would depend on the place where the tests were carried out. If conducted at the USAE Waterways Experiment Station, Vicksburg, Miss., then test sections on the order of 20 feet wide by 150 feet long are possible, as indicated by Webster (References 36 and 37). Thus, five different test sections, each 30 feet long, could be investigated. At WES it is possible to have test sections on both very soft clay (CBR < 1) subgrades or subgrades of loose sands and silts. It is recommended that a sand subgrade be utilized initially. One section would be unreinforced as a control, and the other sections would consist of different types and geometries of reinforcement. The test sections would be instrumented for vertical and horizontal deformations. Inductance-type soil strain gages would be attached to the reinforcement so that horizontal deformations could be determined (Reference 56). Settlement profiles could be determined either by cross-sectional surveys or transverse settlement gages (Reference 57). The response of the various reinforced systems would be obtained by use of the F-4 load cart. The cart would be repeatedly towed over the control and reinforced sections until either subgrade failure or deep rutting of the surface occurred. Prior to failure, surface deflections would be obtained by the traveling laser beam system developed by Elton (Reference 58) presently at WES. In this manner, the number of passes of the F-4 load cart could be correlated with performance of the reinforced sections. The observations would verify predictions of prototype performance under full-scale traffic conditions and allow empirical corrections to be made to design procedures developed from the analytical and experimental work conducted in Phase I of the research.

2. ADDITIONAL LABORATORY AND ANALYTICAL INVESTIGATIONS

A limited series of laboratory investigations should be carried out as part of the Phase II research program. Additional plate load experiments should be carried out on (a) clay subgrades and (b) on the geogrids with coarse granular material such as pea gravel utilized for the top surface layer. As mentioned previously, one of the advantages of geogrid reinforcement is in their ability to interlock coarser granular particles to provide tensile resistance, in addition to increased frictional resistance. Additional multiple-layer reinforcement systems should also be investigated to supplement previous research. Tests on soft clay subgrades would enable behavior and performance to be extended to a wide variety of natural soil types.

3. ADDITIONAL ANALYTICAL WORK

The potential of the strain diffusion theoretical development described in Section II has barely been realized. Work on this aspect was begun rather late in the project and, consequently, it could not be completed in the time remaining. This technique is not only applicable to ALRS and other pavement systems but also to an entire class of foundation (settlement) problems. The possibility of being able to avoid having to determine or estimate traditional constitutive relations for a wide variety of soils is extremely attractive. It is therefore recommended that additional analytical work also be carried out as part of Phase II.

SECTION VI

CONCLUSIONS AND RECOMMENDATIONS

1. CONCLUSIONS

- a. Significant increases in bearing capacity due to both the depth of the reinforcement and the number of reinforcement layers were observed. However, the improvement effect decreased as the depth of the first layer increased.
- b. As observed by others, a strain-hardening effect due to the presence of the reinforcement was also observed in these tests.
- c. At shallow depths of reinforcement, an increase in the modulus of subgrade reaction was observed.
- d. The concept of a "critical depth," if it exists, was found to be somewhat less than $0.5 B \tan \phi$; it is probably about $1/3 B$ (or $1/3 D$).
- e. For the geometries tested, behavior of reinforcement systems in terms of maximum load on the plate and bearing capacity ratio when loaded in plane strain was the opposite of that observed for the circular plate tests.
- f. Based on a limited series of tests, edge fixity conditions are not considered to be important. The bearing capacity tended to decrease for these tests.
- g. The benefit of multiple-reinforcement layers is greater if the depth and spacing are relatively small with respect to the diameter of the loaded area.
- h. The behavior and degree of improvement using geogrids were about the same as with the woven polyester, even though the grids have a significantly greater tensile strength and modulus than the geotextile. This difference was probably due to the lack of any contribution of "interlock" with the sand used in the tests.
- i. Geometric scaling of load, bearing capacity, etc. was not possible; apparently factors other than diameter of loaded plate influence the response of geotextile-reinforced systems.
- j. Surface depression profiles due to the loaded plate could be predicted approximately from the strain-diffusion hypothesis developed in Section 2.

2. RECOMMENDATIONS

Recommendations for additional research in earth reinforcing were outlined in Section V. Full-scale reinforcing systems should be tested under prototype loading conditions. Construction problems, as well as field performance, can be modeled adequately to effectively permit prediction of prototype behavior.

Some additional laboratory and analytical work, also outlined in Section V, is desirable before site-specific design procedures for fabric-reinforced ALRS systems can be finalized.

REFERENCES

1. Wager, O. and Holtz, R. D., "Reinforcing Embankments by Short Sheet Piles and Tie Rods," New Horizons in Construction Materials, pp. 177-186. Envo Publishing Company, Lehigh Valley, PA, 1976.
2. Holtz, R. D., "Modern Corduroy and Fascine for Vehicle and Construction Mats," New Horizons in Construction Materials, pp. 225-236. Published by Polyteknisk Forlag, Copenhagen, Denmark, 1975.
3. Holtz, R. D., "Special Applications--Earth Reinforcing," State-of-the-Art Report, Proceedings of the Symposium on Earth Reinforcing, ASCE, Pittsburgh, pp. 77-97, 1978.
4. Holtz, R. D., "Laboratory Studies of Reinforced Earth Using a Woven Polyester Fabric," Proceedings of the International Conference on the Use of Fabrics in Geotechnics, Paris, Vol. I, pp. 113-117, 1977.
5. Salomone, W. G., "A Soil-Reinforcement Interaction Model," Ph.D. Thesis, Purdue University, 1978.
6. Holtz, R. D., "Recent Developments in Reinforced Earth," Proceedings of the 7th Scandinavian Geotechnical Meeting, pp. 281-291, published by Polyteknisk Forlag, Copenhagen, Denmark, 1975.
7. Holtz, R. D. and Massarsch, K. R., "Improvement of the Stability of an Embankment by Piling and Reinforced Earth," Proceedings of the VI European Conference on Soil Mechanics and Foundation Engineering, Vienna, Vol. 1.2, pp. 473-478, 1976.
8. Haliburton, T. A., Anglin, C. C. and Lawmaster, J. D., Selection of Geotechnical Fabrics for Embankment Reinforcement, Report to U.S. Army Engineer District, Mobile, Oklahoma State University, Stillwater, 1978.
9. Haliburton, T. A. and Fowler, J., "Design and Construction of Fabric Reinforced Embankments," The Use of Geotextiles for Soil Improvement, ASCE Convention, Portland, Oregon, pp. 89-118, April, 1980.
10. Fowler, J., Design, Construction and Analysis of Fabric-Reinforced Embankment Test Section at Pinto Pass, Mobile, Alabama, Technical Report EL-81-7, U.S.A.E. Waterways Experiment Station, Vicksburg, Mississippi, 1981.
11. Haliburton, T. A., Anglin, C. C. and Lawmaster, J. D., "Testing of Geotechnical Fabric for Use as Reinforcement," Geotechnical Testing Journal, ASTM, Vol. 1, No. 4, pp. 203-212, 1978.
12. Haliburton, T. A. and Lawmaster, J. D., "Experiments in Geotechnical Fabric-Reinforced Soil Behavior," Geotechnical Testing Journal, ASTM, Vol. 4, No. 4, pp. 153-160, 1981.

13. Haliburton, T. A., Lawmaster, J. D. and King, J. K., Potential Use of Geotechnical Fabric in Airfield Runway Design, Report to U.S. Air Force Office of Scientific Research, Oklahoma State University, Stillwater, p. 121, 1980.
14. Vidal, H., "La Terre Armee," Annales de l'Institute Technique de Batiment et des Travaux Publics, No. 223-224, 1966.
15. Schlosser, F. and Vidal, H., "La Terre Armee," ("Reinforced Earth,") Bulletin de Liaison des Laboratoires Ponts et Chaussees, No. 41, pp. 101-144, 1969. English translation by the authors, 44 pp.
16. Hausmann, M. R. and Lee, I. K., "Strength Characteristics of Reinforced Soil," New Horizons in Construction Materials, pp. 165-176. Envo Publishing Company, Lehigh Valley, PA, 1976.
17. Juran, I. and Schlosser, F., "Theoretical Analysis of Failure in Reinforced Earth Structures," Proceedings of the Symposium on Earth Reinforcing, ASCE, Pittsburgh, pp. 528-555, 1978.
18. Bell, J. R., Greenway, D. R. and Vischer, W., "Construction and Analysis of a Fabric Reinforced Road Embankment," Proceedings of the International Conference of the Use of Fabrics in Geotechnics, Paris, Vol. 1, pp. 71-76, 1977.
19. Broms, B. B., "Polyester Fabric as Reinforcement in Soil," Proceedings of the International Conference on the Use of Fabrics in Geotechnics, Paris, Vol. I, pp. 129-135, 1977.
20. Bassett, R. H. and Last, N. C., "Reinforcing Earth Below Footings and Embankments," Proceedings of the Symposium on Earth Reinforcing, ASCE, Pittsburgh, pp. 202-231, 1978.
21. Binquet, J. and Lee, K. L., "Bearing Capacity Analysis of Reinforced Earth Slabs," Journal of the Geotechnical Engineering Division, ASCE, Vol. 101, No. GT12, pp. 1241-1255, 1975.
22. Binquet, J. and Lee, K. L., "Bearing Capacity Analysis of Reinforced Earth Slabs," Journal of the Geotechnical Engineering Division, ASCE, Vol. 101, No. GT12, 1257-1276, 1975.
23. Koerner, R. M. and Welsh, J. P., Construction and Geotechnical Engineering Using Synthetic Fabrics, Wiley, New York, 1980.
24. Koerner, R. M. and Welsh, J. P., "Construction and Geotechnical Engineering Using Synthetic Fabrics (Geotextiles)," Supplementary Course Notes for ASCE Continuing Education Course, Revision No. 5, p. 66, (unpublished), 1981.
25. Bender, D. A. and Barenberg, E. J., "Design and Behavior of Soil-Fabric-Aggregate Systems," Transportation Research Record No. 671, 1978.

26. Kinney, T. C., "Fabric Induced Changes in High Deformation Soil-Fabric-Aggregate Systems," Ph.D. Thesis, University of Illinois at Urbana, Champaign, 1979.
27. Kinney, T. C. and Barenberg, E. J., "Soil Movement in Geotextile Reinforced Roads," The Use of Geotextiles for Soil Improvement, Preprint 80-177, ASCE Convention, Portland, Oregon, pp. 119-141, April, 1980.
28. Lai, J. S. and Robnett, G. L., "Design and Use of Geotextiles in Road Construction," Proceedings of the 3rd Conference, Road Engineering Association of Asia and Australia, Taipei, 1981.
29. Giroud, J. P. and Noiray, L., "Design of Geotextile-Reinforced Roads," Journal of the Geotechnical Engineering Division, ASCE, Vol. 107, No. GT9, pp. 1231-1254, 1981.
30. Sivakugan, N., "Design Charts for Geotextile Reinforced Unpaved Roads," unpublished term paper, Purdue University, May, 1982.
31. Hamilton, J. H. and Pearce, R. A., Guidelines for Design of Flexible Pavements Using Mirafi woven Stabilization Fabrics, Report to the Celanese Corporation, Law Engineering Testing Company, Houston, p. 47, 1981.
32. Burns, C. D. and Barber, V. C. (1969), Expedient Surfacing and Drainage of Roads, Streets, and Parking and Storage Areas in Theater of Operations, Report 1, U.S.A.E. Waterways Experiment Station, Vicksburg, Mississippi, Misc. Paper S-69-11, 1967.
33. Burns, C. D. and Barber, V. C., Expedient Surfacing and Drainage of Roads, Streets, and Parking and Storage Areas in Theater of Operations, Report 2, U.S.A.E. Waterways Experiment Station, Vicksburg, Mississippi, Misc. Paper S-69-11, 1971.
34. Webster, S. L., Construction of Sandbag Bridge Abutments, unpublished report, U.S.A.E. Waterways Experiment Station, Vicksburg, Mississippi, 1970.
35. Webster, S. L. and Alford, S. J., Investigation of Construction Concepts for Pavements Across Soft Ground, Technical Report S-78-6, U.S.A.E. Waterways Experiment Station, Vicksburg, MS 1978.
36. Webster, S. L., Investigation of Beach Sand Trafficability Enhancement Using Sand-Grid Confinement and Membrane Reinforcement Concepts, Report 1, Sand Test Sections 1 and 2, Technical Report GL-79-20, U.S.A.E. Waterways Experiment Station, Vicksburg, Mississippi, 1979.
37. Webster, S. L., Investigation of Beach Sand Trafficability Enhancement Using Sand-Grid Confinement and Membrane Reinforcement Concepts, Report 2, Sand Test Sections 3 and 4, Technical Report GL-79-20, U.S.A.E. Waterways Experiment Station, Vicksburg, Mississippi, 1981.
38. Rankilior, P. R., Membranes in Ground Engineering, Wiley, London, 1981.

39. McNerney, M. T., Interim Field Procedure for Bomb Damage Repair, Report ESL-TR-79-01, Air Force Engineering and Services Center, Tyndall AFB, Florida, 1979.
40. Cooksey, D. L., Bomb Crater Repair Techniques for Permanent Airfields, Report I, Series I Tests, Technical Report GL-81-12, U.S.A.E. Waterways Experiment Station, Vicksburg, Mississippi, 1981.
41. Rone, C. L., Sullivan, A. L. and Shamburger, J. H., Evaluation of Materials for Contingency Runways, Report CEEDO-TR-78-46, U.S.A.E. Waterways Experiment Station, Vicksburg, Mississippi, 1979.
42. Harr, M. E., Mechanics of Particulate Media, McGraw-Hill, New York, 1977.
43. Harr, M. E., Foundations of Theoretical Soil Mechanics, McGraw-Hill, New York, 1966.
44. Bourdeau, P. L., Harr, M. E. and Holtz, R. D., "Soil-Fabric Interaction - An Analytical Model," Proceedings of the Second International Conference on Geotextiles, Las Vegas, Vol. II, pp. 387-391, August, 1982.
45. Andrawes, K. Z., McGown, A. and Wilson-Fahmy, R. F., "The Behavior of a Geotextile-Reinforced Sand Loaded by a Strip Footing," Proceedings of the VIII European Conference on Soil Mechanics and Foundation Engineering, Helsinki, Vol. 1, May, 1983.
46. Yoder, E. J. and Witzak, M. W., Principles of Pavement Design, Wiley, New York, 1975.
47. Ali, G. A., "A Laboratory Investigation of the Application of Transfer Functions to Flexible Pavements," Ph.D. Thesis, Purdue University, 1972.
48. Holtz, R. D. and Broms, B. B., "Walls Reinforced by Fabrics - Results of Model Tests," Proceedings of the International Conference on the Use of Fabrics in Geotechnics, Paris, Vol. I, pp. 113-117, 1977.
49. Ingold, T. S. and Templeman, J. E., "The Comparative Performance of Polymer Net Reinforcement," Proceedings of the International Conference on Soil Reinforcement, Paris, Vol. I, 1979.
50. Butterfield, R. and Andrawes, K. Z., "An Air Activated Sand Spreader for Forming Uniform Sand Beds," Geotechnique, Vol. 20, No. 1, pp. 97-100, 1970.
51. Brumund, W. F. and Leonards, G. A., "Experimental Study of Static and Dynamic Friction Between Sand and Typical Construction Materials," Journal of Testing and Evaluation, ASTM, Vol. 1, No. 2, pp. 162-165, 1973.
52. Terzaghi, K. and Peck, R. B., Soil Mechanics in Engineering Practice, 2nd Edition, Wiley, New York, 1967.
53. Perloff, W. H. and Baron, W., Soil Mechanics - Principles and Applications, Ronald Press, New York, 1976.

44. Steward, J., Williamson, R., and Mohney, J., Guidelines for Use of Fabrics in Construction and Maintenance Low-Volume Roads, U.S. Forest Service, Portland, Oregon, 1977. Also published as Federal Highway Administration Report No. FHWA-TS-78-205, 1978.
45. Jarrett, P., Statement made at Session 4C: Slopes and Embankments, of the Second International Conference on Geotextiles, Las Vegas, 3 August, 1982.
46. Brown, S. F. and Brodrick, B. U., "Instrumentation for the Nottingham Pavement Test Facility," Transportation Research Record 810, pp. 73-79, 1981.
47. Harr, M. E. and Ng-A-Qui, N. T., Noncontact Nondestructive Determination of Pavement Deflection Under Moving Loads, Report No. FAA-RD-777-127, 1977.
48. Elton, D. L., "Non-Contact, Non-Destructive Pavement Profile, Texture and Deflection Measurements," Ph.D. Thesis, Purdue University, 1982.

(The reverse of this page is blank)

SECOND INTERNATIONAL CONFERENCE ON GEOTEXTILES -
SESSION 4B: UNPAVED ROADS II

APPENDIX A

Las Vegas, U S A

BOURDEAU, P. L.
Federal Institute of Technology, Lausanne, Switzerland
HARR, M. E. and HOLTZ, R. D.
Purdue University, West Lafayette, Indiana, USA

Soil-Fabric Interaction—An Analytical Model

Un modèle analytique d'interaction entre un sol et une membrane géotextile

A new analytical model for soil-membrane geotextile interaction is presented. A qualitative interpretation of the mechanical role of the membrane is proposed using a probabilistic concept for the vertical stress diffusion in a particulate media (Harr, 1977). A generalization is also offered for multilayered geotextile-reinforced systems.

An iterative numerical procedure is used to obtain solutions. Results are presented for a uniformly distributed load and typical values of soil and geotextile properties. The efficiency of the geotextile increases as the aggregate under the membrane becomes more compressible as long as the geotextile is sufficiently strong and possesses sufficient frictional resistance.

Un nouveau modèle est proposé pour analyser l'interaction entre un sol et une membrane géotextile. Il est proposée une interprétation qualitative du rôle mécanique de la membrane, qui utilise un concept probabilistique pour la diffusion des contraintes verticales dans un milieu particulaire (Harr, 1977). Une généralisation est également offerte pour des systèmes renforcés par plusieurs membranes géotextiles.

Une méthode numérique itérative est utilisée pour obtenir des solutions. Des résultats sont présentés pour une charge distribuée uniformément et des valeurs courantes des propriétés du sol et du géotextile. L'efficacité du géotextile accroît avec la compressibilité du sol sous-jacent à la membrane, à condition que le géotextile soit suffisamment résistant et possède une résistance à la friction suffisante.

INTRODUCTION

In order to describe the mechanical behavior of a layered soil system reinforced by a geotextile, the entire range of physical properties of the soil, geotextile, and the load must be considered. Long before the first reinforced earth projects were built, the problem of a soft (silt, water) soil reinforced by a freely spaced flexible but inextensible sheet was solved by Terzaghi and Peckard (1). The solution was later extended by Harrigan and Getraud (2), but very few other closed-form analytical solutions have been formulated. Most of the recent research were applied numerical methods wherein the soil-reinforcement system was represented by a discretized continuum or a discrete finite element method (e.g., Hirschman (3), Hirschman and Baggett (4), and Holtz, et al. (5)). Recently, a three-dimensional procedure for unpaved roads reinforced with geotextiles was proposed by Bourdeau and Holtz (6).

In spite of this progress, it is felt that a better understanding of the problem can be reached by taking into account such factors as, e.g., the random heterogeneity of the subgrade on which the geotextiles are typically used (7,8), and the particulate nature of the soils. The objective of the present study was to consider this latter factor for the two-dimensional, plane stress case.

MATHEMATICAL DEVELOPMENT

The present approach to assess the transmission of soil stress, as though soils compute stresses

using the linear theory of elasticity, the "Boussinesq solution". Such solutions require the existence of a continuum. Harr (8), taking cognizance of the particulate nature of real soils, introduced the concept of "distribution of stress at a point". Given a unit vertical load acting normal to the surface of the soil (Fig. 1a), the vertical normal stress $S_z(x, z)$ at point (x, z) was found to be a Poisson variate, defined by the probability of the soil, with an expected value

$$E[S_z(x, z)] = \frac{1}{2\pi z^2} \exp\left[-\frac{x^2}{2z^2}\right] \quad (1)$$

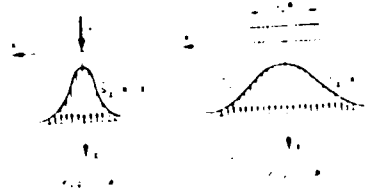
It is noted the coefficient of lateral stress (lateral strain), ν , is related to the coefficient of lateral earth pressure, S_x/S_z , in the solution of the diffusion equation

$$\frac{\partial^2 S_z}{\partial x^2} = 0 = \frac{\partial^2 S_z}{\partial z^2} \quad \text{with} \quad \nu = \frac{\partial S_x}{\partial S_z} \quad (2)$$

and it is seen to be a normal variate with an equivalent mean value of zero and a standard deviation of $\sqrt{2}z$.

For a unit pressure uniformly distributed over a strip of width $2a$ (Fig. 1b) Harr obtained

$$E[S_z(x, z)] = \left(\frac{2-a}{2z}\right) - \left(\frac{a-x}{2z}\right) \quad (3)$$



$$\sigma_z = \frac{P}{\pi} \left[\frac{z}{r^2 + z^2} + \frac{2z^3}{(r^2 + z^2)^2} - \frac{3z}{r^2 + z^2} \right]$$

where σ_z is the vertical stress at depth z from the surface of the road, P is the load, r is the radius of the load, and z is the depth.

The vertical stress at any point in the road is given by the above equation.

$$\sigma_z = \frac{P}{\pi} \left[\frac{z}{r^2 + z^2} + \frac{2z^3}{(r^2 + z^2)^2} - \frac{3z}{r^2 + z^2} \right]$$

For the 1st layer:

$$\sigma_z = \frac{P}{\pi} \left[\frac{z}{r^2 + z^2} + \frac{2z^3}{(r^2 + z^2)^2} - \frac{3z}{r^2 + z^2} \right]$$

$$\sigma_z = \frac{P}{\pi} \left[\frac{z}{r^2 + z^2} + \frac{2z^3}{(r^2 + z^2)^2} - \frac{3z}{r^2 + z^2} \right]$$

It should be noted that the above will be valid only if the capacity of specific materials is known. In other words, the modulus of elasticity of the material.



Consider that a geotextile membrane of infinite extent is used at the interface of two layers, Fig. 3. The layers are characterized by their moduli of elasticity, E_1 and E_2 . A line load of intensity P is applied to the surface, and it is assumed a stress σ_z is induced in the membrane. The membrane is assumed to be of negligible thickness and offers no bending resistance. Assuming small deflections and slopes, vertical equilibrium requires:

$$E_1 \epsilon_1 = E_2 \epsilon_2 = P$$

where ϵ_1 and ϵ_2 are the strains in the two layers, equivalent to a stress σ_z in each layer. The stress between the two layers is assumed to be zero.

$$\sigma_z = \frac{P}{\pi} \left[\frac{z}{r^2 + z^2} + \frac{2z^3}{(r^2 + z^2)^2} - \frac{3z}{r^2 + z^2} \right]$$

where σ_z is the vertical stress at depth z from the surface of the road, P is the load, r is the radius of the load, and z is the depth.

$$\sigma_z = \frac{P}{\pi} \left[\frac{z}{r^2 + z^2} + \frac{2z^3}{(r^2 + z^2)^2} - \frac{3z}{r^2 + z^2} \right]$$

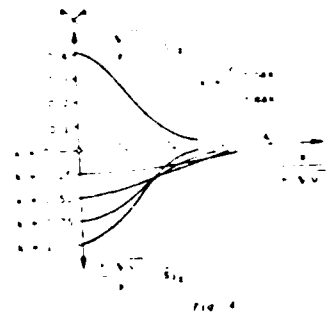
The vertical stress at any point in the road is given by the above equation.

$$\sigma_z = \frac{P}{\pi} \left[\frac{z}{r^2 + z^2} + \frac{2z^3}{(r^2 + z^2)^2} - \frac{3z}{r^2 + z^2} \right]$$

For the 1st layer:

$$\sigma_z = \frac{P}{\pi} \left[\frac{z}{r^2 + z^2} + \frac{2z^3}{(r^2 + z^2)^2} - \frac{3z}{r^2 + z^2} \right]$$

It should be noted that the above will be valid only if the capacity of specific materials is known. In other words, the modulus of elasticity of the material.



Numerical values of the ratio λ are yet to be determined. Its measure is seen to depend upon the deformability of the geotextile and of the underlying soil. Following Rosen and Harr (9) and Nieuwenhuis (10), the underlying soil (layer II) is taken to offer a reaction force being proportional to its deflection (Winkler model), that is:

$$S_2 = k_s h_2 = E_2 w(x) \quad (8)$$

where $w(x)$ is the deflection of the membrane and E_2 is the coefficient of subgrade reaction (Fig. 5).

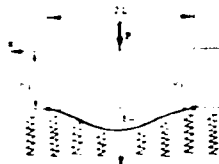


Fig. 5

Thus, for the equilibrium and usage of the membrane as shown in Fig. 4, the respective tangential stresses T_1 and T_2 at all points oppose the direction of the displacement of the membrane. Consequently, we find that:

$$T_1 = E_1 \frac{dw}{dx} \quad T_2 = -E_2 \frac{dw}{dx} \quad (9)$$

where $E_1 = \frac{dF_1}{d\epsilon}$ and $E_2 = \frac{dF_2}{d\epsilon}$

$$\text{and } T_1 = \int_0^x T_1 dx \quad T_2 = \int_0^x T_2 dx$$

The deflection condition is:

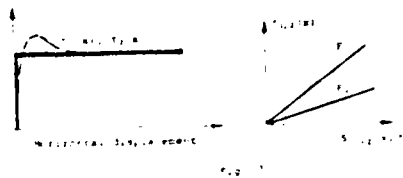
$$\int_0^L \sqrt{1 + \left(\frac{dw}{dx}\right)^2} dx = L = \int_0^L \sqrt{1 + \left(\frac{dw}{dx}\right)^2} dx \quad (10)$$

where E_1 is the elongation modulus $\left(\frac{dF_1}{d\epsilon} = \frac{1}{\epsilon}\right)$ of the membrane and E_2 is the tension in the membrane.



Fig. 6

Model wall tests by Holtz and Bruns (11) and pull-out tests performed with woven polyester fabrics (Kraft, 12) have shown that full frictional resistance of the geotextile is achieved with only small displacements. Accordingly, a rigid-perfectly plastic friction law was adopted to represent the behavior at the soil/fabric interface. Thus, a Mohr-Coulomb yield criterion is introduced for the frictional stresses f_1 and f_2 (Fig. 7).



Thus, the frictional resistance is in proportion to the resultant normal (vertical) stress at the point in question.

If also a ϕ shear strain exists:

$$f_1 = F_1 \left[S_1 \tan(\phi) + c \right] \quad (11)$$

$$f_2 = F_2 \left[S_2 \tan(\phi) + c \right] = F_2 \left[E_2 w(x) \tan(\phi) + c \right] \quad (12)$$

Consequently, f_1 and f_2 in Eq. (9) are dependent on $w(x)$. E_1 and E_2 are corresponding coefficients of friction.

The finite difference form of Eq. (9) is:

$$T_1 = E_1 \frac{F_1 \tan(\phi) + c}{h_1} \Delta w \quad T_2 = -E_2 \frac{F_2 \tan(\phi) + c}{h_2} \Delta w \quad (13)$$

In matrix notation this can be written as:

$$[T] = [B] \Delta w \quad (14)$$

where $[B]$ is a tri-diagonal matrix:

A numerical solution of the system was obtained using the following iterative algorithm with 100 nodes in the x direction (per half length L) selected along the membrane (Fig. 8). It is assumed that E_1 , E_2 , c , F_1 , F_2 , ϕ and λ are given.

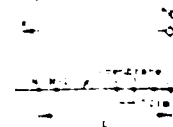


Fig. 8

1. At each nodal point, calculate $S_{ij}(w, h_j)$ from Eqn. (6) and $T_{ij}(w)$ from the first of Eqns. (11).
2. Form the $[B]$ matrix, Eqn. (13), with $\gamma(w) = 0$, $M_1 = \text{constant}$, and solve the linear system for the w_i .
3. Check if the deformation condition, Eqn. (10), is satisfied. If not, change the value of T_{ij} and repeat step 2.
4. Having satisfied step 3, calculate the resulting values of $T_{ij}(w)$.
5. Form the new matrix $[B]$ using the new values of T_{ij} and (13) and return to step 2.
6. The solution is achieved when the deflection at $w = 0$, $w = 0$ converges to a constant value when this is realized $T_{ij} = T_{ij}^0$ which can then be compared to the maximum tensile strength T_{max} of the geotextile membrane.

DISCUSSION OF RESULTS

The above procedure was programmed and some results were obtained for typical values of soil and geotextile properties to illustrate the relative influence of the various parameters. These results are shown in Figs. 9a and 9b and Fig. 10. Calculations were obtained for both a frictionless membrane (case I, shown dashed) and one that requires friction (case II, shown solid). The frictionless case has no relevancy to common geotextiles. However, it was included in the early stages of the study to aid in the development of the numerical algorithm. On the other hand, the frictional case is of considerable practical importance. In these plots the curves marked "1" represent an "improvement factor", $1 = M_{max} / w_{max}$, where M_{max} is the maximum deflection with the membrane and w_{max} is the maximum deflection without the membrane. It is noted that the efficiency of the membrane increases, as measured by $1 = M_{max}$, as the underlying soil becomes more compressible (smaller values of F_{ij}). For heavy loads, the factor $1 = M_{max}$ can exceed 50%. However, as shown, the geotextile must also be able to sustain large tensile forces (T_{ij}). At the present time, it appears that only heavy woven geotextiles and geogrids can meet such requirements for the cases shown.

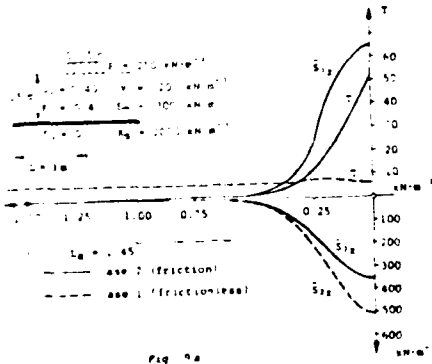


Fig. 9a

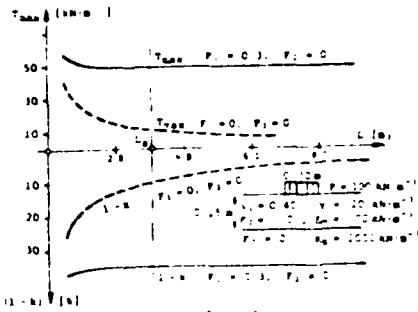


Fig. 9b

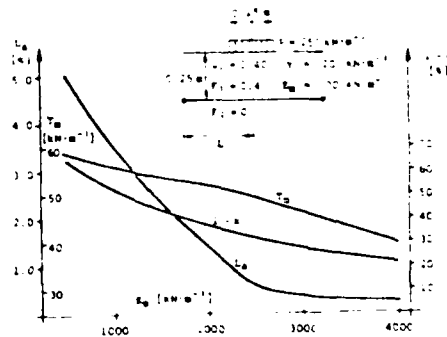


Fig. 10

The required length of fabric L_{ij} is seen to decrease rapidly as the friction increases and the underlying soil becomes stiffer.

Finally, it should be noted that the developed model does not consider failure induced by the lack of adequate bearing capacity. However, it does indicate two important possible modes of distress: (1) that of the tensile force T_{ij} exceeding the tensile strength, and (2) the slipping "pull out" of the fabric if its length L is less than the required value of L_{ij} .

ACKNOWLEDGMENTS

This research was supported by the Engineering Research Division of the United States Air Force Engineering and Services Laboratory. The interest and encouragement shown by the contract monitors, Captains J. D. Williams and R. E. Gavigan, is gratefully appreciated. The paper is based on original research carried out by the first author for his doctoral dissertation while he was a visiting scholar at Purdue University.

The manuscript was typed by Catherine Ralston.

REFERENCES

1. Westergaard, H. W. (1938) "A problem of elasticity suggested by a problem in soil mechanics: Soft materials reinforced by numerous strong horizontal sheets", in contribution to the "Mechanics of Soils", dedicated to the late Professor by his friends on the occasion of his sixtieth birthday anniversary. The Macmillan Company, New York.
2. Harrison, W. J. and Fordard, J. M. (1972) "Elastic theory applied to reinforced earth", *Journal of the Soil Mechanics and Foundations Division, ASCE*, Vol. 98, No. 1012, pp. 1357-1365.
3. Heermann, L. R. (1977) "Non-linear finite element analysis of reinforced systems", *Proc. Int. Conf. on the Use of Fabrics in Geotechnics and Structures*, Trondheim, Norway.
4. Hashemi, M. R. and Bagheri, M. J. (1977) "Analysis of soil-fabric interaction", *Proc. Int. Conf. on the Use of Fabrics in Geotechnics*, Paris, Vol. 3, pp. 347-48.
5. McGown, A., Anderson, E. A., Mashhour, M. M., Miles, B. (1961) "Stress behaviour of soil-fabric and embankments", *Proc. 8. ICODI*, Stockholm, Vol. 3, pp. 139-144.
6. Giroud, J. P. and Nouray, L. (1981) "Geotextile reinforced unpaved road design", *Journal of the Geotechnical Engineering Division, ASCE*, Vol. 107, No. 109, pp. 1233-1236.
7. Ladouze, E. (1977) "Mecanique des renforts dans le sol", *Proc. Int. Conf. on the Use of Fabrics in Geotechnics*, Paris, Vol. 3, pp. 155-160.
8. Barr, M. E. (1977) *Mechanics of Particulate Media*, Wiley-Interscience, New York.
9. Rucker, J. C., Barr, M. E. (1976) "Identification of aggregate characteristics from Prototype Testing of Landing Mats", *TR Report*, No. 137.
10. Nienhuis, J. D. (1977) "Geotextiles and the bearing capacity of road bases", *Proc. Int. Conf. on the Use of Fabrics in Geotechnics*, Paris, Vol. 3, pp. 3-6.
11. Holtz, R. D. and Brown, B. B. (1977) "Waste reinforced by fabrics - results of model tests", *Proc. Int. Conf. on the Use of Fabrics in Geotechnics*, Paris, Vol. 3, pp. 113-118.
12. Holtz, R. D. (1977) "Laboratory studies of reinforced earth using a woven polyester fabric", *Proc. Int. Conf. on the Use of Fabrics in Geotechnics*, Paris, Vol. 3, pp. 149-154.

APPENDIX B

LISTING OF COMPUTER PROGRAMS

```

PROGRAM MAIN(INPUT,OUTPUT,TAPES=INPUT;TAPES=OUTPUT)
C
C *****
C * THIS PROGRAM EMPLOYS A 2D SYSTEM OF TWO LAYERS OF *
C * SOIL REINFORCED BY A MEMBRANE AT THE INTERFACE. *
C * WINKLER MODEL FOR THE LOWER LAYER. *
C * TANGENTIAL INTERACTION IS RIGID-PLASTIC *
C * ITERATIVE SOLUTION TO THE FINITE DIFFERENCE EQUATION *
C * DIMENSION OF VECTORS = 300 *
C * MODE BATCH *
C *****
C
COMMON /BL1/EPSILO1,EPSILO2,TO,DELTAT,ITMAX,ITER,WM,
* EM,L,WR,IOUT(30),JOUT,XLA,A,TMAX,XTMAX
COMMON /SIMPS/F(300),NS,HS,FINT
COMMON /MAT1/XA(300,3),XB(300),W(300),NP
COMMON /MAT2/T(300),TAU(300),LAMBDA,H
COMMON /TG1/TAU1M(300),TAU2M(300),TAU1(300),TAU2(300),X(300)
COMMON /TG2/SIZ(300),S2Z(300)
C
REAL KS,OUI,L,LDIF,NU1,LAMBDA
C
C INPUT DATA
C *****
C
DO 100 I=1,30
100 IOUT(I)=0
C
WRITE(6,901)
901 FORMAT(/,/,1X,130(1H*),/,/,45X,15HPROGRAM FABRIC4,
* /,/,1X,130(1H*),/)
WRITE(6,905)
905 FORMAT(/,/,1X,37HCONVENTION: TENSILE STRESSES NEGATIVE)
READ(5,1103)A
READ(5,1103)H1
1103 FORMAT(F10.3)
READ(5,1103)NU1
READ(5,1103)KS
LAMBDA=KS
READ(5,1103)EM
READ(5,1103)P
READ(5,1103)L
READ(5,1103)F1
READ(5,1103)F2
READ(5,1103)GAMA
READ(5,1115)NSTEP
1115 FORMAT(I6)
C
200 H=L/NSTEP
C
C NUMBER OF NODES
C
NP=NSTEP+1
READ(5,1103)TO
READ(5,1103)DELTATO
READ(5,1214)EPSILO1
READ(5,1214)EPSILO2

```

```

        READ(5,1218)ITERMAX
        READ(5,1218)ITMAX
1214    FORMAT(F10.8)
1218    FORMAT(I3)
C
C   INTERMEDIATE OUTPUT COMMAND
C
        READ(5,1219)NOUT
1219    FORMAT(I2)
        IF (NOUT. NE. 0)GO TO 210
        GO TO 230
210    DO 220 I=1,NOUT
220    READ(5,1219)IOUT(I)
230    CONTINUE
C
C   OUTPUT
C   *****
C
        WRITE(6,2001)
2001    FORMAT(/,1X,21HDATA FOR COMPUTATION: ,/,21H*****
C
        WRITE(5,2005)
2005    FORMAT(45X,12HGENERAL DATA,/)
        WRITE(6,1111)H1,NUI,KS,EM,P,L,F1,F2,A
1111    FORMAT(/,1X,3HH1=,E12.4,1X,1HM,9X
        1 ,4HNUI=,E12.4,9X
        2 ,3HKS=,E12.4,1X,6HKN.M-3,3X
        3 ,3HEM=,E12.4,1X,6HKN.M-1,3X
        4 ,2HP=,E12.4,1X,1HM,10X
        5 ,1X,2HL=,E12.4,1X,1HM,10X
        6 ,3HF1=,E12.4,10X
        7 ,3HF2=,E12.4,10X
        8 ,2HA=,E12.4)
        WRITE(6,1212)GAMA,NSTEP
1212    FORMAT(1X,5HGAMA=,E12.4,1X,6HKN.M-3,2X,6HNSTEP=,I4)
        WRITE(6,2101)
2101    FORMAT(/,40X,34HDATA OF THE ITERATION COMPUTATIONS)
        WRITE(6,2102)TO,DELTA0,EPSILO1,EPSILO2,ITERMAX,ITMAX
2102    FORMAT(/,1X,3HTO=,E12.4,1X,6HKN.M-1,4X,8HDELTA0=,E12.4,1X
        1 ,6HKN.M-1,/,1X,8HEPSILO1=,E12.4,6X,8HEPSILO2=,E12.4,5X
        2 ,8HITERMAX=,I4,13X,6HITMAX=,I4)
C
C
C   INITIALIZATION OF VECTORS
C   *****
C
        DO 300 I=1,300
        TAU(I)=0.
        TAU1(I)=0.0
        TAU2(I)=0.0
        TAU1M(I)=0.0
        TAU2M(I)=0.0
        T(I)=0.0
        XA(I,1)=0.0
        XA(I,2)=0.0
        XA(I,3)=0.0
        XB(I)=0.0
        F(I)=0.0
        X(I)=0.0

```

```

      W(I)=0.0
      S2Z(I)=0.0
300   S1Z(I)=0.0
C
C   CALCULATION OF TAU1M
C   *****
C
      Q=P/(2*A)
      DO 350 I=1,NP
      X(I)=(I-1)*H
      Y1=(X(I)-A)/(H1*SQRT(NU1))
      Y2=(X(I)+A)/(H1*SQRT(NU1))
      HT=(Y2-Y1)/NSTEP
      DO 320 J=1,NSTEP
      F(J)=Y1+((J-1)*HT)
      F(J)=EXP(-(F(J)**2)/2)
320   F(J)=F(J)/SQRT(8*ATAN(1.0))
      HS=HT
      NS=NSTEP
      CALL SIMPSON
350   S1Z(I)=FINT*Q
C
C
C   CALCULATION OF DELTAP
      DO 370 I=1,NP
370   F(I)=S1Z(I)
      NS=NSTEP
      HS=H
C
      CALL SIMPSON
      WRITE(6,1221)FINT
1221  FORMAT(/,1X,7HPSI(L)=,E12.4)
      DELTAP=P-(2*FINT)
      WRITE(6,1222)DELTAP
1222  FORMAT(1X,7HDELTAP=,E12.4,7H KN.M-1)
      DO 400 I=1,NP
      TAU1M(I)=(S1Z(I)+(GAMA*H1))*F1
400   CONTINUE
C
C   WMAX WITHOUT MEMBRANE
C
      WM=S1Z(1)/LAMBDA
C
C   COUNTER OF PRINCIPAL ITERATIONS ITER
C
      ITER=0
      JOUT=1
C
C   ITERATION COMPUTATION FOR MAIN CYCLE
C
450   ITER=ITER+1
      DELTAT=DELTATO
C
C   FIRST ITERATION : COMPUTATION WITHOUT TANGENTIAL FORCES
C
      IF (ITER. NE. 1) GO TO 530
C
500   DO 520 I=1,NP
520   T(I)=TO

```

```

C
C ITERATIVE COMPUTATION FOR SECONDARY CYCLE
C
530 CALL ITERA
C
C CALCULATION OF S2Z AND TAU2M
C
      DO 550 I=1,NP
      S2Z(I)=W(I)*LAMBDA
550   TAU2M(I)=(S2Z(I)+(GAMA*H1))*F2
C
C COMPUTATION OF TANGENTIAL FORCES
C
      CALL TANG
C
C COMPUTATION OF EFFECTIVE LENGTH
C
      IF (F1. NE. 0) GO TO 565
      IF (F2. NE. 0) GO TO 565
      XLA=L
      GO TO 575
565   CONTINUE
C
      DO 570 I=1,NP
      IF (T(I). NE. 0)GO TO 570
      XLA=X(I)
      GO TO 575
570   CONTINUE
C
575   CONTINUE
C
C CONTROL OF THE MAIN CONVERGENCE ON W0
C
      IF (ITER. EQ. 1)GO TO 600
      DELTAW=(W0L-W(1))/W(1)
      ADELTAW=ABS(DELTAW)
      IF (ADELTAW. LT. EPSILO1)GO TO 680
C
C COMPUTATION TOO LONG
C
      IF (ITER. EQ. ITERMAX) GO TO 900
600   W0L=W(1)
C
C INTERMEDIATE OUTPUT
C *****
C
      IF (ITER. NE. 1)OUT(JOUT))GO TO 620
      CALL OUTPT
      JOUT=JOUT+1
620   GO TO 450
C
C IF CONVERGENCE TAKES PLACE END OF COMPUTATION
C
680   CONTINUE
C
C CALCULATION OF T(X)
C
      N=NP-2

```

```

DO 700 I=1,N
700 F(I)=(-3*W(I))+(4*W(I+1))-W(I+2)
F(I)=SQRT(1+(F(I)/(2*H))**2)
F(NP-1)=(W(NP)-W(NP-1))/H
F(NP-1)=SQRT(1+F(NP-1)**2)
F(NP)=F(NP-1)
DO 720 I=1,NP
720 T(I)=T(I)*F(I)
C
C CALCULATION OF TMAX
C
TMAX=T(1)
XTMAX=0.0
DO 730 I=2,NP
IF (T(I).GE.TMAX)GO TO 730
TMAX=T(I)
XTMAX=X(I)
730 CONTINUE
C
WR=W(1)/WM
CALL OUTPT
C
GO TO 999
C
C COMPUTATION TOO LONG
C
900 WRITE(6,1801)
1801 FORMAT(/,/,1X,32HNO CONVERGENCE IN THE MAIN CYCLE)
GO TO 680
999 WRITE(6,9001)
9001 FORMAT(/,1X,18HEND OF COMPUTATION)
C
C
C STOP
C END
C
C SUBROUTINE ITERA
C
C *****
C SUBROUTINE ITERA
C CYCLES OF SECONDARY ITERATION OF FABRIC4
C SOLUTION OF FINITE DIFFERENCE EQUATIONS OF THE
C VERTICAL AND HORIZONTAL EQUILIBRIUM
C FROM THE RESULTS OF THE PREVIOUS PRINCIPAL ITERATION
C FORM THE MATRIX(SUBROUTINE MATRIX)
C SOLUTION OF THE LINEAR SYSTEM(SUBRTM. SLIMTRI)
C CONTROL OF THE SECONDARY CONVERGENCE
C *****
C
C COMMON /BL1/EPSILO1,EPIL02,TD,DELTAT,ITMAX,ITER,WM,EM,L,WR
C 1 ICUT(30),JCUT,XLA,A,TMAX,XTMAX
C COMMON /MAT1/XA(300,3),XB(300),W(300),NP
C COMMON /MAT2/T(300),TAU(300),LAMBDA,H
C COMMON /SIMPS/F(300),NS,HS,FINT
C COMMON /TG2/S12(300),S2Z(300)
C COMMON /TG1/TAU1M(300),TAU2M(300),TAU1(300),TAU2(300),X(300)

```

```

C
C      REAL LAMBDA,LDIFF,L
C
C      INITIALIZE
C      COUNTER OF THE SECONDARY ITERATIONS IT
C      IT=1
C
C      COUNTER OF THE JUMPS OF THE ROOTS DURING CONVERGENCE
C      XSAUT=0.0
C      DIFF=0.0
C
C      DIFFERENCE FROM THE PREVIOUS ITERATION
C      100  LDIFF=DIFF
C
C      FORMATION OF THE MATRIX COEFFICIENTS
C      CALL MATRIX
C
C      SECOND MEMBER OF THE SYSTEM
C
C      NSTEP=NP-1
C      DO 200 I=2,NSTEP
200  XB(I)=S1Z(I)*H*H
C      XB(1)=0.0
C      XB(NP)=0.0
C
C      SOLUTION OF THE SYSTEM
C      CALL SLIMTRI
C
C      CONTROL OF CONVERGENCE
C      CALCULATION OF SRA
C
C      N=NP-2
C      DO 300 I=1,N
300  F(I)=(-3*W(I))+(4*W(I+1))-W(I+2)
C      F(I)=SQRT(1+(F(I)/(2*H))**2)
C      F(NP-1)=(W(NP)-W(NP-1))/H
C      F(NP-1)=SQRT(1+F(NP-1)**2)
C      F(NP)=F(NP-1)
C      NS=NSTEP
C      HS=H
C      CALL SIMPSON
C      SRA=FINT-L
C
C      CALCULATION OF SRB
C
C      DO 350 I=1,NP
350  F(I)=F(I)*ABS(T(I))
C      NS=NSTEP
C      HS=H

```

```

      CALL SIMPSON
      SRB=FINT/EM
C
C   TEST OF CONVERGENCE
C
      DIFF=SRA-SRB
      ADIFF=ABS(DIFF)
      ADIFF=ADIFF/SRA
      IF (ADIFF. LT. EPSILO2)GO TO 600
C
C   TESTS ON THE JUMPS OF THE ROOTS
C
      PROD=DIFF*LDIFF
      IF (PROD. LT. 0) GO TO 550
C
C   STEPS OF THE JUMP
C
540   CONTINUE
      TO=TO+DELTAT
      DO 545 I=1,NP
545   T(I)=T(I)+DELTAT
      IT=IT+1
      IF (IT. GT. ITMAX)GO TO 580
      GO TO 100
C
C   JUMP
C
550   XSAUT=XSAUT+1
      XSIGN=-1
570   DELTAT=XSIGN*((1/(2*XSAUT))*DELTAT)
      TO=TO+DELTAT
      DO 575 I=1,NP
575   T(I)=T(I)+DELTAT
      IT=IT+1
      IF (IT. GT. ITMAX)GO TO 580
C
C   INTERMEDIATE OUTPUT
C
      IF (ITER. NE. IOUT(JOUT))GO TO 578
      WRITE(6,2001)ITER
2001  FORMAT(/,1X,5HITER=,I4)
      WRITE(6,1001)DELTAT
1001  FORMAT(1X,7HDELTAT=,E12.4)
      WRITE(6,1411)
1411  FORMAT(85X,4HSRA=,E12.4,5X,4HSRB=,E12.4,5X,5HDIFF=,
1     E12.4,5X,5HADIFF=,E12.4)
      WRITE(6,1012)PROD
1012  FORMAT(1X,5HPROD=,E24.4)
578   GO TO 100
C
580   WRITE(6,1420)ITER,IT
1420  FORMAT(/,/,1X,37HNO CONVERGENCE IN THE SECONDARY CYCLE,1X,
1     SHITER=,I4,3HIT=I4)
      STOP
C
600   CONTINUE
      RETURN
      END
C
C

```

```

C          SUBROUTINE TANG
C
C *****
C *          SUBROUTINE    TANG          *
C *          *
C *          COMPUTATION OF THE NODAL TANGENTIAL FORCES FOR
C *          FABRIC4
C *          PRIMARY TANGENTIAL STRESSES S12 AND S22
C *          SECONDARY TANGENTIAL STRESSES(ELASTO-PLASTIC)
C *          TENSILE NODAL FORCES IN THE MEMBRANE T
C *          *
C *****
C
C          COMMON /BL1/ EPSILO1, EPSILO2, TO, DELTAT, ITMAX, ITER, WM, EM, L, WR
1          , IOUT(30), JOUT, XLA, A, TMAX, XTMAX
C          COMMON /TG1/ TAU1M(300), TAU2M(300), TAU1(300), TAU2(300), X(300)
C          COMMON /TG2/ S12(300), S22(300)
C          COMMON /MAT1/ KA(300,3), XB(300), W(300), NP
C          COMMON /MAT2/ T(300), TAU(300), LAMBDA, H
C          COMMON /SIMPS/ F(300), NS, HS, FINT
C
C          REAL LAMBDA
C
C          SECONDARY FORCES ARE ZERO AT THE EXTREMES
C
C          F(1)=0.0
C          TAU1(1)=0.
C          TAU2(1)=0.
C          TAU(1)=0.
C
C          F(NP)=0.
C          TAU(NP)=0.
C          TAU1(NP)=0.
C          TAU2(NP)=0.
C
C          FINT=0.
C          TINT=0.
C          NSTEP=NP-1
C
C          DO 500 I=2, NSTEP
C
C          COMPUTATION STARTS FROM THE END OF THE MEMBRANE
C          AUXILLIARY INDEX IA
C
C          IA=NSTEP-I+2
C          JA=IA+1
C
C          LIMIT OF THE MOBILIZED STRESS
C          RIGID PLASTIC MODEL
C
450          TAU1(IA)=TAU1M(IA)
          TAU2(IA)=TAU2M(IA)
500          TAU(IA)=TAU1(IA)+TAU2(IA)
C

```

```

C TENSILE FORCES IN THE MEMBRANE
C
  DO 500 I=2,NP
  J=I-1
  B=(TAU(J)+TAU(I))*H/2
  TINT=TINT+B
  T(I)=T(I)+TINT
C
C NO COMPRESSIONS
C
  IF (T(I).LT.0)GO TO 600
  T(I)=0.
  TAU(I)=0.
  TAU1(I)=0.
  TAU2(I)=0.
600 CONTINUE
C
  RETURN
  END

C
C SUBROUTINE MATRICE
C
C *****
C * SUBROUTINE MATRICE *
C * MATRIX COEFFICIENTS FOR FABRIC4 *
C *****
C
COMMON /MAT1/XA(300,3),XB(300),H(300),NP
COMMON /MAT2/T(300),TAU(300),LAMBDA,H
C
REAL LAMBDA
C
  DO 200 I=2,NP
  XA(I,1)=T(I)
  XA(I,2)=LAMBDA*H*H
  YA(I,2)=XA(I,2)+(2*T(I))
  XA(I,2)=XA(I,2)+(H*TAU(I))
  XA(I,3)=T(I)+(H*TAU(I))
200 CONTINUE
C
C BOUNDARY CONDITIONS
C
  XA(1,1)=0.
  XA(1,2)=1.
  XA(1,3)=1.
  XA(NP,1)=0.
  XA(NP,2)=1.
  XA(NP,3)=0.
C
  RETURN
  END

```

```

C
C      SUBROUTINE SLIMTRI
C
C *****
C *
C *          SUBROUTINE    SLIMTRI
C *
C * SOLUTION BY THE DIMINISHON OF A TRI-DIAGONAL LINEAR
C * SYSTEM
C *
C *****
C
C      COMMON /MAT1/XA(300,3),XB(300),W(300),NP
C
C      ELIMINATION
C
C      DO 100 I=2,NP
C      FACT=XA(I,1)/XA(I-1,2)
C      XA(I,2)=XA(I,2)+(XA(I-1,3)*FACT)
100  XB(I)=XB(I)-(XB(I-1)*FACT)
C
C      COMPUTATION OF W(I) BY SUBSTITUTION
C
C      W(NP)=XB(NP)/XA(NP,2)
C      DO 200 J=2,NP
C      I=NP+1-J
200  W(I)=(XB(I)-(XA(I,3)*W(I+1)))/XA(I,2)
C
C      RETURN
C      END
C
C
C      SUBROUTINE SIMPSON
C
C *****
C *
C *          SUBROUTINE    SIMPSON
C *
C * NUMERICAL INTEGRATION USING SIMPSON RULE
C *
C *****
C
C      COMMON /SIMPS/F(300),NS,HS,FINT
C
C      SIMPSONS FORMULA (NS HAS TO BE EVEN)
C
C      FINT=0.
100  DO 110 J=2,NS,2
C      XINT=F(J-1)+4*F(J)+F(J+1)
C      XINT=XINT*HS/3
110  FINT=FINT+XINT
C
C      RETURN
C      END

```

```

C
C
C      SUBROUTINE OUTPT
C
C *****
C      SUBROUTINE  OUTPT
C      OUTPUT FOR FABRIC4
C *****
C
COMMON /BL1/EPSILO1, EPSILO2, TO, DELTAT, ITMAX, ITER, WM, EM, L, WR
1  , IOUT(30), JOUT, XLA, A, TMAX, XTMAX
COMMON /TG1/TAU1M(300), TAU2M(300), TAU1(300), TAU2(300), X(300)
COMMON /TG2/S1Z(300), S2Z(300)
COMMON /MAT1/XA(300,3), XB(300), W(300), NP
COMMON /MAT2/T(300), TAU(300), LAMBDA, H
C
REAL LAMBDA, L
C
WRITE(6, 1515) ITER, W(1), T(1), T(NP), TMAX, XTMAX, XLA, WM, WR
1515  FORMAT(/, /, 1X, 27HRESULTS OF THE COMPUTATION: , 5X, 5HITER=, I6,
1  /, 1X, 20H*****
2  /, 25X, 5HW(1)=, E12.4, 5X, 1HM,
3  /, 25X, 5HT(1)=, E12.4, 5X, 6HKN.M-1,
4  /, 25X, 5HT(L)=, E12.4, 5X, 6HKN.M-1,
5  /, 25X, 5HTMAX=, E12.4, 5X, 6HKN.M-1,
6  /, 25X, 6HXTMAX=, E12.4, 5X, 1HM,
7  /, 25X, 4HXLA=, E12.4, 5X, 1HM,
8  /, 25X, 3HWM=, E12.4,
9  /, 25X, 3HWR=, F6.3, )
C
WRITE(6, 1525)
1525  FORMAT(/, 3X, 1HN, 7X, 1HX, 10X, 3HS1Z, 10X, 3HS2Z, 9X, 4HTAU1, 9X,
1  4HTAU2, 10X, 3HTAU, 12X, 1HT, 12X, 1HW, /)
DO 300 I=1, NP
300  WRITE(6, 1526) I, X(I), S1Z(I), S2Z(I), TAU1(I), TAU2(I), TAU(I)
1  , T(I), W(I)
1526  FORMAT(1X, I3, 1X, E12.4, 7(1X, E12.4))
C
C
RETURN
END

```



```

C      DO 100 L=1,K
      N1=L*N1
100    CONTINUE
C
C      N11=(N1)**2
C
C      X1=R*X
      DELS=(-0.25*(X**2)**K)/N11
      DELS1=(-0.25*(X1**2)**K)/N11
C
      S1=S1+DELS1
C
      DELS2=DELS/(K+1)
C
      S2=S2+DELS2
C
      IF (ABS(DELS1).GT. 0.0001) GO TO 150
      IF (ABS(DELS2).GT. 0.0001) GO TO 150
C
      GO TO 250
C
150    CONTINUE
C
200    CONTINUE
250    CONTINUE
C
      S2=S2*0.5*X
C
      IF (X1. LT. 7.0)GO TO 290
C
270    CONTINUE
C
      USE APPROXIMATE BESSEL FUNCTION FOR LARGE ARGUMENTS
C
      THETA=X-PI/4.0
      S1=(SQRT(2/PI/X))*COS(THETA)
C
      IF (X. GT. 7.0) GO TO 290
C
      THETA1=X-3.0*PI/4.0
      S2=(SQRT(2/PI/X))*COS(THETA1)
290    CONTINUE
C
C
      C(I)=(A2)*(S1)*(S2)
      IF (I. EQ. 1)GO TO 300
C
C      COMPUTE THE STRAIN
C
      DELD=0.5*(C(I)+C(I-1))*DELX
      D=DELD+D
C
      IF (ABS(DELD). LT. 0.0001) GO TO 400
C
300    CONTINUE
C
400    CONTINUE

```

```

C      D1(J)=Q*D
C      IF (J. EQ. 1)GO TO 600
C      CALCULATE THE SETTLEMENT
C      DELRO=0.5*(D1(J)+D1(J-1))*DELZ
      RO=RO+DELRO
      IF (ABS(DELRO). LT. 0.0001) GO TO 700
C      600  CONTINUE
C      700  CONTINUE
C      CALCULATE THE SETTLEMENT RATIO
C      IF (R. EQ. 1.000)RO1=RO
      RO=RO/RO1
C      WRITE(6,750)R,RO
      750  FORMAT(/,F10.3,9X,F10.3)
C      800  CONTINUE
C      STOP
      END

```

END

DATE
FILMED

11 - 83

DTIC